WASM: Minerals, Energy and Chemical Engineering

Evaluation of the Wettability Characteristics of CO_2-Brine-Rock-Clay Mineral Systems: Implications for CO_2 Sequestration

Cut Aja Fauziah

0000-0002-5983-7011

This thesis is presented for the Degree of

Doctor of Philosophy

of

Curtin University

April 2021

DECLARATION OF ACADEMIC INTEGRITY

To the best of my knowledge and belief, this thesis contains no material previously published by any other person, except where due acknowledgement has been made.

This thesis contains no material, which has been accepted for the award of any other degree or diploma in any university.

Signature: Cut Aja Fauziah

Date: 19 April 2021

COPYRIGHT

I warrant that I have obtained, where necessary, permission from the copyright owners to use any third-party copyright material reproduced in the thesis (e.g. questioners, artwork, unpublished letters), or to use any of my own published work (e.g. journal articles) in which the copyright is held by another party (e.g. publishers, co-authors).

Signature: Cut Aja Fauziah

Date: 19 April 2021

DEDICATION

I dedicate my thesis to the memory of my father and mother, Sayid Ahmad and Cut Aja Hamidah, for their endless love, affection, prayers, and encouragement that make me able to be the individual I am today.

You both have gone but your belief in me has made this journey possible.

I wish that you had been proud to see my achievement of the graduation in a Doctor of Philosophy degree.

ACKNOWLEDGMENTS

All praise and thanks to God, the Almighty Allah for His showers of blessings throughout my PhD journey to complete the study successfully.

I would like to express my deep and sincere gratitude to my supervisor, Associate Professor Ahmed Barifcani and co-supervisor Dr Christopher Lagat for their guidance, support, knowledge, and encouragement during my PhD study. My utmost gratitude also goes to my associate supervisor Professor Stefan Iglauer for his assistance and support from the beginning I started my study. His knowledge, devoted efforts and essential comments in manuscript writings have guided me to transform my work into the best manner and the quality publications. My gratitude also extends to Dr Drew Parson (previous) and Dr Hamid Roshan (current), as my external associate supervisors for their contributions in the valuable discussion and advice, especially in manuscript preparation and writing; and Chairperson of my thesis committee Associate Professor Mofazzal Hossain for his time, encouragement, and expertise throughout this project. Special thank goes to Dr Ahmed Al-Yaseri, my colleague, my brother and my real 'supervisor' for his continued and never-ending support and guidance from the very beginning I started this research, which guided me to be where I am right now.

I would like to thank to Professor Maxim Lebedev for his contribution and assistance in providing the AFM data in this research. I also thank the Department of Mines, Industry Regulations and Safety (DMIRS), NGL Geochemistry Laboratory-CSIRO Energy, and RSO CSIRO-Mineral Resources of Western Australia for providing the

Harvey 1 core samples, the analyses of organic content, and the compositional analysis of the Harvey 1 core samples, respectively.

I would like to acknowledge my sponsor, LPDP-Indonesia endowment fund for education, Ministry of Finance of the Republic of Indonesia for the financial support through the PhD scholarship.

My sincere appreciation to all faculty members and colleagues at the Department of Petroleum Engineering, Curtin University for whom I have great regards. Much gratitude goes to Jamiu Ekundayo who always helped and supported me through the hardship during my study. I would like to extend my gratitude to Emad Al-Khdheeawi, it has been a great pleasure knowing and working with you, especially in writing successfully many international conference papers. Special thanks to 'party group' (Anastasia, Atif, Gonzalo, Miftah, Nilesh, and Partha), you made my life more colourful and enjoyable.

Last but by no means least; I would like to express my deepest gratitude to my late father and mother, my sisters and brothers, and all my family members for prayers, encouragement, and support throughout my life and my study.

ABSTRACT

Carbon capture and storage (CCS) has been proposed as an efficient method to reduce anthropogenic carbon dioxide (CO_2) emissions into the atmosphere and thus mitigate global climate change. One of the essential concerns of CCS is to ensure that the buoyant CO_2 remains trapped underground in the geological formation. To optimise storage efficiency and to minimise risk CO_2 leakage, therefore, specific reservoirs need to be selected. In this context, rock wettability is a fundamental subject of research that intensely and directly influences containment security and storage capacity. Specifically, wettability of CO_2-brine-rock-clay systems is an important physicochemical factor of reservoir characterisation. Despite significant previous research efforts, there remains a high uncertainty associated with the understanding of the wettability of CO_2-brine-rock-clay systems and how it evolves with CO_2 exposure.

This research is a collection of experimental work on wettability of various CO_2/brine/rock/clay systems through the measurement of advancing and receding water contact angles. The tilted plate technique and a high temperature-high pressure goniometer methodology were used in this study. The measurements were conducted at various pressures (0.1 MPa, 5 MPa, 10 MPa, 15 MPa and 20 MPa) and elevated temperatures (305 K, 323 K, 333 K and 334 K) that simulate the typical subsurface, aquifer reservoir conditions. The rock samples used for wettability measurements included the South West Hub (Harvey-1) sandstones, Berea, and Bandera Gray sandstones. Clay solid substrates formed by compaction of powdered clay minerals, precisely montmorillonite, illite and kaolinite, were also used. These are variable but important cohort of the many rock-forming minerals present in reservoir and caprocks. They are also critical in CO_2 sequestration functions.

The research investigated the effect of pressure and temperature, clay type, organic content, pore systems and surface roughness on wettability to determine the impacts on reservoir storage capacity and containment security. The study also addressed characterisation for nitrogen/brine/clay and nitrogen/oil (n-decane)/clay contact angle to enhance fundamental knowledge, which will be applicable to oil production and fundamental an understanding of the development of solid earth. In addition, this work reported novel mathematical correlations to predict the advancing and receding contact

angles of three clay minerals as a function of gas density for helium, nitrogen, argon, and carbon dioxide-brine systems.

The results of this study indicate that the advancing and receding water contact angles increased with increase in pressure for most of the CO_2-brine-rock-clay systems. It is related to the increasing CO_2 density, which strengthens the intermolecular interactions between the CO_2 and mineral, and therefore leads to de-wetting of the surface. However, there was only a small reduction in advancing and receding contact angles with an increase in temperature. The wettability analysis demonstrated that the contact angle is very sensitive to the content of organic matter. Moreover, the sandstones turned slightly more hydrophobic after core flooding, indicating that the sandstones became more CO_2-wet after CO_2 injection. These results suggest that CO_2 flooding leads to an increase in the CO_2-wettability of sandstone. Thus, an increase in vertical CO_2 plume migration, solubility trapping, and a reduction in the residual trapping capacity, especially when extrapolated to more prolonged field-scale injection and exposure times. However, low permeability formations with significant CO_2 injection issues, CO_2-wetting of the reservoir rock surface, and adequate seal for containment security could help better pressure management. These analyses thus have important implications for assessing the feasibility of long-term CO_2 storage and enabling large-scale industrial carbon geological storage projects.

PUBLICATIONS

Journal publications:

1. Fauziah, C. A., Al-Yaseri, A. Z., Jha, N. K., Lagat, C., Roshan, H., Barifcani, A. & Iglauer, S. 2020. Carbon dioxide wettability of South West Hub sandstone, Western Australia: Implications for carbon geo-storage. International Journal of Greenhouse Gas Control, 98, 103064. https://doi.org/10.1016/j.ijggc.2020.103064

2. Fauziah, C. A., Al-Yaseri, A. Z., Beloborodov, R., Siddiqui, M. A., Lebedev, M., Parsons, D. F., Roshan, H., Barifcani, A. & Iglauer, P. S. 2019. Carbon dioxide/brine, nitrogen/brine and oil/brine wettability of montmorillonite, illite and kaolinite at elevated pressure and temperature. Energy & Fuels, 33(1), 441-448. https://doi.org/10.1021/acs.energyfuels.8b02845

3. Li, P., Zhang, J., Rezaee, R., Dang, W., Li, X., **Fauziah, C. A**., Nie, H. & Tang, X. 2021. Effects of swelling-clay and surface roughness on the wettability of transitional shale. Journal of Petroleum Science and Engineering, 196, 108007. https://doi.org/https://doi.org/10.1016/j.petrol.2020.108007

Under review papers:

1. Dependence of clay wettability on gas density. Submitted to journal of Greenhouse Gases Science and Technology (Under consideration after revision).

2. Effect of CO2 flooding on wettability evolution of sandstone. Submitted to Colloid and Surfaces A: Physicochemical and Engineering Aspects (Under review).

Conference publications:

1. Fauziah, Cut Aja., Al-Khdheeawi, Emad A., Lagat, Christopher., Iglauer, Stefan and Barifcani, Ahmed. 2021. Influence of gas density on the clay wettability: Implication for CO_2 geo-sequestration. 15th International Conference on Greenhouse Gas Control Technologies, GHGT-15; 15th - 18th March 2021. Abu Dhabi, UAE. http://dx.doi.org/10.2139/ssrn.3818907

2. Al-Khdheeawi, E. A., Fauziah, C. A., Mahdi, D. S. & Barifcani, A. 2021. A new approach to improve the assessments of CO_2 geo-sequestration capacity of clay minerals. International Petroleum Technology Conference. D021S006R002. https://doi.org/10.2523/iptc-21278-ms

3. Fauziah, C. A., Al-Khdheeawi, E. A., Barifcani, A. & Iglauer, S. 2020. Wettability measurements on two sandstones: An experimental investigation before and after CO_2 flooding. The APPEA Journal, 60(1), 117-123. https://doi.org/https://doi.org/10.1071/AJ19099

4. Fauziah, C. A., Al-Khdheeawi, E. A., Iglauer, S. & Barifcani, A. 2020. Effect of clay minerals heterogeneity on wettability measurements: Implications for CO_2 storage. Offshore Technology Conference Asia. Kuala Lumpur, Malaysia: Offshore Technology Conference. https://doi.org/10.4043/30449-MS

5. Al-Khdheeawi, E. A., Mahdi, D. S., Ali, M., **Fauziah, C. A**. & Barifcani, A. 2020. Impact of caprock type on geochemical reactivity and mineral trapping efficiency of CO_2. Offshore Technology Conference Asia. Kuala Lumpur, Malaysia: Offshore Technology Conference.. https://doi.org/10.4043/30094-MS

6. Fauziah, C. A., Al-Khdheeawi, E. A., Iglauer, S. & Barifcani, A. 2020. Influence of total organic content on CO_2–water– sandstone wettability and CO_2 geo-storage capacity. SPE Europec featured at 82nd EAGE Conference and Exhibition. Amsterdam, the Netherlands: Society of Petroleum Engineers. https://doi.org/10.2118/200564-MS

7. Fauziah, C. A., Al-Khdheeawi, E. A., Barifcani, A. & Iglauer, S. 2019. Wettability measurements of mixed clay minerals at elevated temperature and pressure: Implications for CO_2 geo-storage. SPE Gas & Oil Technology Showcase and Conference. Dubai. Society of Petroleum Engineers. https://doi.org/10.2118/198591-MS

TABLE OF CONTENTS

LIST OF FIGURES

LIST OF TABLES

Chapter 1 Introduction

1.1 Background

The spike in industrial activities following the 1750 industrial revolution has led to a proportionate increase in atmospheric carbon dioxide (CO_2) (Figure 1.1) (Surampalli et al., 2014; Lindsey, 2020). An obvious consequence of this reality is an excess use of machines, which sharply raised a demand for energy to support the new development era. Conventional energy (i.e. fossil fuels) such as coal and hydrocarbon have become the primary sources of energy, and would likely remain the viable available sources for years to come (Surampalli et al., 2014; Rackley, 2017; Leung et al., 2014). The conventional energy consumption is accounted for over 85% of the world's energy use (IEA, 2015).

The constant increase in the use of these primary energy sources has caused an extensive change in the atmosphere, particularly related to increase in CO_2 emissions, a primary anthropogenic greenhouse gas (Leung et al., 2014; Yu et al., 2008). Apart from fossil fuels' combustion process, CO_2 emissions from deforestation and industrial activity are also responsible for the increase in the ambient CO_2 concentrations, leading acidification of oceans, global warming, and consequently, climate change (IPCC, 2014; IPCC, 2005; Surampalli et al., 2014). The 2019 mean concentration of atmospheric CO_2, globally, was found to be approximately 410 ppm, with the annual rate of rise 100 times faster than preceding natural increases over the past 60 years (Lindsey, 2020). The global atmospheric CO_2 concentration is expected to be more than 900 ppm by the end of the 21st century, if the worldwide energy demand continues to grow with fossil fuel sources (Lindsey, 2020; IPCC, 2005). Therefore, there is a

serious need to take a global action to reduce the worldwide CO_2 emissions for the longer term.

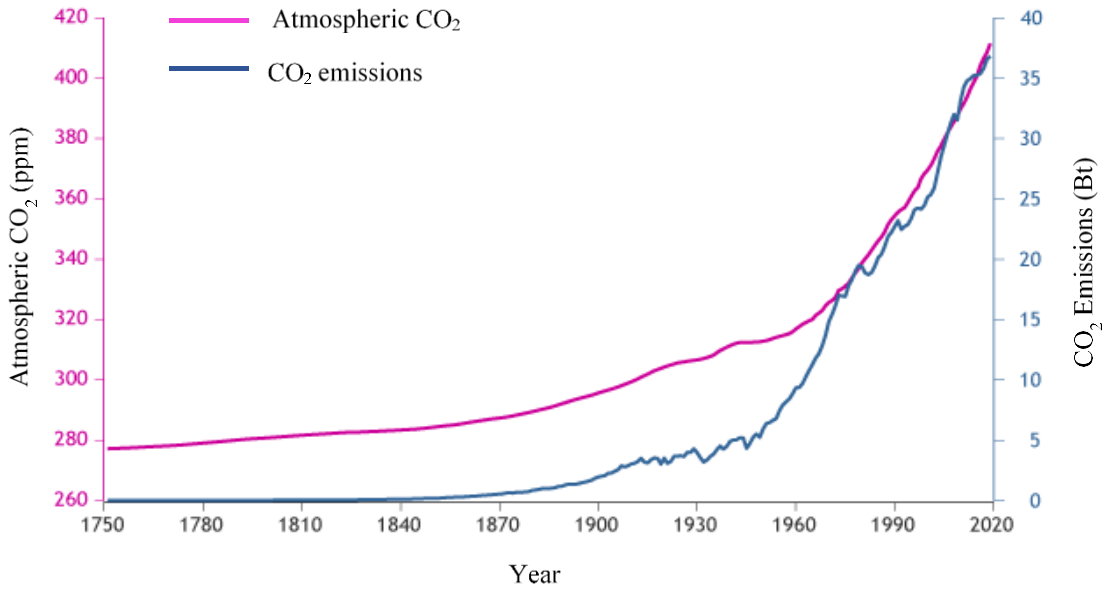

Source: modified from Lindsey (2020)

Figure 1. 1 CO_2 concentration versus annual emission (1750 – 2019)

The figure shows that CO_2 emissions increased considerably to 5 billion tons in the mid-20th century, and then it jumped to more than 35 billion tons per annum by the end of the 2019.

Several technology options have been proposed to mitigate CO_2 emissions and adopted by various countries, including 1) improving the use of energy conservation and low carbon fuels, 2) deploying renewable energy such as solar wind and hydropower, and 3) CO_2 capture and storage (CCS) (IPCC, 2005; Leung et al., 2014). The latter option is considered as the most feasible method to reach the large-scale CO_2 emissions reduction from large point sources (IPCC, 2005). The CCS process comprises

separating CO_2 from the extensive point emission sources such as industrial areas and power plants, then transporting to a storage site, and injecting or storing into underground formations such as depleted hydrocarbon reservoirs and deep aquifers for long-term separation from the atmosphere (IPCC, 2005). Sequestering CO_2 into deep geological formations (CO_2 storage) has more advantages than CO_2 recycling and enhanced oil recovery in active hydrocarbon reservoirs (Underschultz and Strand, 2016).

During the injection of CO_2 into an aquifer, various parameters are involved in controlling the CO_2 movement within the porous media, in terms of aquifer petro-physical properties, fluid densities and viscosities, the CO_2 solubility in the formation fluid (brine), as well as the rate and duration of injection (Pentland et al., 2011a). Besides, a leading issue with CCS is CO_2 leakage because of its lower density comparative to the formation water. Mechanisms such as structural (Jamaluddin et al., 1998; Iglauer et al., 2015a), mineral (Matter et al., 2016; Xu et al., 2003), residual (Qi et al., 2009; Rahman et al., 2016), dissolution (El-Maghraby et al., 2012; Jeon et al., 2018), and adsorption trappings (Arif et al., 2017d; Busch et al., 2004) have been investigated for mitigating CO_2 leakage in different solids.

Wettability is a leading factor controlling the integrity of rock in storing and containing CO_2 (Iglauer et al., 2015b; Iglauer, 2017). It is also the primary factor affecting the management of CCS in geological formations. Moreover, interfacial interactions including rock wettability, interfacial tension, capillary pressure, residual saturation, and relative permeability control multiphase flow behaviour, and fluid migration in porous media at reservoir-scale (Iglauer et al., 2015a). The surface rock and interfacial

tension between two immiscible liquids are the main factors that determine the relative permeability, the residual saturation, and the capillary pressure (Anderson, 1986b; Morrow, 1990; Hirasaki, 1991). The wettability examines how the immiscible liquids interact with the rock/mineral surfaces and affect the liquid flows. In fact, there is a difference between the liquid spreading in water-wet rock and oil/gas-wet rocks. Capillary pressure decreases as interfacial tension decreases, while capillary increases because of reduced interfacial tension. In this context, the CCS process is specifically affected by the interfacial interactions of gas-fluid-rock (Iglauer et al., 2015b; Yang et al., 2008; Chalbaud et al., 2009).

The wettability is typically determined from contact angles measured in the laboratory under geological conditions for various fluid-solid systems. While existing literatures have established temperature, pressure, salinity, total organic content, surface roughness, and rock/clay types as the main factors affecting wettability (Iglauer et al., 2015b; Iglauer, 2017), there is no consensus on how these factors influence the experimental results. For example, while some researchers reported increasing contact angle with pressure (Alnali et al., 2018; Al-Yaseri et al., 2016; Fauziah et al., 2019b; Fauziah et al., 2019a; Saraji et al., 2013), others have reported the opposite of pressure effect on contact angle (Espinoza and Santamarina, 2010; Farokhpoor et al., 2013; Wang et al., 2012a). Similarly, other research reports indicate a decreasing contact angle with temperature (Bikkina, 2011; Saraji et al., 2013; Fauziah et al., 2019b), while others have reported increasing contact angle with temperature (Alnali et al., 2018; Al-Yaseri et al., 2017b; Farokhpoor et al., 2013). Similar contrasting views have also been found in several studies involving measurements of contact angles for CO_2-brine-muscovite substrates (mica) systems at high temperatures and pressures (Chiquet et

al., 2007; Farokhpoor et al., 2013; Arif et al., 2016a; Broseta et al., 2012; Wan et al., 2014; Wang et al., 2012b). These studies have revealed that the contact angle is positively correlated with pressure and salinity, but negatively related to temperature (Chiquet et al., 2007; Farokhpoor et al., 2013; Arif et al., 2016a; Broseta et al., 2012; Wan et al., 2014; Wang et al., 2012b).

Despite the abundance of research publications in this domain, there is still a lack of understanding in wettability characteristics of CO_2-rine-rock-clay mineral systems. This study could fill some knowledge gaps that persist, as summarised below:

1. The study for CO_2/brine, nitrogen (N_2)/brine and oil/brine wettability of different clay types, especially wettability characterisations of pure clays; montmorillonite, illite and kaolinite, which is compacted from clay powder into a solid substrate for varied experimental conditions, remains limited.
2. This study examines the wettability of compacted clays: montmorillonite, illite and kaolinite to understand a correlation between gas densities and wettability on pure clays, and to develop a new mathematical model. The existing reported data are shown only for quartz.
3. The study shows how an actual reservoir storage rock (Harvey-1 well storage reservoir core material) behaves in regards to what wettability properties can be expected because of CO_2 injection into a representative storage formation. Specifically, this study introduces a method to remove artificial organic matter from the rock for more indicative interpretations of in situ conditions.
4. The reported data of wettability on Berea and Bandera Gray sandstones still have high inconsistencies, especially on how CO_2 injection changes sandstone's

wettability, in correlation with microstructural alteration in the sandstone caused by CO_2 flooding.

1.2 Research objectives

The primary focus of this thesis is to present the details of the experimental studies conducted on montmorillonite, illite and kaolinite wettability for CO_2-brine, N_2/brine and N_2/oil systems; gas density on clay wettability; CO_2 wettability of Harvey sandstones; and CO_2 wettability of Berea and Bandera Gray sandstones, measured at various pressures and temperatures. The specific objectives of this research are explained as follows:

1. Investigate the wettability of montmorillonite, illite and kaolinite for CO_2/brine, N_2/brine and N_2/oil (n-decane) fluid systems. To achieve this objective, contact angle measurements were conducted for these clay minerals in CO_2/brine, N_2/brine and N_2/oil (n-decane) systems at various pressures (5 MPa, 10 MPa, 15 MPa and 20 MPa) and temperatures (305 K and 333 K). Additionally, zeta potential was measured to investigate the link between wettability and the macroscopic contact angle.
2. Investigate the relationship between gas densities and wettability of the different solid-gas systems, and develop mathematical models to predict contact angles, from pressure and gas density, for these clays (montmorillonite, illite and kaolinite).
3. Investigate the wetting behaviour of an actual storage reservoir rock. To achieve this objective, wettability of CO_2-brine-South West Hub sandstone (GSWA Harvey-1) was measured for pressures from 0.1 MPa to 20 MPa, and temperature

of 334 K. Organic carbon isotope tracking ($\delta^{13}C_{org}$) was suggested to eradicate the effect of superficial organic matter caused by drilling mud penetration..

4. Analyse how CO_2 injection can change sandstone wettability and correlate the changes with microstructural alteration in the sandstone caused by CO_2 flooding and evaluate the implications for CO_2 trapping capacity and containment security predictions.

1.3 Significance of the Study

The study will contribute to a significantly clearer comprehension of wettability characteristics of CO_2-brine-rock-clay mineral systems. The result will help to accurately characterise the wettability, which is the key physicochemical factor for controlling multiphase flow in porous media, especially the wettability of rock and minerals when in contact with CO_2 and brine. The new knowledge will considerably improve prediction of containment security and storage capacity, which will consequently affect the viability of extended CO_2 storage and support for industrial-scale CCS projects.

1.4 Methodology of the Study

As previously stated, wettability is often determined experimentally using contact angle evaluations conducted at reservoir conditions. In this study, the contact angle measurements were performed using the high temperature-high pressure goniometer unit with a tilted plate technique. The tested core samples were characterised using various techniques such as scanning electron microscopy-energy dispersive x-ray spectroscopy (SEM-EDX), atomic force microscope (AFM), total organic carbon (TOC) and organic carbon isotopic composition ($\delta^{13}C_{org}$) analyses, and quantitative

x-ray diffraction (XRD). The clay powder samples, including montmorillonite, illite, and kaolinite are mechanically compacted to create solid samples. Data obtained from zeta potential evaluations were used to investigate the relationship between the clay surface charge and the macroscopic contact angle.

1.5 Thesis organisation

There are seven chapters in this thesis as outlined below:

Chapter 1 - Provides the introduction of the thesis, a quick insight into the need for carbon capture and storage technology to mitigate CO_2 emissions and the factors that influence its process, and presents the primary objectives of the research.

Chapter 2 - Reviews the present literature about wettability characteristics of CO_2-brine-rock-clay mineral systems.

Chapter 3 - Apparatus and experimental procedure applied in the study is comprehensively described in this chapter.

Chapter 4 - Describes wettability of montmorillonite, illite and kaolinite for CO_2/brine, N_2/brine and N_2/oil (n-decane) fluid systems. This chapter has been published in the journal of Energy & Fuels.

Chapter 5 - Presents the correlation between gas densities and wettability on montmorillonite, illite and kaolinite. This chapter has been submitted to the journal of

Greenhouse Gases Science and Technology and the status now is under consideration after revision.

Chapter 6 - This chapter discusses the wettability of CO_2-brine-Harvey-1 sandstone, and it has been published in the International Journal of Greenhouse Gas Control.

Chapter 7 - Presents wettability characterisation of CO_2-brine-Berea and Bandera Gray. This chapter is currently under review in the journal of Colloid and Surfaces A: Physicochemical and Engineering Aspects.

Chapter 8 - A summary of the key findings and conclusions from the research. It also provides recommendations for further research outlooks.

Figure 1.2 - Shows layout of the thesis structure and objectives.

Note - Chapters 4 and 6 are the author's publications; Chapters 5 and 7 are papers that have been submitted to the journals for publication, which are reproduced as standalone chapters. Because of the standalone, structure some illustrations (figures, diagrams, equations) may appear in multiple places in the thesis. Appendix A includes the appropriate copyright permissions.

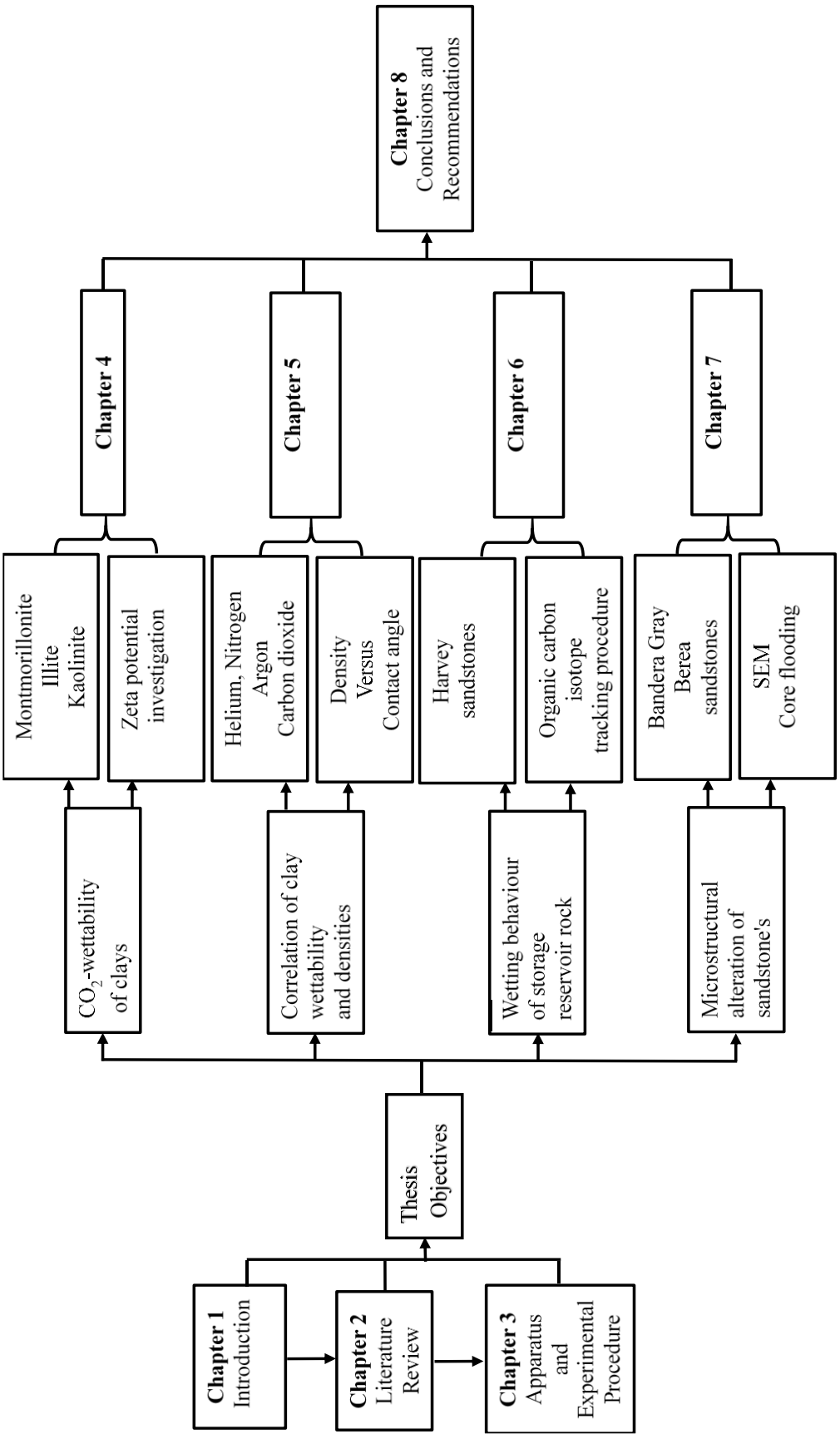

Figure 1. 2 Layout of the thesis structure and objectives

Chapter 2 Literature Review

2.1. Introduction

This chapter presents a detailed review of existing literature related to the wettability of carbon dioxide (CO_2)-brine-rock-clay minerals systems, and their important implications for CO_2 geological sequestration. The chapter firstly introduces carbon capture and storage (CCS), and illustrates trapping mechanisms. Wettability techniques and the effects on multiphase flow characteristics as they affect the transport of CO_2, fluid spreading and dynamic in the reservoir are thus presented. The chapter concludes with a brief overview of the knowledge gaps and allied challenges with the new studies on CO_2-brine-rock-clay minerals wettability.

2.2. Carbon capture and storage

CCS is viewed as a vital technology to mitigate the emissions of CO_2 to the atmosphere, from the use of non-renewable carbon-rich fossil fuel at the global level (IPCC, 2005). CCS is the process of capturing CO_2 from large sources of emission (i.e. industrial areas and power stations), transporting it to a storage site and permanently storing CO_2 into deep geological rock formations, as described in Figure 2.1 (IPCC, 2005; Lackner, 2003). In the CCS operating system, three main CO_2 capture options are proposed: 1) post-combustion capture, 2) pre-combustion capture, and 3) fuel combustion in oxygen (oxy-fuel) (Gibbins and Chalmers, 2008; Thomas and Benson, 2005; Cuéllar-Franca and Azapagic, 2015). 1) Post-combustion capture includes the separating of CO_2 from waste gas streams to produce a relative pure CO_2 stream. The methods for separating CO_2 involve utilising of chemical absorption, adsorption process, and high-pressure membrane filtration. 2) Pre-combustion capture

consists of converting the fuel to a mixture of carbon dioxide and hydrogen by gasification process. The next process is separation of CO_2 to produce a hydrogen fuel gas. 3) Oxy-fuel combustion is based on combustion process, such as combustion of fossil fuel plants, the iron and steel industry. The fuel is combusted with the recycled flue gas enriched with oxygen to yield more concentrated CO_2 for easier purification (Cuéllar-Franca and Azapagic, 2015; Vishal and Singh, 2016; Surampalli et al., 2014).

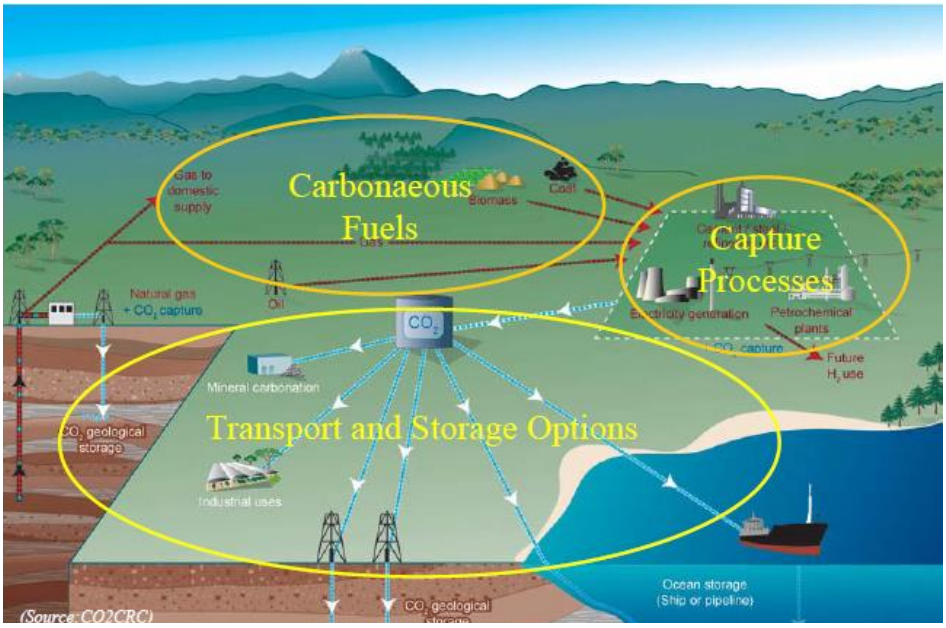

Source: adapted from IPCC (2005)

Figure 2. 1 Schematic diagram of CCS process

Three geological storage formations for the CO_2 storage that have obtained a broad consideration include 1) depleted oil and gas reservoirs, 2) deep saline aquifers and 3) coal seams (Figure 2.2) (IPCC, 2005). In saline aquifers as well as oil and gas reservoirs, CO_2 storage is typically placed at depths below 800 m, where the CO_2 becomes liquid or supercritical phase because of the ambient pressure and temperature condition. At such conditions, the density of CO_2 typically ranges from half to about 80% of the density of water, resulting in buoyant forces and CO_2 tending to move

upwards. Therefore, to limit the upwards flow of CO_2, due buoyancy, the cap rock over the specific storage reservoirs has to be an effective seal (IPCC, 2005). Moreover, coal seams are considered as another option for the underground storage, in which the CO_2 injection into coal seams will have advantages for both CO_2 storage and enhance methane recovery (IPCC, 2005; Bachu et al., 2007).

Table 2. 1 Approximate range of storage capacity for geological storage options

Geological Storage Options	**Approximate lower storage volume ($GtCO_2$)**	**Approximate upper storage volume ($GtCO_2$)**
Depleted oil and gas reservoir	675	900[a]
Deep saline aquifer	1,000	Possibly 10^4
Coal seams	3-15	200

Source: modified from IPCC (2005)

[a] Including undiscovered oil and gas fields would increase the volume by 25%

It is evident from Figure 2.2 that coal seams are at the shallower depth compared with a saline aquifer, which is located at the deepest state of the storage media. In contrast, the storage capacity in aquifers is estimated to be higher than other geological storage options. Table 2.1 shows the estimated storage capacity of the geological storage options. It is obvious, therefore, that the enormous quantities of CO_2 can be stored in geological formations, thus providing a better alternative to reduce CO_2 emissions in the atmosphere (Thomas and Benson, 2005).

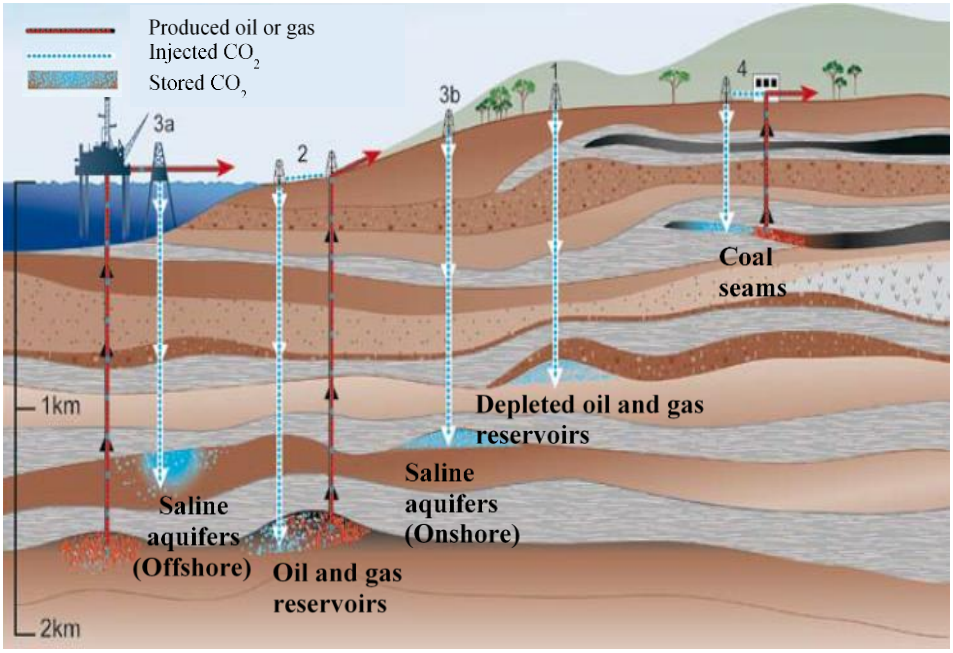

Source: modified from IPCC (2005)

Figure 2. 2 Geological storage options for CO_2 storage

A number of large-scale CO_2 storage projects currently are in operation worldwide. These have captured and stored millions of tonnes of CO_2 annually. Many more projects have been planned. Specifically, oil and gas companies have been operating geological CO_2 storage projects for a number of years. They have successfully demonstrated that securely storing a large quantity of CO_2 in deep underground is possible (IPCC, 2005; IPCC, 2014). A list of CO_2 storage projects (active and planned) around the world is presented in Table 2.2.

Table 2. 2 CO_2 storage projects

Geological storage projects	Established	CO_2 capture capacity (Mt/year)	Storage formation
Sleipner (Norway)*	1996	1	Natural gas field, offshore
Weyburn-Midale (Canada)*	2000	3	Enhanced Oil Recovery (EOR), oilfield, onshore
In Salah (Algeria)*	2004	3.8 Mt of CO_2 stored since 2004	Natural gas field, onshore
Cranfield (US)*	2008	1.5	EOR, oilfield, onshore
Snovhit (Norway)*	2008	0.7	Natural gas field, sandstone formation, offshore
GreenGen (China)**	2011	0.1 - First phase 2 - Planned in the third stage	Integrated Gasification Combined Cycle (IGCC), EOR (the third stage)
Quest (Canada)**	2015	Planned for up to 1.2 Mt/year	Deep saline aquifer
Gorgon (Australia)**	2016	3.4 to 4 - Expected	Saline aquifer, onshore

Sources: modified data from IPCC (2005), and CCSBrowser (2020)

*Active projects
**Planned projects

2.3. Carbon dioxide trapping mechanisms

CCS efficiency and containment security depend on several CO_2 storage mechanisms resulting from CO_2 injection into the storage reservoir formations. There are several physical and chemical trapping mechanisms, which control the CO_2 migration and distribution in the porous media, including structural, residual, solubility, mineral and

adsorbtion trappings. The details of outlined trapping mechanisms are discussed in the subsequent sections.

2.3.1 Structural trapping

Structural trapping is the primary mechanism for CO_2 storage during the first stages of a CCS project. In this process, the mechanism refers to the barrier presented by sealing caprock, which is a permeability barrier situated above the porous and permeable geological storage formation. This prevents undesirable CO_2 upward migration and CO_2 capillary leakage (Gershenzon et al., 2015; Hesse et al., 2008). CO_2 enters through the porous medium and accumulates on top of brine due to buoyancy forces and underneath the caprocks or seal (Bachu et al., 1994; Wollenweber et al., 2010). Caprocks are impermeable strata, typically mudrocks, clays, shales, and carbonates. These can be largely composed of halite, anhydrite, calcite, kaolinite, muscovite, and other minerals (Chiquet et al., 2007). The structural trapping process is relatively rapid.

Structural trapping is affected by the wettability of the rock-CO_2-brine system and CO_2-brine-interfacial tension as an important physicochemical factor. It is also governed by the height of CO_2 column immobilised below the low permeability caprock (Arif et al., 2017a; Broseta et al., 2012). This correlation can be described through a capillary force-buoyancy force balance, as shown in equation below (Dake, 1978), and can determine the structural trapping potential.

$$h = \frac{2\gamma cos\theta_r}{\Delta\rho g R} \qquad (2.1)$$

h, γ, θ_r refer to the height of CO_2 column permanently trapped by the caprock, the interfacial tension of CO_2-brine, and the receding contact angle of water, respectively. $\Delta\rho$ is the difference in densities between CO_2 and brine, g is the acceleration because of gravity, and R is the mean pore throat radius of the caprock. Practically, to prevent the capillary leakage occurring, the injection pressure of CO_2 must not exceed the breakthrough or threshold pressure of the caprock, which is the least pressure needed to mobilise brine in the seal layer (Chiquet et al., 2007).

2.3.2 Residual trapping

Residual trapping, or capillary trapping, is a mechanism that depends on hysteresis between drainage and imbibition capillary pressure and relative permeability curves. Capillary forces inhibits the buoyancy of CO_2 leading to its physical immobilization in the pore spaces (Rahman et al., 2016; Pentland et al., 2011a; Hesse et al., 2008; Juanes et al., 2006). This mechanism occurs rapidly, and it does not depend on the existence of an impermeable caprock. Following CO_2 injection into the formation, brine is firstly replaced by the injected CO_2. As the CO_2 movement continues, the displaced brine returns, disconnects and traps the residual CO_2 as isolated droplets at the preceding edge of the plume within the pore spaces. Figure 2.3 shows this residual trapping concept. At laboratory scale, the residual CO_2 saturation can be estimated by setting up the injection brine through a core of the reservoir placed in a high-pressure core holder, which represents the residual trapping potential (Saadatpoor et al., 2010; Qi et al., 2009; Kumar et al., 2004).

There are several factors that affect the residual trapping process, including rock wettability (Farokhpoor et al., 2013; Iglauer et al., 2015b), interfacial tension

(Chalbaud et al., 2009), geometry and pore throat size (Al-Menhali et al., 2015; Suekane et al., 2010). In addition, other factors such as injection rate, heterogeneity and the viscous ratio to gravity drive ratio essentially influence the last immobilised saturation. An increase in viscous ratio to gravity drive ratio and heterogeneity will improve the sweeping efficiency, and lead to increase in CO_2 trapping as remaining/residual gas (Bryant et al., 2008; Mo and Akervoll, 2005; Ide et al., 2007).

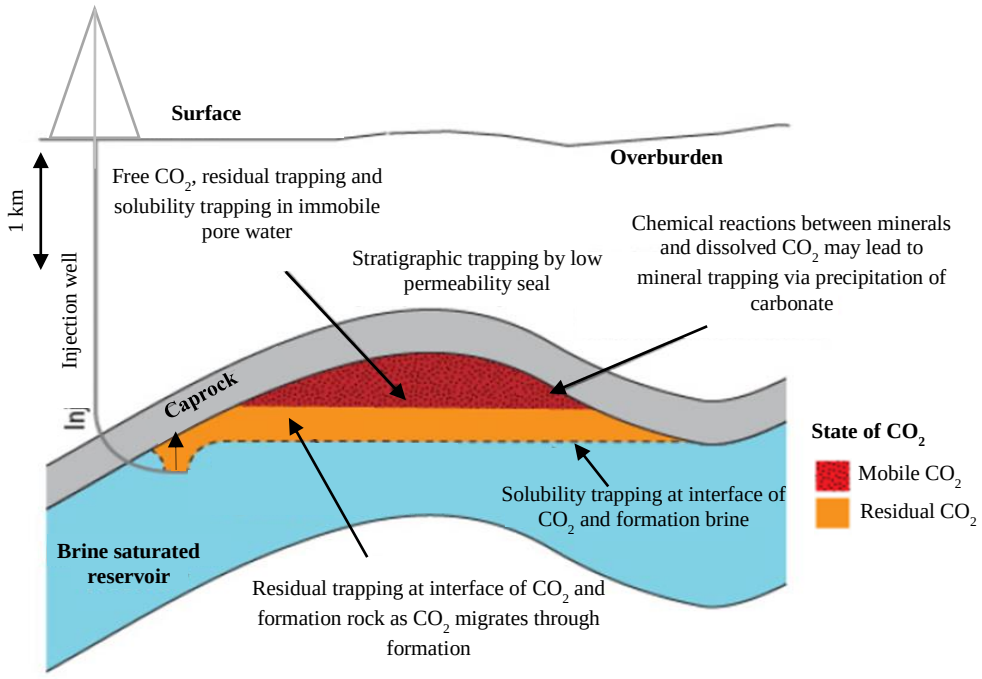

Source: adapted from Burnside and Naylor (2011)

Figure 2. 3 Trapping mechanisms at in-situ conditions

2.3.3 Solubility trapping

Solubility trapping is a geochemical storage process in which the injected CO_2 is dissolved in the formation brine. CO_2 then migrates downward in the reservoirs as the CO_2-saturated brine has higher density (Iglauer, 2011; IPCC, 2005). At the point where CO_2 interacts with the ambient formation brine, mass exchange occurs with CO_2

dissolving into the brine until an equilibrium condition is reached. Therefore, the CO_2 solubility is influenced by salinity, temperature and pressure of the formation brine (Zhang and Song, 2014; Riaz and Cinar, 2014). CO_2 dissolves in the formation brine by molecular diffusion, in which the brine is saturated with CO_2 and a concentration gradient of CO_2 is formed spatially. This is a slow process from mid to long-term scales, since the molecular diffusion coefficient is small. It will take thousands of years for CO_2 to be fully dissolved in brine formation, depending on the reservoir permeability, as shown in Figure 2.4 (Riaz et al., 2006; Ennis-King and Paterson, 2003).

2.3.4 Mineral trapping

Storing CO_2 in the geological storage formation can be implemented permanently through geochemical interactions between the dissolved CO_2 and rock minerals existing in the reservoirs (Flett et al., 2007; Xu et al., 2003). This mechanism is known as mineral trapping, which is essential for a long-term CO_2 entrapment in geological storage. In this mechanism, the injected CO_2 reacts with the formation brine to form weak carbonic acid and bicarbonate ions resulting in an increased acidity of the pore solution (Gunter et al., 1993; Pearce et al., 2015). The following is the reactions that occur in the mineral trapping mechanism (Bachu et al., 1994; Xu et al., 2001; Vishal and Singh, 2016).

Initially, the injected CO_2 dissolves in the formation brine to produce carbonic acid and bicarbonate ions:

$$CO_2 + H_2O \rightarrow H_2CO_3$$

$$H_2CO_3 = H^+ \rightarrow HCO_3^-$$

Therefore, as the acidity increased, the rock's primary minerals are dissolved leading to more complex dissolution of the cations and bicarbonate ions, which then react to precipitate carbonate minerals.

$$Ca^{2+} + HCO_3^- \rightarrow CaHCO_3^-$$

$$HCO_3^- + Ca^{2+} \rightarrow CaCO_3 + H^+$$

$$HCO_3^- + Mg^{2+} \rightarrow MgCO_3 + H^+$$

$$HCO_3^- + Fe^{2+} \rightarrow MgCO_3 + H^+$$

In the next reaction, the carbonic acid formed above can also attack the silicate minerals, as shown below:

$$2CO_2 + H_2O + CaSiO_3 \rightarrow Ca^{++} + 2HCO_3 + SiO_2$$

The mineral trapping mechanism takes place over a long geologic timescale in its process, and is thus classified as a very slow trapping mechanism (Gunter et al., 1993).

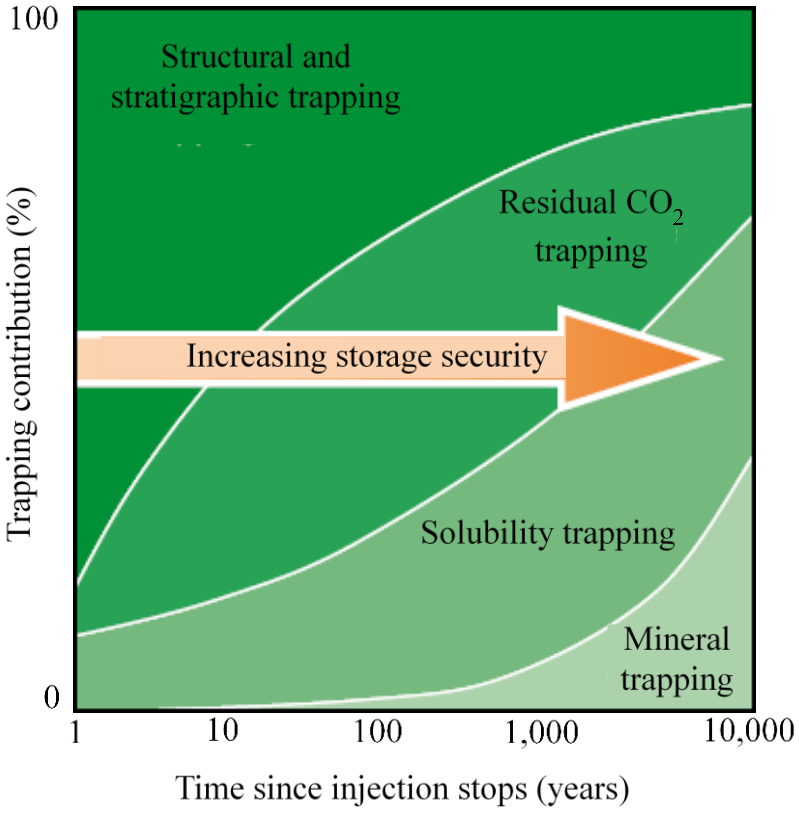

Source: modified from IPCC (2005)

Figure 2. 4 Mechanisms of CO_2 trapping over time

2.3.5 Adsorption trapping

The four trapping mechanisms described above generally apply for geological storage of CO_2 in conventional gas and oil reservoirs, such as sandstones and carbonates reservoirs. However, the adsorption trapping process dominantly applies to coal seams (Golding et al., 2011; Gray, 1987; White et al., 2005). CO_2 injection in coalbeds has the dual advantage of enhanced gas recovery and CO_2 storage, since the CO_2 adsorption capacity in coal can be nine times more than that of methane adsorption (Busch et al., 2004; Clarkson and Bustin, 2000). Adsorption capacity is associated with temperature (Bustin and Clarkson, 1998; Perera et al., 2011), pressure (Bae and Bhatia, 2006; Krooss et al., 2002), and rank of coal (Mastalerz et al., 2004; Siemons and Busch, 2007). In addition to coal seams, shales that are rich in organic matter are, too,

considered as a CO_2 storage formation through adsorption trapping (Busch et al., 2008; Li and Elsworth, 2015). Presently, this area is an emerging research ground (Eshkalak et al., 2014; Fernø et al., 2015).

2.4. Wettability

Wettability properties currently attract considerable interest due to their potential applications in industrial processes, for instance, in CCS, enhanced oil recovery, oil industry, marine, lubrication, spray quenching, liquid coating, manufacturing and materials. Wettability is "the preference of a solid to interact with a fluid in the presence of another fluid" (Craig, 1971). To measure the wettability in the system, a number of approaches have been developed, including qualitative and quantitative methods. The use of imbibition rates, capillary pressure curves, flotation, microscope examination, relative permeability curve, reservoir logs, displacement capillary pressure, nuclear magnetic resonance, dye adsorption, glass slide method permeability/saturation relationships, and capillarimetric constitute the qualitative methods. On the other hand, contact angles, imbibition and forced displacement Amott), and USBM are classified as quantitative methods. (Anderson, 1986a). Specifically, the rock-brine (fluid) wettability system can be projected qualitatively using the interpretation of the capillary pressure and relative permeability data (Bryant and Blunt, 1992; Parker et al., 1987).

Wettability method that involves the contact angle measurements is the most preferred and effective quantitative method to examine the wettability in pure liquids/fluids and proxy rocks/minerals. The main reason for this preference is that the contact angle measurement allows for sensitivity analysis of the temperature, pressure, surface

roughness, and salinity influence on wettability (Anderson, 1986b; Kaveh et al., 2014; Mittal, 2003; Giraldo et al., 2013; Lander et al., 1993). The contact angle shows the extent of wetting as a result of a solid-liquid interaction in a system. The contact angles with small angles (< 90°) indicate high wettability, while the contact angles with large angles (> 90°) show low wettability (Yuan and Lee, 2013; Zhao et al., 2010; Gharbi and Blunt, 2012).

In petroleum engineering, wettability is normally attributed to the measurement of a reservoir rock's affinity in the presence of rock-fluid-oil system, and is the main physicochemical factor, which controls fluid flow behaviour in porous media. In case of reservoir characterisation, rock wettability is attributed to the flow of fluids, within the pore column, over one another, the fluid distributions, and residual saturations (Iglauer et al., 2015b; Chaudhary et al., 2013; Pentland et al., 2011a). Specifically, in reservoir simulations, it is well recognised that the interfacial interactions, including wettability, interfacial tension, capillarity and relative permeability are inter-correlated and are the main input simulation parameters. Above all, wettability of rock surface and interfacial tension between two immiscible liquids, have been identified as the main factors controlling the irreducible saturation, the relative permeability and the capillary pressure (Anderson, 1986b; Morrow, 1990; Hirasaki, 1991). The relationship between the interfacial tension, wettability and capillary pressure can be characterised by the Young-Laplace equation (Laplace et al., 1829; Young, 1805):

$$P_c = P_{nw} - P_w = \frac{2\gamma_{aq,CO_2}\cos\theta}{R} \qquad (2.2)$$

P_w; P_c; P_{nw}; refer to pressure in wetting phase, capillary pressure and pressure in non-wetting phase, respectively. $\gamma_{aq,CO2}$ indicates interfacial tension between liquid phase and CO_2-rich phase. R is the pore constriction of radius, and θ is the contact angle. Depending on the wetting phase, the capillary pressure could be either positive or negative. This is related to the contact angles being either less or more than 90°. When CO_2 is immobilized within the rock pores, the capillary trapping occurs, and its process depends on the rock wettability, the interfacial tension with the brine (aqueous phase), the CO_2-rich phase, and the pore size distribution (Eq. 2.2) (Pentland et al., 2011b; Mills et al., 2011).

The contact angle techniques, the wetting frameworks and contact angle theories will be outlined in detail in subsequent sections, and, in later sections, the discussion will focus on the wettability of CO_2-rock-mineral-brine systems and its implications for CO_2 geological storage.

2.4.1 Technique of contact angle measurement

Various techniques for measuring contact angle have been widely developed and extensively used in many systems and industries. The techniques include sessile drop and tilting plate techniques, which are broadly used in the petroleum industry (Anderson, 1986a). In this study, the contact angle measurements were obtained by the sessile drop with a tilted plate technique. This technique enables to simultaneous measurements of the advancing and receding contact angles for the wettability evaluation (Lander et al., 1993). Other techniques of contact angle measurement are capillary penetration method for powders and granules, Wilhelmy balance method,

individual fibre, capillary rise at a vertical plate capillary tube, and capillary bridge method (Yuan and Lee, 2013).

2.4.2 Theoretical framework of wettability and contact angle

Thomas Young in 1805 (Young, 1805), who was the first person to recognise the correlation between the contact angle and the interfacial tension, defined the contact angle as the equilibrium of forces at the contact line between a liquid droplet and an ideal solid surface. The formation yields three surface tensions (i.e. solid-gas, solid-liquid, liquid-gas) when the liquid contacts a solid surface. At such condition, the wetting of fluid can be estimated accordingly (Yuan and Lee, 2013).

In case of wettability of CO_2/brine/mineral systems, brine and mineral come in contact with each other in the presence of CO_2 in reservoir formations. The three different interfacial forces act on the liquid droplet, as shown in figure 2.5. The three interfacial force fields are CO_2-brine interfacial tension (γ_{cw}), solid-CO_2 interfacial tension (γ_{sc}) and solid-water interfacial tension (γ_{sw}). In this case, solid indicates sandstones, carbonates, or proxy minerals such as quartz and calcite. Therefore, the macroscopic contact angle by Young's equation (Eq. 2.3) is determined by force equilibrium of the three interfacial tensions (Young, 1805):

$$cos\theta = \frac{\gamma_{sc} - \gamma_{sw}}{\gamma_{cw}} \qquad (2.3)$$

For a specified set of experimental conditions, the contact angles is determined through the denser liquid phase (water). The three phases forming the contact angle define a reservoir rock to be either water-wet, intermediate-wet, or oil/CO_2-wet. According to

the literature, the three phases of contact angles range from $0 \leq \theta < 75^{\circ}$, $75^{\circ} \leq \theta < 105^{\circ}$, and $105^{\circ} \leq \theta \leq 180^{\circ}$ for terms of water-wet, intermediate-wet, and oil-wet, respectively (Treiber and Owens, 1972). However, other literature has classified the ranges of contact angle from $0 \leq \theta < 90^{\circ}$, $\theta = 90^{\circ}$, and $90^{\circ} < \theta \leq 180^{\circ}$ for water-wet, intermediate-wet, and oil-wet, respectively (Dake, 1978). In addition to the above definitions, Iglauer et al. (2015b) have distinguished five typical wettability states with different ranges of contact angles. The states include strongly water-wet (<50°), weakly water-wet (50-70°), intermediate-wet (70-110°), weakly CO_2-wet (110-130°), and strongly CO_2-wet (130-180°). Table 2.4 summarises the wettability states for different contact angle ranges from different literature.

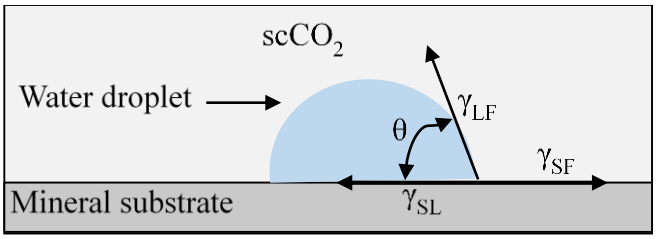

Source: adapted from Iglauer et al. (2015b)

Figure 2. 5 Force field acting on a three-phase CO_2-brine-mineral system

Table 2. 3 Wettability states based on contact angle ranges

Wettability state	**Contact angle (θ) (°) ranges**	**Literature**
Water-wet	$0 \leq \theta < 75^{\circ}$	Treiber and Owens (1972)
Intermediate-wet	$75^{\circ} \leq \theta < 105^{\circ}$	
Oil-wet	$105^{\circ} \leq \theta \leq 180^{\circ}$	
Water-wet	$0 \leq \theta < 90^{\circ}$	Dake (1978)
Intermediate-wet	$\theta = 90^{\circ}$	
Oil-wet	$90^{\circ} < \theta \leq 180^{\circ}$	
Complete wetting	0	Iglauer et al. (2015b)
Strongly water-wet	0-50	
Weakly water-wet	50-70	
Intermediate-wet	70-110	
Weakly CO_2-wet	110-130	
Strongly CO_2-wet	130-180	
Complete non-wetting	180	

Source: contact angle ranges from different literature (modified from Iglauer et al. (2015b))

Other theoretical frameworks of wettability include the Wenzel model, which emphases homogeneous surface wetting. The Wenzel model considers chemical homogeneity and rough surfaces. This indicates that the contact angle on solid rough surface is real and varies from an ideal surface. Note that no real surfaces are ideal, as

a result, the models were advanced to define the contact angle on the real surfaces. The Wenzel equation is, therefore, used to explain the influence of surface roughness on the contact angle (Wenzel, 1936):

$$cos\ \theta_{rough} = r\ cos\ \theta_{smooth} \qquad (2.4)$$

θ_{rough} and θ_{smooth} represent the Young's contact angle on the rough and ideal surface, respectively. r denotes the ratio of the actual and the projected solid surface roughness. For an ideal surface and rough surface, r is equal to 1 and greater than 1, respectively.

The Wenzel equation further indicates that a rough surface increases the relative contact of the fluid (water)-solid, which leads to increase in hydrophobicity, and thus increases in contact angle (Yang et al., 2010). As the surface roughness increases the surface wetting, therefore, the hydrophobic surfaces turn into more hydrophobic, while the hydrophilic surfaces turn into more hydrophilic (Seo et al., 2015; Chau et al., 2009).

Cassie-Baxter is another model that describes the contact angle on a real surface. This model was originally used to describe wetting character at porous surfaces, and rough hydrophobic surfaces. In addition, the Cassie-Baxter equation is used for prediction of contact angle trend change. It is also used for validation of the measured contact angle data, as shown in the equation below (Cassie and Baxter, 1944):

$$cos\ \theta_c = f_i\ cos\ \theta - (1 - f_i) \qquad (2.5)$$

Where θ_c, f_i, and θ denote the predicted Cassie-Baxter contact angle, the fractional projected area of materials and the smooth area contact angle, respectively. The contribution of CO_2 remaining under the droplet is denoted by $(1- f_i)$ (Milne and Amirfazli, 2012; Alnali et al., 2018).

The models proposed by Cassie and Wenzel have been extensively applied to investigate the real (heterogeneous and rough) surface characters. Hence, the real surface characters can be estimated or described by Wenzel's and Cassie's equations (Chau et al., 2009).

2.4.3 Advancing and receding contact angles

This research used the sessile drop tilted plate to measure the contact angles. This method allows measuring simultaneously the two different contact angles, in terms of advancing and receding, over the equilibrium of contact angle. The water advancing contact angle is significant to residual trapping capacity, and the receding contact angle is significant to structural trapping capacity. Right before the droplet commence movement, measurement of the advancing water contact angle (θ_a) is carried out at the leading edge of the droplet. On the other hand, measurement of the receding contact angle (θ_r) is conducted at the trailing end of the droplet (Yuan and Lee, 2013; Broseta et al., 2012). The advancing contact angle usually has a higher value than that the receding contact angle. This difference is caused by hysteresis of the contact angle. Figure 2.6 illustrates the schematic of the measurement of advancing and receding contact angles by application of a tilted plate technique.

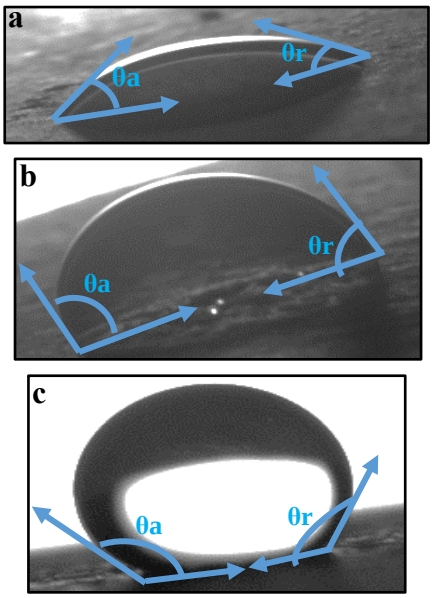

Figure 2. 6 The advancing and receding contact angles in three different phases

Note: (a) water-wet, (b) Intermediate-wet, and (c) oil-wet

2.4.4 Contact angle hysteresis

Young's equation (Eq. 2.3) applies to a specific fluid-solid system, where the angle is shaped between the fluid on a homogenous and an ideal surface. As mentioned in Section 2.4.3, the contact angle formed from expanding a fluid droplet is named as the advancing contact angle. Additionally, the contact angle shaped from the contracting gas bubble is termed as the receding contact angle. Surface roughness and heterogeneous surface wetting cause the difference between the advancing and the receding contact angles. This difference is referred as the contact angle hysteresis *(H)* (Kwok and Neumann, 1999):

$$H = \theta_a - \theta_r \quad (2.6)$$

Hysteresis usually ranges from 5 to 20, but higher values can be expected (Johnson Jr and Dettre, 1964). If the rough surface exists, then Young's equation for analysing the contact angle is not applicable. The contact angles on rough surfaces are generally higher than those on homogenous surfaces (Grundke et al., 1996). Therefore, the interpretation of contact angles defined by Eq. 2.3 results in inaccurate outcomes, because the contact angles would certainly represent the surface topography, instead of reflecting the surface energy. For this reason, the Wenzel's and Cassie-Baxter's methods are applied in the analysis of the equilibrium contact angles on heterogeneous and rough surfaces, as explained under heading 2.4.2.

2.5. Wettability of CO_2-storage rock minerals

Wettability of CO_2-rock minerals system has a main impact on the CO_2 sequestration management in subsurface geological formations. Wettability directly affects containment security, injectivity, structural and residual trapping capacities, and indirectly mineral and dissolution trapping capacities. There is also a different effect on wettability for different minerals (Iglauer et al., 2015b). Therefore, having a full understanding of the wetting properties in geological carbon storage sites and its effect on multiphase porous flow is essential for storage capacity and risk assessments. Wettability characteristics of different minerals will be discussed in detail in subsequent sections.

2.5.1 Clay

2.5.1.1 Clay characteristics and properties

Generally, the term clay refers to naturally occuring, earthy, fine-grained fractions of materials, and develop into a plastic state when mixed with a small amount of water

(Grim, 1953). According to the Joint Nomenclature Committees (JNCs), clay is described as "a naturally occurring material composed primarily of fine-grained minerals, which is generally plastic at appropriate water contents and will harden when dried or fired" (Guggenheim and Martin, 1995), Figure 2.7 shows the physical phase alteration of clay.

"Naturally occurring" conditions of clays imply that synthetic clays and clay-like materials are not considered as clay. Plasticity refers to the moistened material property, which can be moulded to any shape. Clays are mainly inorganic materials, which include large quantities of organics materials. Based on chemical analyses, clays primarily consist of silica, alumina, water, and considerable quantities of iron, alkalies, and alkaline earths. The term of "fine-grained' basically cannot be applied, in general, because there is no universally upper limit size for the clay particles, which is defined differently by different disciplines and professions. For examples, the clay particle size used in geology and sedimentology is less than 4 μm, in soil science is less than 2 μm, while in colloid science is less than 1 μm (Guggenheim and Martin, 1995; Grim, 1953; Bergaya and Lagaly, 2013).

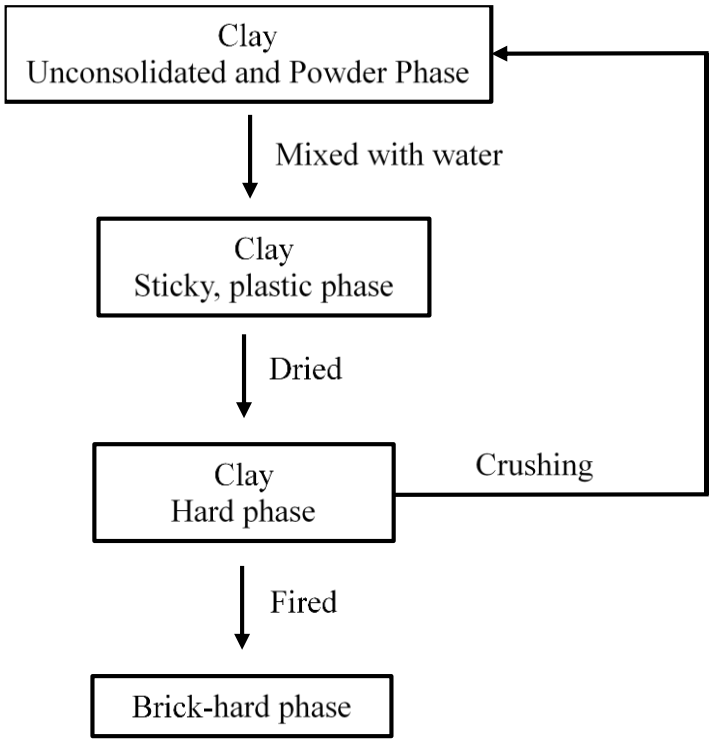

Source: modified from Mukherjee (2013)

Figure 2. 7 The physical phase alteration of clay

The term ‘clay minerals’ refers to minerals that produce the plasticity property, which are known as phyllosilicates and made up from fine-grained segments of sediments, rocks, and soils (Bergaya and Lagaly, 2013). The JNCs defined the clay minerals as “phyllosilicate and non-phyllosilicate minerals impart plasticity to a clay and hardens upon drying or firing” (Guggenheim and Martin, 1995). From the definition above, clay minerals may include natural and synthetic, phyllosilicates and non-phyllosilicate materials, and may not have size particle criteria. Clay minerals can be categorised by particular properties, in terms of the layered structures, the anisotropy layers, and various surfaces including external basal, edge surfaces and interlayer surfaces. The other category is that the surface can be changed by either adsorption, ion exchange or grafting process. Other properties of clay minerals are large surface area, large degree of layer assembling, colloidal size particles, modest layer charge, high capacity of

cation exchange, and low capacity of anion exchange with slightly depends on pH variable (Bergaya and Lagaly, 2013).

Other authors used the term of clay material for any fine-grained fractions, earthy, natural, and argillaceous materials. Various factors control the clay material properties and need to be understood in order to fully classify clay materials. These factors include (Grim, 1953):

1. Clay mineral composition

   This is related to the characteristic and abundance of the clay mineral constituents.

2. Non-clay mineral composition

   This defines the characteristic and abundance of the non-clay minerals as well as particle size distributions.

3. Organic materials

   This describes the type and the number of organic materials that are contained in the clay minerals.

4. Interchangeable ions and solvable brines

   This is related to the solvable brine contained in clay materials, which is trapped in the clay with the natural process i.e. weathering or alteration process.

5. Texture

   This explains the particle size distribution, the particle shape, the particle alignment in a porous space, and the particle force.

Clays and clay rock/minerals are the foremost common material in sedimentary deposits within the Earth's crust. They account for nearly half of the mass of lithospheric sediments. They have a volume of 270 million cubic kilometres (km^3) in

the crust. 85% of the total carbonaceous organic matter is related to clay, including argillaceous cement in sedimentary rocks and carbonate rocks (Laszlo, 1987; Vassoyevich et al., 1976). In geoengineering, clay materials are vital components of many minerals in the reservoir and cap rocks, including quartz, carbonate, hematite and pyrite (Iglauer et al., 2015b; Guidotti, 1984). Clays and clay minerals not only play the significant role within the genesis of petroleum hydrocarbons, but also in their concentration. Therefore, it is important to study the post-sedimentation alteration of clay deposits as new sedimentary materials cover them. The composition and structure of clay sediments, their physical and mechanical properties also change during the rock formation process (lithogenesis), and clays are progressively transformed into clay rock and shale, and then into argillite and schist (Vassoyevich et al., 1976; Osipov et al., 2003).

Moreover, geo-technology industry, agriculture, building constructions, and other industries widely use clays and clay minerals. The clay minerals applications in different sectors are closely associated with their composition and structures (Murray, 1991). The composition and structure of clays will be outlined comprehensively in subsequent sections.

2.5.1.2 Clay constituent and structure

The mineral constituents of clay could be divided into two types (Mukherjee, 2013):

1. Clay minerals, forming plasticity when they are mixed with water and harden when they are dried or fired, such as kaolinite, illite, montmorillonite, etc.
2. Associated minerals that do not give plasticity to clays, include silicate minerals, such as micas, quartz, and feldspars; iron oxides and hydroxides, such as

magnetite, hematite, etc; and aluminium oxides and hydroxides, such as corundum, boehmite, etc.

In addition to those, clays generally consist of certain amorphous materials and/or organic materials. These non-mineral constituents are referred to *associated phases* (Mukherjee, 2013). The diagram of clay constituents is illustrated in Figure 2.8.

As mentioned above, clay minerals may consist of natural or artificial, phyllosilicates or non-phyllosilicates. Tetrahedral (T) and an octahedral (O) sheet, which may consolidate in either a 1:1 or 2:1 proportion to make an anisotropic TO or TOT layer, support all the structures of phyllosilicates. The 1:1 layer structure includes the recurrence of one (1) tetrahedral and one (1) octahedral sheet. The 2:1 layer structure consists of one octahedral sheet that is inserted in between two tetrahedral sheet. The layered double hydroxides (LDH) have an octahedral sheet (O) base. The layers could be negatively charged, either positively charged, or uncharged. As an alternative concept, an assembly of layers refers to a particle, and an assembly of particles refers to an aggregate. Based on this concept, the arrangement of particles and aggregates can be differentiated into interlayer, interparticle, and interaggregate pores. This arrangement results in clay minerals having the different morphologies, such as plates, laths, tubules and fibres. Ultimately, all phyllosilicates thus have porous properties with different size and shape (Bergaya and Lagaly, 2013). Figure 2.9 shows the diagram of the clay mineral layer, particle, aggregate, and assembly of aggregates.

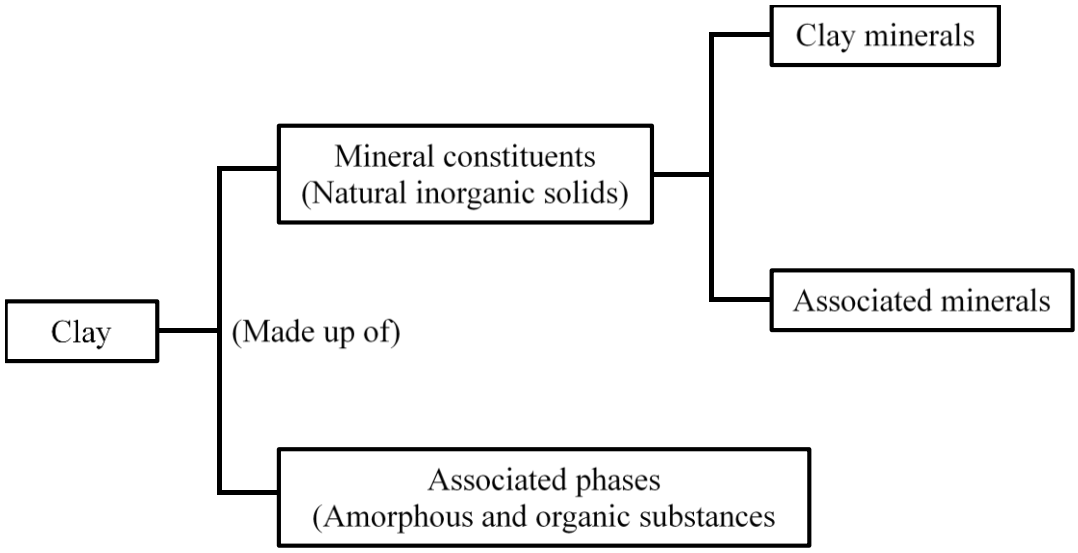

Source: modified from Mukherjee (2013)

Figure 2. 8 The diagram of clay constituents

The atomic structures of layered clay minerals consist of silica (Si) tetrahedra, and aluminium (Al) or magnesium (Mg) octahedra, Figure 2.10. Two basic units are engaged with the atomic grids of the clay minerals. One unit comprises two sheets of oxygen atoms or hydroxyls, in which magnesium aluminium, or iron atoms are set in octahedral direction and have an equal distance from six oxygen atoms or hydroxyls. The second unit is made of silica tetrahedrons. To each tetrahedron, a silica atom is located at the centre and surrounded by four oxygen atoms, or hydroxyls. The silica tetrahedral groups are also coordinated to shape a hexagonal structure (Mukherjee, 2013; Grim, 1953)

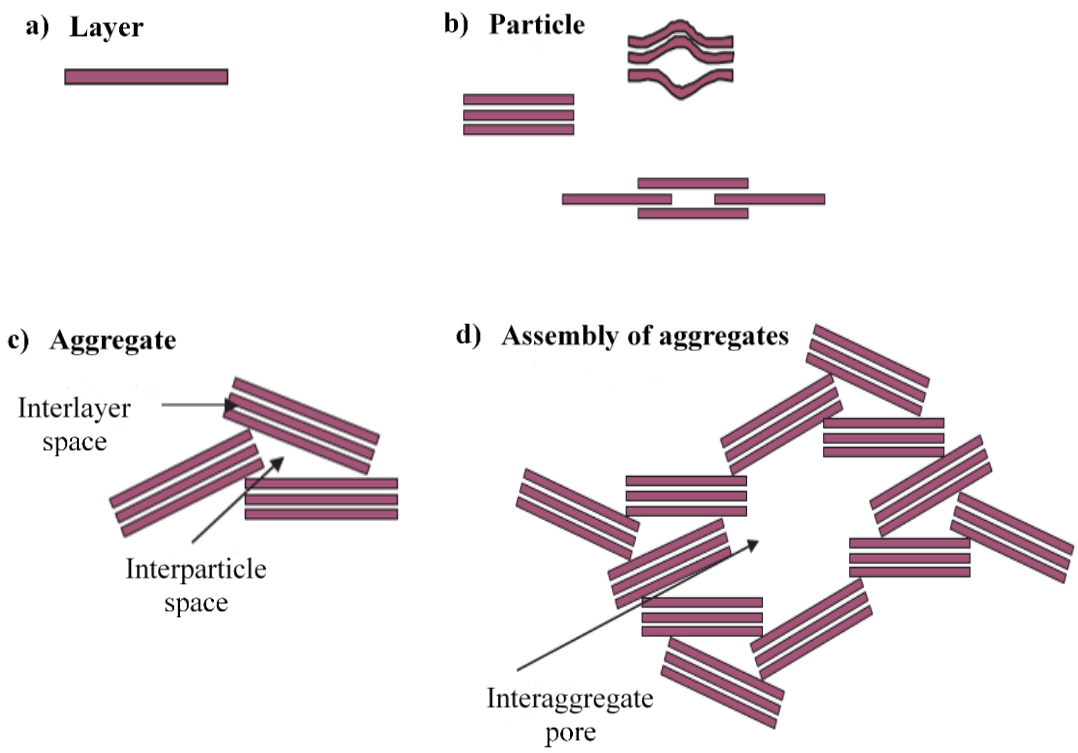

Source: modified from Bergaya and Lagaly (2013)

Figure 2. 9 The schematic of clay layers

Note: clay layers include (a) the layer of clay mineral; (b) the particle, made-up of loaded layers that can provide a lenticular pore; (c) the aggregate; (d) the assembly of aggregates with enfolding the interaggregate pore.

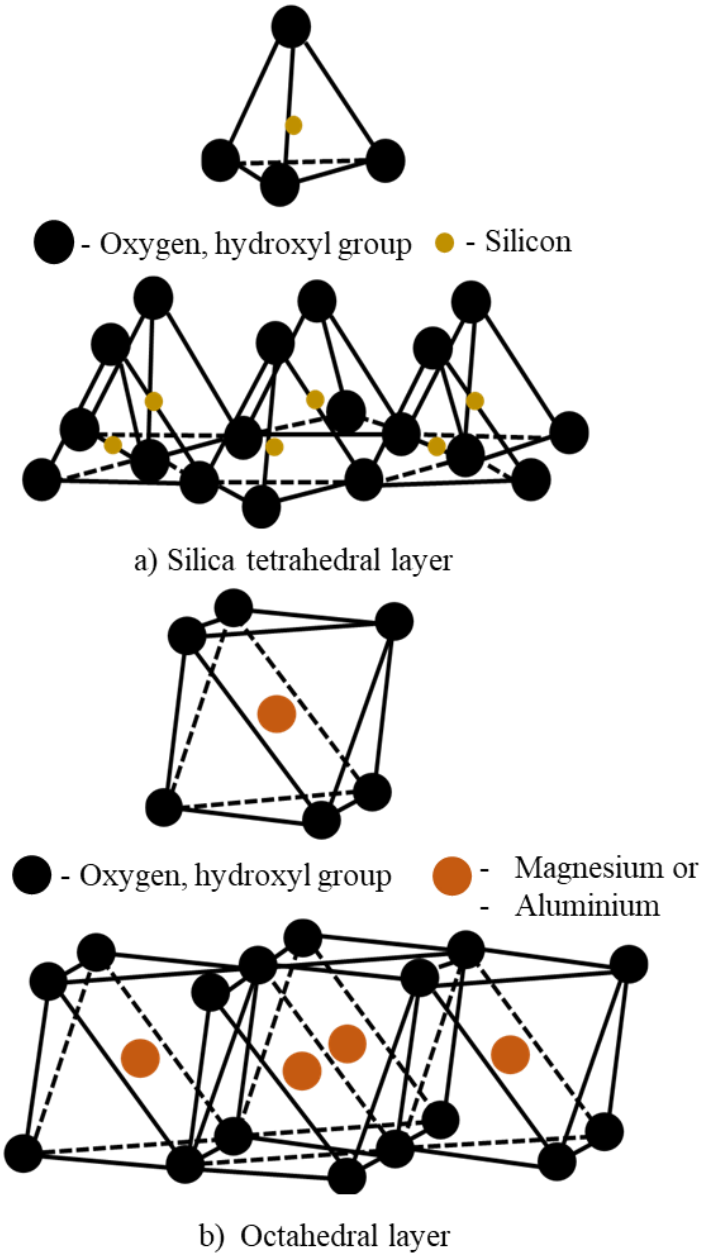

Source: modified from Pan et al. (2020b)

Figure 2. 10 The atomic structures of layered clay minerals

In short, structurally, three basal oxygen atoms contributed from silicon atom make the structure of a sheet. The fourth oxygen atom, which is perpendicular to the present sheet structure, forms a part of the closest and parallel the magnesium/aluminium-octahedral sheet. The aluminium atom, which is composed of two oxygen atoms from

tetrahedral sheet shares four hydroxyl groups (-OH) with adjoining aluminium atoms. Every octahedral sheet is hooked up along with the aid of shared octahedral edges (Zhang et al., 2016b). However, there is no literature reported obviously on how magnesium-octahedron is formed (Pan et al., 2020b).

2.5.1.3 Clay wettability

Clay wettability performs a key function in numerous characteristic phenomena, particularly when the surface of mineral interrelate with reservoir liquid. Some of the clay wettability applications are applied in the process of CCS (Kaveh et al., 2016; Espinoza and Santamarina, 2012; Umar et al., 2019), oil movement and accumulation in certain (i.e. shale) reservoirs (Xi et al., 2019), process industries, geology, agriculture (Murray, 1999), CO_2-EOR (Lashgari et al., 2019), and fracturing fluid loss (Ge et al., 2015). The clays' applications are closely associated with their structure and composition. The wettability of three different clays is studied in detail in the following section, with providing experimental evaluations and simulations of dynamics of molecules.

1. Kaolinite

Kaolinite, with the chemical formula $Al_2Si_2O_5$ (OH_4), is classified as a two-layer clay mineral (1:1 layer), with a silica tetrahedral sheet joint through octagonal oxygen and hydroxyl, and shared with a sheet of alumina octahedral layer (Murray, 1999). Kaolinite is mainly formed by weathering process, which is transformed from the chemical weathering reaction called hydrolysis, as shown in reaction below (Mukherjee, 2013):

$$2\,KAlSi_3O_8 + 3\,H_2O \rightarrow Al_2Si_2O_5\,(OH)_4 + 4\,SiO_2 + 2\,KOH$$

Theoretically, kaolinite has a chemical composition of 46.3% silica, 39.8% alumina and 13.9% water, a fine particle size, a low surface area, a neutral surface, and a well-recognised crystal structure (Murray, 1991). However, those crystal structures generally occur as fine particles or micron-sized particles. This phenomenon is difficult to signify their wettability through direct contact angle measurements (Yin et al., 2012). Various experimental techniques have been done to overcome this problem, especially to analyse kaolinite wettability, including spontaneous imbibition and liquid-liquid extraction (Luo et al., 2019), clay film (Pan et al., 2019a; Pan et al., 2020a), floatation tests (Hu et al., 2003), nuclear magnetic resonance (NMR) (Lipsicas et al., 1985), atomic force microscopy (AFM) (Yin and Miller, 2012), and cryo-scanning electron microscopy (SEM) (Durand and Rosenberg, 1998).

Experimental results for kaolinite wettability show that kaolinite was obviously strongly water-wet to weakly water-wet, and contact angles increased with increasing in pressure (Pan et al., 2019a; Pan et al., 2020a; Fauziah et al., 2019b). However, another study states that contact angle was unresponsive to pressure (Wang et al., 2012b). Molecular dynamic simulations show that octahedral surfaces ranged from completely water-wet to weakly water-wet, with independent of pressure, temperature, brine, and force field. Meanwhile, tetrahedral surfaces were mostly intermediate-wet and strongly oil/CO_2-wet. Molecular dynamic simulations also show that the temperature (Tian et al., 2018), pH (Tian et al., 2018), and external electrical fields (Liao et al., 2019) have an effect on molecular adsorption onto the surface of kaolinite.

2. Montmorillonite

Montmorillonite is a 2:1 layered clay mineral with two silica tetrahedral layers joined to a central octahedral layer, with a chemical formula of $(Na, Ca)_{0.33}(Al\ Mg)_2(Si_4O_{10})(OH)_2 \cdot nH_2O$ (Murray, 1999; Bergaya and Lagaly, 2013). The weathering process of basic igneous rocks and the sedimentary products that are derived from the rocks forms montmorillonite (Mukherjee, 2013). Isomorphous substitutions in clay minerals result in the charge of development, and occur in those layers, such as Al^{3+} replaced by Mg^{2+}, Fe^{2+}, and Fe^{3+} in octahedral layer, and Al^{3+} substituted by Si^{4+} in tetrahedral layer. Hence, the surfaces of these layers have negative charges that will attract the cation exchange (generally Ca^{2+}, Mg^{2+}, Na^{+}, and K^{+} in brine solution). These cations have a tendency to be hydrated which results in increase in the space among the stacked layers. Consequently, this causes clay swelling (Uddin, 2008; Pan et al., 2020b; Zhang et al., 2017).

Experimental investigations on montmorillonite wettability show that montmorillonite was more water-wet to intermediate-wet, which was mostly influenced by thermo-physical environments (Shang et al., 2010; Pan et al., 2019a; Pan et al., 2020a; Fauziah et al., 2019b; Borysenko et al., 2009; Ballah et al., 2016). This is in line with the molecular dynamic simulations, which show that montmorillonite is more water-wet to intermediate-wet. This result depends on its specific microscopic layer, which include exchangeable cation, surface charge, and ion adsorption (Yi et al., 2018; Zhang et al., 2016a; Underwood et al., 2015).

3. Illite

Illite is a type of dioctahedral 2:1 phyllosilicate with variable degrees of lattice replacement (mainly Si^{4+} is replaced by Al^{3+} in the tetrahedral layer) with chemical formula $(K,H_3O)(Al,Mg,Fe)_2(Si,Al)_4O_{10}[(OH)_2 \cdot (H_2O)]$. In this case, cations have a tendency to be involved in the surface of illite in order to recompense the negative surface charges (Zheng and Zaoui, 2017).

Experimental results for illite wettability reveal that illite was strongly water-wet to weakly water wet (range of $10° < \theta < 60°$) (Shang et al., 2010; Hu et al., 2003; Fauziah et al., 2019b; Wang et al., 2012b; Botto et al., 2017). This was consistent with molecular dynamics simulations, where illite is strongly water-wet to intermediate-wet with contact angles range from 30° to 78° (Mohammed and Gadikota, 2020). In addition, the contact angles increased with elevated pressure and decreased with elevated temperature (Fauziah et al., 2019b). .

2.5.2 Sandstones wettability

Sandstones reservoirs can have varying amounts of clay laminae or subordinate thin shale beds and lenses, which have an effect on the inner movement of CO_2 injection. Sandstone and carbonate formations comprise the main underground storage reservoirs for CCS and EOR applications. Several geological CO_2 storage projects have been implemented in sandstone lithology. These include the Sleipner project, Norway; the Minami-Nagoaka project, Japan; the In-Salah project, Algeria; and the Gorgon project, Australia (IPCC, 2005). Clean and pure quartz as well as the composite rock surfaces are normally used for contact angle measurements as

substitution minerals for sandstone (Kaveh et al., 2014). However, assessing the wettability characteristics for both natural and proxy minerals is essential.

Measuring contact angles of natural cores at in-situ conditions is currently an intricate procedure. Thus, published data of contact angle measurements on sandstone at reservoir conditions are scarce. These limitation on data are due to complexity of contact angle measurements on natural complex rocks, including pore morphology, heterogeneity of pore system, and drop penetration within the rock samples (Kaveh et al., 2014). Kaveh et al. (2014) further conducted contact angle measurements on the Bentheimer sandstone in CO_2-deionised water system at high pressures and a constant temperature of 318 K by application of the captive bubble technique. Obtained results indicate that contact angles increased minimally with pressure. In addition, the Bentheimer sandstone stayed strongly water-wet during the experimental study (Kaveh et al., 2014).

Other researchers have investigated the wetting behaviour of the Mount Simon sandstone. They report that the wettability of CO_2-sandstone has insignificant effect on pressure, such as the contact angles slightly decreased from 35^o to 34° when the pressure was raised from 20 MPa to 25 MPa at 40 °C, in high concentrate brine of 5.12 M NaCl. This also implies that the wettability of CO_2-brine-sandstone system is strongly water-wet at high brine salinity environment (Botto et al., 2017). Meanwhile, Tudek et al. (2017) investigated the effect of surface roughness on the wettability of CO_2-brine-Mount Simon sandstone through the sessile drop method. The results indicate that the contact angles increased with the surface roughness increasing. Other studies showed a decrease in contact angles with the increase in surface roughness on

various surfaces such as quartz (Al-Yaseri et al., 2016; Wang et al., 2013) and calcite (Arif et al., 2017c) and thus suggested that the wettability is more water-wet on the rougher surfaces (Iglauer et al., 2015b). However, the report proposes that the wetting phase of the Mount Simon sandstone is generally strongly water-wet (Tudek et al., 2017).

The others have measured the wettability of CO_2-brine in the South West Hub sandstone (GSWA Harvey-1) at different pressures (from 0.1 MPa to 20 MPa) and at 334 K, using the sessile drop with a tilted plate technique (Fauziah et al., 2020). The study shows that increased pressure results in higher contact angles measurements. Results also suggest that the system is weakly water-wet to intermediate-wet. Likewise, Alnali et al. (2018) examined the CO_2-brine-Warro sandstone wettability (the sample taken from Warro-1 well, Perth Basin, Western Australia) using the sessile drop method. The result is consistent with Fauziah et al. (2020), where contact angles increased with pressure, and the wettability ranges in the weakly water-wet to intermediate-wet region.

In summary, the wettability of CO_2-Mount Simon sandstones investigated by Kaveh et al. (2014), Botto et al. (2017), and Tudek et al. (2017) measured through sessile drop or captive bubble methods, is strongly water-wet. Whereas, the South West Hub sandstone wettability (Fauziah et al., 2020) and CO_2-brine-Warro sandstone (Alnali et al., 2018) is weakly water-wet to intermediate-wet. The variation on the results obtained are probably due to various factors, including mineralogy of the sandstones, surface roughness, and method of cleaning surface of the sandstones. In addition to these factors, the mineralogy of the sandstones are quite diverse, and analysis of

wettability shows that the contact angle measurement is very sensitive to the presence of amount of organic matter. This can cause, for instance, the surface charge to be changed (Al-Yaseri et al., 2016; Kaveh et al., 2014; Fauziah et al., 2020), and thus affect the wettability (Arif et al., 2019; Iglauer et al., 2015b).

2.5.3 Quartz wettability

Quartz represents the major part of mineral constituents in cap rock sediments (Kaveh et al., 2016; Iglauer et al., 2015a) and reservoir rocks (Al-Yaseri et al., 2016). Therefore, understanding the wettability of CO_2-quartz characteristics is essential. In this context, some studies have been conducted to measure the wettability of quartz by contact angle method. Some studies evaluated the contact angle of CO_2-brine on quartz substrate as a function of pressure. These evaluations suggest that there is a substantial inconsistency in the reported results. For example, Espinoza and Santamarina (2010) described that the effect of pressure has an insignificant impact on the wettability of quartz, i.e. the contact angles slightly decreased with an increase in pressure. These results are in line with other studies, conducted by Farokhpoor et al. (2013), Mutailipu et al. (2019) and Bikkina (2011). In general, these studies reveal that the wettability of quartz together with CO_2 is strongly water-wet. However, there is a slightly different result from Bikkina (2011). The wettability of quartz surface shifted into weakly water-wet when the second cycle of CO_2 injection was conducted. This wettability variation is due to the dissolution of CO_2 between quartz and brine.

Conversely, works of other researchers on contact angle measurements using the captive bubble method show that an increase in pressure results in an increase in contact angle values (Chiquet et al., 2007; Broseta et al., 2012; Saraji et al., 2013).

These results are consistent with Iglauer et al. (2014a), and Al-Yaseri et al. (2016), who measured the contact angle with sessile drop method. The trend is also in line with Botto et al. (2017), where the captive drop method was used to measure the contact angles.

Other scholars have also investigated the effect of temperature on quartz surfaces through contact angle measurements. The results indicate that the contact angle increased with temperature (Farokhpoor et al., 2013; Al-Yaseri et al., 2016; Liu et al., 2015). However, other researchers suggest that the temperature has insignificant effect on the contact angle measurements (Bikkina, 2011; Mutailipu et al., 2019). Likewise, Saraji et al. (2014) have reported that there was a slight decrease in contact angles with elevated temperature. In summary, the reported data indicate that the variety of measurement methods have no effect on the contact angle values obtained, i.e. captive bubble or sessile drop or captive drop. Moreover, the results generally propose that the wettability of quartz is strongly water-wet.

2.5.4 Carbonate wettability

Carbonate aquifers and hydrocarbon reservoirs consist of substantial amounts of calcite and dolomite as in limestones and dolostones and can include small amounts of carbonate minerals including azurite and malachite (Burchette, 2012; Moore and Wade, 2013; Ahr, 2011). Carbonate reservoirs or rocks (dolomites and limestones) contribute about 50% of global oil and gas production. Their petrological structures can have multiple porosity systems and typically relate to heterogeneity of petro-physical characteristics (Mazzullo, 2004). Together with sandstones, carbonate rocks are important lithologies, for CO_2 storage formations (Arif et al., 2017c).

Little has been published on the contact angle measurement of CO_2-brine-carbonate systems but the data results' variability is high. Some studies have been conducted to measure the carbonate wettability through contact angle measurements and researchers have observed several inconsistencies. For example, the advancing and receding contact angle increased with increasing pressure on dolomite surfaces (Mutailipu et al., 2019; Yang et al., 2008). Works by other scholars show small effect of pressure on carbonate-rich Rousse caprock surfaces (Siddiqui et al., 2018; Tonnet et al., 2010).

The influence of temperature on the wettability of CO_2-brine-carbonate has also been investigated. Discrepancies are evident amongst the results of contact angle evaluations. For example, the water contact angles were both seen to increase (Al-Yaseri et al., 2017b), and decrease with temperature (Yang et al., 2008; Tonnet et al., 2010). Such difference can be related to particular factors, including mineral compositions i.e. the sample mainly consisted of magnesium (Al-Yaseri et al., 2017b), while the other samples mostly contained calcium (Yang et al., 2008; Tonnet et al., 2010).

From the above studies, there are differing datasets of the carbonate-CO_2 wettability. Al-Yaseri et al. (2017b) proposed that the wettability of carbonate (dolomite) is weakly water-wet to intermediate-wet, while Yang et al. (2008) indicated that the wettability is weakly CO_2-wet. In addition, Tonnet et al. (2010) and Mutailipu et al. (2019) suggested that the wettability of carbonate (limestone) is strongly water-wet to intermediate-wet.

2.5.5 Calcite wettability

Several studies have been conducted to measure calcite wettability through contact angle measurements. Espinoza and Santamarina (2010) observed the effect of pressure and salinity on CO_2-brine-calcite contact angles. The authors found that the advancing and receding contact angles of calcite in CO_2-brine system reduced very slightly with increase in pressure. However, with CO_2-deionised water, the reduction in contact angles of calcite was more pronounced as pressure increased. The result is consistent with Bikkina (2011), and Farokhpoor et al. (2013). From the above measurements, it was observed that the strong water-wet nature of calcite generally remained the same at low and high pressures. This was also in line with the findings of Mills et al. (2011) and Wang et al. (2012b).

Investigation of the dependency on pressure for the wettability of CO_2-deionised water-calcite system has been conducted by other scholars (Arif et al., 2017c). The results revealed a strong positive relationship between the contact angle and pressure. This was in agreement with the earlier findings by Broseta et al. (2012). These authors also observed that the contact angle on calcite exhibited an obvious increase with increasing pressure. The findings suggest that there is a slight shift in calcite wettability from strong water-wet, at low pressure to intermediate-wet, at high pressure.

Arif et al. (2017c) studied the effect of temperature on CO_2-brine-calcite surface, and found that advancing and receding contact angles decreased as temperature increased. The results implied that the calcite wettability becomes weak to strong water-wet as the temperature increased, which was also consistent with other studies involving

Weyburn limestone surface (Yang et al., 2008), and calcite-rich Rousse caprock surface (Broseta et al., 2012).

2.6. Factors affecting wettability

Various factors that affect the wettability of CO_2-brine-rocks, including pressure, temperature, surface roughness, brine composition, organic content, and clay type have been investigated. The mineralogy of the rock surface has also some effects on wettability change and fluid equilibration. Other researchers upon further investigation have indicated that a procedure of surface cleaning needs to be applied during contact angle measurements in order to help preclude biased results (Iglauer et al., 2015b). Having a full understanding of those factors, therefore, is essential to characterise the wettability alterations in specific CO_2-brine-rocks systems. These factors are discussed in detail below.

2.6.1 Pressure

Pressure is an important parameter that affects contact angles positively, i.e. an increase in pressure would cause an increase in CO_2-wettability (Iglauer, 2017; Broseta et al., 2012; Farokhpoor et al., 2013; Kaveh et al., 2012). This behaviour is related to the increasing density of CO_2 gas, which improves the intermolecular interactions between the mineral and CO_2, and leading to de-wetting of the surface (Iglauer et al., 2015a; Al-Yaseri et al., 2016; Iglauer et al., 2012). However, contrasting views about the effect of pressure on contact angle have been reported by other researchers, most of which posited that the relationship between pressure and contact angle is not necessarily positive (Guiltinan et al., 2017; Bikkina, 2011; Espinoza and Santamarina, 2010). Therefore, it is evident that a significant discrepancy exists in the literature

about the true effect of pressure on contact angle. Some researchers have attributed such this discrepancy to factors such as contamination, surface roughness, or chemical heterogeneity of the substrate (Iglauer et al., 2015b; Butt et al., 2006).

2.6.2 Temperature

Most CO_2-wettability studies involving clean quartz, calcite (Bikkina, 2011; Saraji et al., 2013), or water-wet mica (Arif et al., 2016a; Broseta et al., 2012; Wan et al., 2014), typically showed negative relationships between contact angles and temperature. Like pressure, some contrasting views have also been found in the literature about the effect of temperature on contact angles. For example, Roshan et al. (2016a) found a positive relationship between contact angle and temperature for shale rocks. Similar relationships have also been found for feldspar (Farokhpoor et al., 2013), and quartz (Sarmadivaleh et al., 2015; Al-Yaseri et al., 2016). The relationship between temperature and contact angle can be related to fluid density and van der Waals forces, both of which contribute to the molecular interactions between the CO_2 and the minerals. This was also the conclusion of a previous studies on the hydrophilic versus hydrophobic surfaces of CO_2-brine-dolomite wettability by Al-Yaseri et al. (2017b).

2.6.3 Surface roughness

The limitation of the Young's equation in accounting for the effect of surface roughness on contact angle was long recognised. That is, the Young's equation is not suitable for non-flat surfaces, in which case, the Wenzel equation (Wenzel, 1936) could be used to capture the effect of surface heterogeneity (Marmur, 2006). Typically, surface roughness can be measured using atomic force microscopy (AFM), and expressed as the root mean square (RMS) roughness. Surface roughness tends to

intensify the wettability of the original surface (Seo et al., 2015); due to the full infiltration of the wetting fluid into the roughness grooves, producing a homogeneous wetting regime (Marmur, 2006; Swain and Lipowsky, 1998). Some studies have revealed that contact angles increase with increasing in surface roughness (hydrophobic surface). Conversely, some other studies have reported that contact angles decrease with increasing in surface roughness (hydrophilic surface) (Al-Yaseri et al., 2016; Arif et al., 2017c).

2.6.4 Salinity

Salinity has an important effect on wettability of CO_2-brine-rock systems. Generally, an increase in salinity increases CO_2-wettability. Several researchers have investigated the effect of salinity on wettability by contact angle measurements, especially for mica, quartz, calcite and shales surfaces (Chiquet et al., 2007; Farokhpoor et al., 2013; Arif et al., 2016a; Broseta et al., 2012; Wan et al., 2014; Wang et al., 2012b; Iglauer et al., 2015a). These results have revealed that the contact angle increases with salinity increases. Conversely, Espinoza and Santamarina (2010) have reported that there is insignificant effect of salinity on wettability.

2.6.5 Organic content

Total organic contents (TOC) have also been found to strongly affect CO_2 wettability (Jha et al., 2019b; Abramov et al., 2019; Iglauer, 2017), and consequently, storage potential (Arif et al., 2017d; Guiltinan et al., 2017; Roshan et al., 2016a). There is a consensus that the storage capability and integrity of a geological formation can be strongly influenced by the presence of a small amount of TOC. This finding has also

been upheld by other researchers (Pan et al., 2018; Siddiqui et al., 2018; Yassin et al., 2017), who found that contact angle generally correlates positively with TOC.

2.6.6 Clay type

Clay mineral surfaces typically negatively charged on their minerals due to their crystalline structure, adding to the complexity of their wettability (Grim, 1953; Brigatti et al., 2013). Fauziah et al. (2019b) have examined wettability on clay surfaces, especially montmorillonite, illite and kaolinite wettability for CO_2-brine system. The results showed that, at typical geological storage conditions, montmorillonite is strongly oil-wet. Kaolinite and illite, however, are strongly water-wet.

Chapter 3 Apparatus and Experimental Procedure

3.1 Introduction

This study on the wettability characteristics of CO_2-brine-rock-clay mineral systems is an experimentally based research. To achieve the aims and objectives of the research, various experiments were conducted. This chapter presents the description of the experimental apparatus, a detailed description of the materials used in the study, and the experimental procedures that were followed in conducting the experiments.

3.2 Experimental Apparatus

Extensive experiments were conducted on clays and sandstone samples at various experimental conditions, simulating reservoir conditions. Figure 3.1 shows a schematic of the apparatus used to conduct the contact angle measurements.

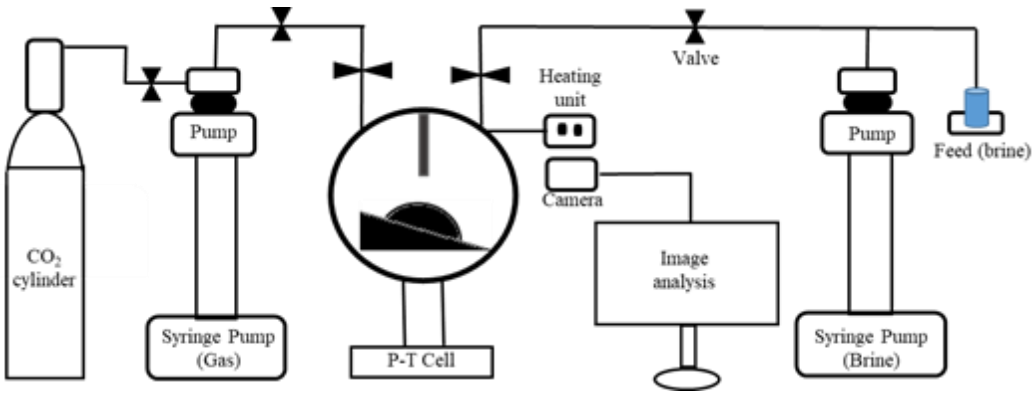

Source: modified from Fauziah et al. (2019b)

Figure 3. 1 The experimental setup of contact angle measurement

The equipment consists of CO_2 cylinder, syringe pump for gas (CO_2), high pressure-high temperature cell with substrate housed on a tilted plate inside, heating unit, high resolution video camera, image visualization and interpretation software, pressure

relief valve, syringe pump for brine and liquid feed/drain system. Figure 3.2 below shows the high pressure-high temperature goniometer setup used for contact angle measurements.

Figure 3. 2 Apparatus of the contact angle measurement

Brief descriptions of the main parts of the high pressure-high temperature goniometer are given in the following section.

3.2.1 High pressure-high temperature cell

The optical cell is fabricated from stainless steel. It is designed for use in simulating reservoir conditions, typically specific salinity, high pressure and high temperature. Figure 3.3 shows the high pressure-high temperature cell. During the experimental procedure, a sample is placed in the cell at a set temperature and pressure, and a droplet of equilibrated liquid/brine is positioned onto the sample surface through a needle. The sample base, on to which the sample is placed inside the vessel, is tilted at an angle of 12° to allow the direct measurement of advancing and receding contact angles. An

industrial heating tape was used to heat the cell up. A high precision syringe pump is connected into the cell through Swagelok fittings, valves and pipes.

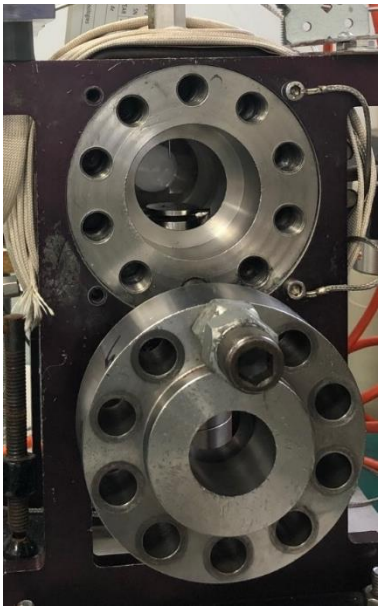

Figure 3. 3 High pressure-high temperature cell

3.2.2 High precision syringe pumps

The system is equipped with two high precision pumps: a syringe pump for gas and syringe pump for water/brine. The gas syringe pump (Teledyne, model 500D syringe pump) was used to pump the gas i.e. CO_2 into the cell to increase the pressure for the measurement. The water/brine syringe pump (Teledyne, model 260D syringe pump) was employed to pump the de-gassed liquid, i.e. brine, into the cell whilst the experiment was running. Both pumps have a pressure accuracy of about 0.1 % at full scale (FS). Figure 3.4 below shows the high precision gas syringe pump and brine syringe pump.

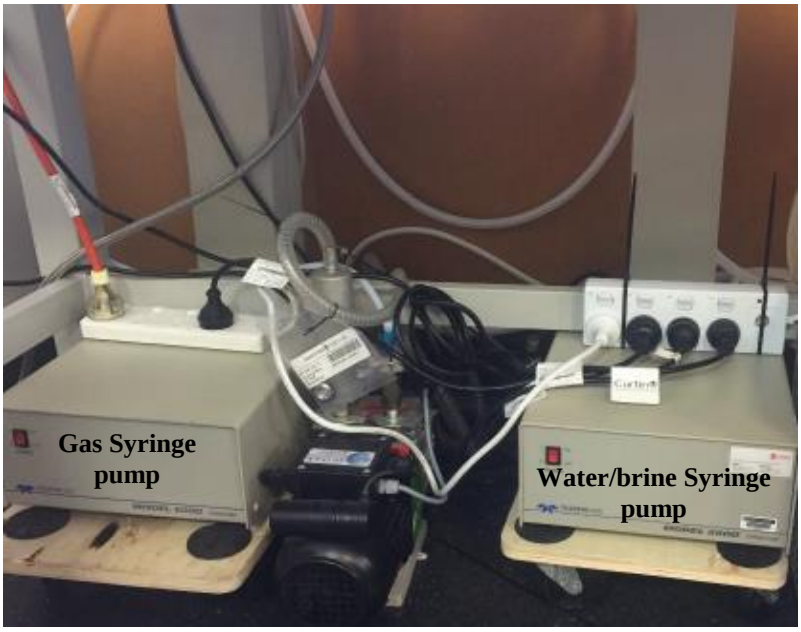

Figure 3. 4 High precision gas and water/brine syringe pumps

3.2.3 Video camera

A high-resolution video camera, with specification of Basler scA (640-70) fm, pixel size = 7.4 μm; frame rate = 71 frames per second; Fujinon CCTV lens: HF35HA-1B; 1.6/35 mm, was employed to record and monitor the processes occurring inside the cell. A light (specification: fibreoptic lightguides, microlight LED) was also utilised to flash onto the cell.

3.2.4 Image J software

The software, Image J, was applied to analyse images. The images were extracted from the video recording files. These were used to measure the advancing and receding contact angle values. The software was installed on the computer, which was connected to the video camera to allow the direct measurements.

3.3 Materials and Sample Preparation

Experimental work began by selecting appropriate samples and chemicals, preparing the samples, such as grinding the samples for clay compaction and other measurements, cleaning treatment, and cutting rock cores into specific sizes.

3.3.1 Materials

Material types used in this research consist of liquid phase, gas phase, oil phase, powder, and rock samples. Details are discussed below:

3.3.1.1 Liquid phase

Sodium chloride (NaCl, 4 wt%)), calcium chloride ($CaCl_2$, 4 wt%), magnesium chloride ($MgCl_2$), potassium chloride (KCl), with purity ≥ 0.995 for all brines, supplied from Scharlab were used in the experiment. Ultrapure de-ionised water (conductivity = 0.02 mS/cm), supplied from David Gray was also used as a base liquid to dissolve the brines to obtain the preferred concentrations. Other brines were also prepared, with a wide range of concentrations including calcium chloride ($CaCl_2$, 1200 mg/L), magnesium sulphate hydrated ($MgSO_4.7H_2O$, 600 mg/L), potassium bromide (KBr, 183 mg/L), sodium bicarbonate ($NaHCO_3$, 125 mg/L), strontium chloride ($SrCl_2$, 100 mg/L), and copper (II) sulphate pentahydrate ($CuSO_4.5H_2O$, 2522 mg/L), by dissolving the brines in deionised water using magnetic stirrer.

3.3.1.2 Gas Phase

Carbon dioxide (CO_2, purity ≥ 0.999, food grade, BOC Australia), nitrogen (N_2, purity ≥ 0.999, BOC Australia), argon (Ar, purity ≥ 0.999, BOC Australia), helium (He,

purity ≥ 0.999, BOC Australia) were used in this study to raise the set pressure in the contact angle measurement.

3.3.1.3 Oil phase

N-decane ($C_{10}H_{22}$, purity ≥ 0.999, Sigma Aldrich, density: 0.73 g/mol, molecular weight: 142.28 g/mol) was used as a model oil and a liquid phase for contact angle measurements.

3.3.1.4 Powder

Clays powder, including montmorillonite (purity ≥ 0.950, Ward Science), illite (purity ≥ 0.850, Ward Science), and kaolinite (purity ≥ 0.950, Ward Science) were used in this measurement. The clay powders were mechanically compacted to obtain the solid clay samples and used for contact angle measurements.

3.3.1.5 Rock samples

Four sandstones samples retrieved from GSWA Harvey-1 well core material (Figure 3.5), Berea and Bandera Gray (Figure 3.6) were used in this study. The petro-physical properties, characterisation and mineralogy of the cores were thoroughly characterised with quantitative X-ray diffraction (XRD), atomic force microscope (AFM), scanning electron microscopy-energy dispersive X-ray spectroscopy (SEM-EDX), total organic carbon (TOC) and organic carbon isotopic composition ($\delta^{13}C_{org}$) analyses.

3.3.1.6 Cleaning agents

Dichloromethane (CH_2Cl_2, purity ≥ 0.999), and acetone were used as cleaning agents for the samples before and after measurement.

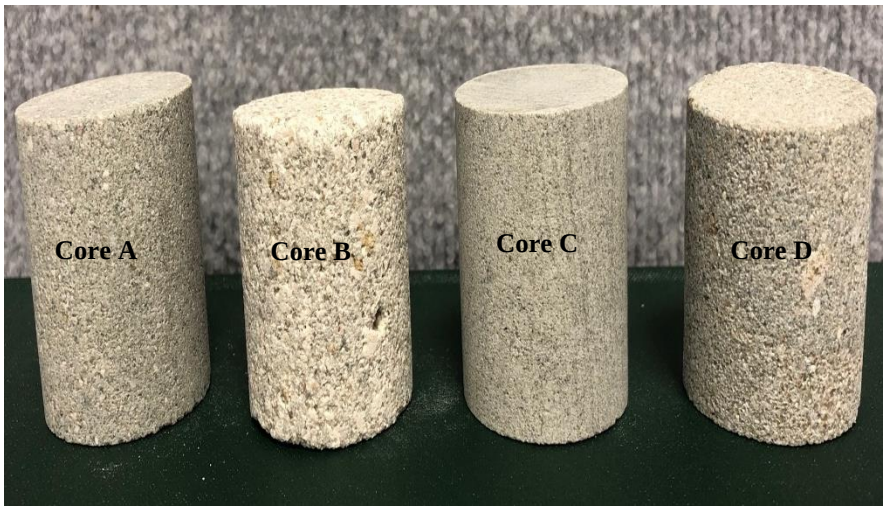

Figure 3. 5 Sandstones retrieved from GSWA Harvey-1 well

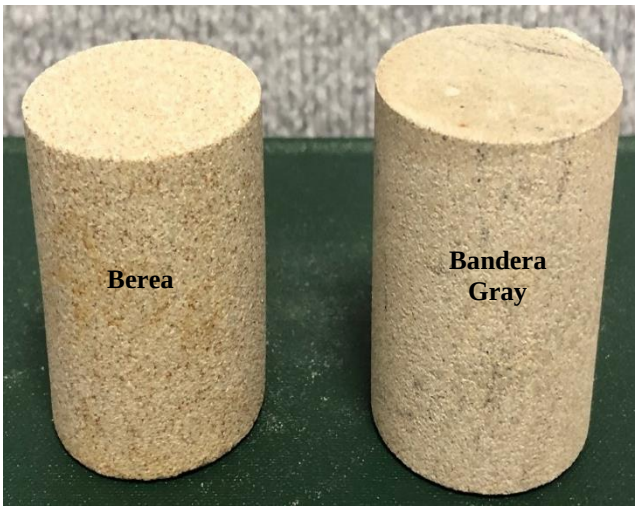

Figure 3. 6 Berea and Bandera Gray sandstones

3.3.2 Sample preparation

Sample preparation involved mechanical compaction of clay powder, cutting and cleaning the rock samples. In wetting analyses, an important requirement was for

appropriate sample preparation and treatment, sufficient sample quality and cleanliness in order to eliminate any possible methodical inaccuracies.

3.3.2.1 Compaction

Clay powder samples were mechanically compacted to create solid montmorillonite, illite, and kaolinite material. Specimens were made of montmorillonite, illite, and kaolinite as well as formation brine (20 wt% NaCl +1 wt% KCl) as moisture fluid. The clay powders were initially mixed with formation brine, the mixture was subsequently poured into a steel cylinder cell (length 10cm and 3.8cm diameter, built in-house), which encloses a circular semi-permeable porous plate (porous alumina, 25% porosity, mean pore size < 2 µm). To simulate the natural sedimentary process, axial stress was exerted on the mixture (10 MPa), and controlled via a high precision 260D ISCO syringe pump series. The excess brine was removed through a drainage tube. The compacted cylindrical samples (diameter of 3.8 cm and length of 1 cm) were removed from the cell after one week and then dried in an oven at 50 °C for 48 hours. The schematic of the mechanical compaction is illustrated in Figure 4.1 and Figure 5.1, and a detailed description of the apparatus and the method is explained in Chapter 4 (Section 4.3.1) and Chapter 5 (Section 5.3.1). Figure 3.7 and Figure 3.8 show the mechanical compaction apparatus, and the compacted clay samples, respectively.

Figure 3. 7 Mechanical compaction apparatus

Figure 3. 8 Compacted montmorillonite, illite and kaolinite

3.3.2.2 Rock/clay cleaning

The Harvey sandstones were cleaned with dichloromethane to remove the artificial intrusions of organic matter contaminations from the drilling mud before the contact angle measurements were conducted. In addition, all samples were placed into air plasma (model Diener plasma, Yocto; Figure 3.8) for 5 minutes to remove organic surface contamination (Love et al., 2005). This cleaning procedure is necessary to ensure accuracy of the results (Iglauer et al., 2014a; Bikkina, 2011).

Figure 3. 9 Air plasma

3.3.2.3 Rock samples

All rock samples including Harvey sandstones, Berea and Bandera Gray were cut into smaller sample discs (5 mm thick, 38 mm in diameter) for measurements, using a high-speed diamond blade.

3.4 Mechanistic quantification

Mechanistic analysis of samples was characterised by X-ray diffraction, atomic force microscope, scanning electron microscope, TOC and organic carbon isotopic composition ($\delta^{13}C_{org}$).

3.4.1 X-ray diffraction

X-ray diffraction (XRD) was used to analyse the mineral constituent of the samples, with instrumental model of X-Ray Diffraction (XRD)-Bruker-AXS D9 Advance Diffractometer.

3.4.2 Atomic Force Microscope (AFM)

Atomic force microscope (AFM, DSE 95-200, Semilab) was used for analysis of surface roughness of the solid samples.

3.4.3 Scanning Electron Microscopy

Scanning electron microscope (SEM, instrumental model Zeiss Neon 40EsB FIBSEM) was used to analyse the samples' microstructural changes in order to investigate any potential alteration in the samples' structure.

3.4.4 TOC and organic carbon isotopic composition ($\delta^{13}C_{org}$)

TOC and organic carbon isotopic composition was used to identify the source of organic content from artificially introduced vs in-situ organic material, using the instrument model elemental analyser-isotope ratio mass spectrometer (EA-IRMS) (Thermo Flash 2000 Elemental Analyser).

3.5 Experimental Procedure

Several experimental procedures were applied on the samples of clay and rock at particular experimental conditions in order to achieve the aims and objectives of the study. These procedures are discussed in detail in the subsequent sections.

3.5.1 Contact angle measurements

The advancing (θa) and receding (θr) water contact angles were measured using the tilted plate technique and a high temperature-high pressure goniometer as per steps detailed below:

1. The brine was prepared in deionised water, and then it was stirred at 100 RPM at room temperature for 1 hour using a magnetic stirrer.
2. The sample was cleaned using the air plasma unit for 5 minutes.
3. The water bath and the reactor controller were heated to the required temperature.

4. The cleaned sample was placed in the sample holder chamber (cell) of the equipment and the chamber then closed with sapphire lens.
5. The brine syringe and gas syringe pumps were filled with brine and CO_2, respectively, and pressurised to the required pressure.
6. The holder chamber was pressurised with the gas by using the gas syringe pump to the required pressure.
7. Once the pressure stabilised in the gas syringe pump, the brine syringe pump was also pressurised to the same value as the gas syringe pump. The brine flow rate, using the brine syringe pump, was through the needle in the chamber.
8. The camera was then started to record the process of droplet fall.
9. The fall of the brine droplet was captured and recorded by the video camera. The pumps were stopped once the initial fall was observed.
10. The pressure in the chamber was then gradually released by using the gas syringe pump to enable the opening of the sapphire lens.
11. The sample was removed from the sample holder in the chamber
12. The light and power were then turned off.
13. The advancing and receding contact angle values were then analysed, with the Image J software, using images from video recording.

3.5.2 Zeta potential

Zeta potential was measured by placing the clay dispersion into a folded capillary cell of the Malvern NanoZS instrument at 25 °C.

3.5.3 Core flooding

Core flooding was also conducted for Berea and Bandera Gray core plugs, a detailed description is given in Chapter 7 section 7.3.2. Subsequently, the samples were used for the contact angle measurements for both treatments, before and after core flooding to investigate the wettability changes caused by CO_2 flooding.

Chapter 4 Carbon dioxide/brine, nitrogen/brine and oil/brine wettability of montmorillonite, illite and kaolinite at elevated pressure and temperature[1]

4.1. Summary

Montmorillonite, illite and kaolinite wettability for carbon dioxide/brine, nitrogen/brine and nitrogen/oil systems were systematically measured through contact angle measurement at various pressures (5 MPa, 10 MPa, 15 MPa and 20 MPa) and temperatures (305 K and 333 K). The zeta potential of each clay was also measured to investigate its link to the macroscopic contact angle. The results show that both advancing and receding water contact angles for carbon dioxide /brine, nitrogen/brine and nitrogen/oil systems increase with an increase in pressure. However, they are only slightly reduced by increasing temperature. It was also showed that montmorillonite has a higher water contact angle in the presence of carbon dioxide, than illite and kaolinite. The same trend was observed for nitrogen/brine and brine/oil systems. Consequently, montmorillonite is strongly oil-wet. Kaolinite and illite, however, are strongly water-wet at typical storage conditions (high pressure, elevated temperature). This has important implications for carbon dioxide geo-storage in determining the flow of carbon dioxide and its entrapment, fluid spreading and dynamics in the reservoir.

4.2. Introduction

Carbon dioxide (CO_2) capture and storage (CCS) is a promising technology to decrease atmospheric CO_2 emissions and enhance production from unconventional resources

[1] Reference: Fauziah at al. 2019 in Journal of Energy and Fuels, 33(1), 441-448. https://doi.org/10.1021/acs.energyfuels.8b02845

(Pacala and Socolow, 2004). However, one of the primary concerns of CCS is to ensure that the buoyant CO_2 remains trapped underground in the geological formation (IPCC, 2005). There are four main CO_2 trapping mechanisms that can create levels of storage volumes in varying amounts and time (IPCC, 2005). These include the following: 1) *Structural* (Jamaluddin et al., 1998; Iglauer et al., 2015a); 2) *residual* (Qi et al., 2009; Hesse et al., 2008); 3) *dissolution* (Iglauer, 2011; Riaz et al., 2006) and 4) *Mineral trapping* (Xu et al., 2003). *Adsorption* trapping, in coal and organic-rich shale, also has been proposed (Busch et al., 2004; Arif et al.). Thus, in order to optimise storage efficiency and to ensure minimum CO_2 leakage, reservoirs with specific properties have to be carefully and systematically selected (Chiquet et al., 2007).

One of the fundamental, underlying reservoir properties, which strongly impacts CO_2 injectivity, storage capacities and containment security, is *wettability* (Iglauer et al., 2015b). Thus it is an imperative that wettability needs to be closely studied and understood in great detail.

In this context, several studies have measured the wettability of clay minerals by contact angle measurements, especially for CO_2-brine-muscovite (mica) systems (Chiquet et al., 2007; Farokhpoor et al., 2013; Arif et al., 2016a; Broseta et al., 2012; Wan et al., 2014; Wang et al., 2012b). These studies examined the contact angle of CO_2-brine on muscovite (mica) substrates at elevated pressures and temperatures. Their results show that the water contact angle increases with pressure and salinity, and decreases with increased temperature. Other researchers have investigated the wetting of CO_2 on organic shales (Barnet Shale), which consisted mainly of clay. Conversely, they reported that increased pressure did not show an increase in contact

angle, and increased temperature did cause an increased contact angle (Guiltinan et al., 2017). Contact angles measured on caprock samples (siltstone, argillaceous siltstone, calcareous sandstones, and calcareous siltstone), taken from a CO_2 storage site in New South Wales, again increased significantly with pressure and temperature (Iglauer et al., 2015a). These studies suggest that there are some significant discrepancies in the reported results. These could be attributed to various factors including chemical heterogeneity of substrate, surface roughness and contamination (Iglauer et al., 2015b; Butt et al., 2006).

To gain a greater understanding of the underlying causes, this research systematically analysed the wettability of clays; montmorillonite, illite and kaolinite through the advancing and receding contact angle measurements. These three clays were chosen for the analysis, since they are essential constituents of many rock-forming minerals present in reservoir and caprocks (Guidotti, 1984; Iglauer et al., 2015b); which are critical in CO_2 sequestration. The measurements were performed for CO_2/brine, nitrogen (N_2)/brine and N_2/oil (n-decane) fluid systems at various pressures (5 MPa, 10 MPa, 15 MPa and 20 MPa) and temperatures (305 K and 333 K). The experimental setups are relevant for geo-sequestration conditions (Nielsen et al., 2012; Al-Yaseri et al., 2016; Arif et al., 2016a). The characterisation for N_2/brine and N_2/oil (n-decane) contact angle was measured to enhance fundamental knowledge, which will be applicable to oil production and fundamental understanding of the development of solid earth. Zeta potential was additionally measured to correlate the macroscopic contact angle to surface chemistry and thus wettability (Iglauer, 2017; Arif et al., 2017b). How pressure and temperature, clay type, pore system and surface roughness influence contact angle were then analysed. Finally, the results were presented and

discussed with providing primary reasons for the observed correlations, and compare them with other reliable literature studies.

4.3. Experimental Methodology

4.3.1 Sample preparation

The clay powder samples were mechanically compacted to create solid montmorillonite, illite, and kaolinite samples. The compaction rig used is illustrated in Figure 4.1 and is described in detail in Beloborodov et al. (2016). The solids were prepared from a brine-based mixture of montmorillonite, illite, and kaolinite. To mimic the brine solution in the reservoir formation, we mixed 4 wt% NaCl, 4 wt% $CaCl_2$, 1 wt% $MgCl_2$ and 1 wt% KCl in deionised water. The brine mixture was added to each of the above clay powders. The prepared mixtures were then poured into an oedometer cell with an enclosed, semi-permeable porous plate (porous alumina, 25% porosity, mean pore size < 2 μm) that retained clay particles but passed the water through during the compaction process. An automatic hydraulic pump (Isco-Teledyne 260D) was used to create constant axial stress applied vertically to the porous plates on both sides of the oedometer. The applied stress was increased, stepwise, until the stabilisation criterion, of 0.01 mm in 16 hours for the sample of ~ 25 mm in height, was met to prevent creep deformations and to fully consolidate the sample at a given step (Beloborodov et al., 2017). All samples were compacted to the same porosity value of 15%. This was estimated as a function of cell volume (V_0), a clay grain density (ρ_m) and clay mass (m), as given by equation 4.1 :

$$\phi = 1 - \frac{m/\rho_m}{V_0} \tag{4.1}$$

Note that the particle size of individual clay grains is generally < 2 μm or < 4 μm (Moore and Reynolds, 1997; Weaver, 1989; Bergaya and Lagaly, 2013). The aggregate grain size of montmorillonite, illite, and kaolinite was about 75 μm, with associations of aligned individual clay particles, as observed on scanning electron microscopy (SEM) images.

After compaction, the samples were gently ejected from the oedometer cell and cut into four subsample discs (5 mm thick, 38 mm in diameter) in the bedding direction of the sample (normal to the applied stress). Subsamples were then oven-dried at 105 °C. Details of the samples are provided in Table 4.1.

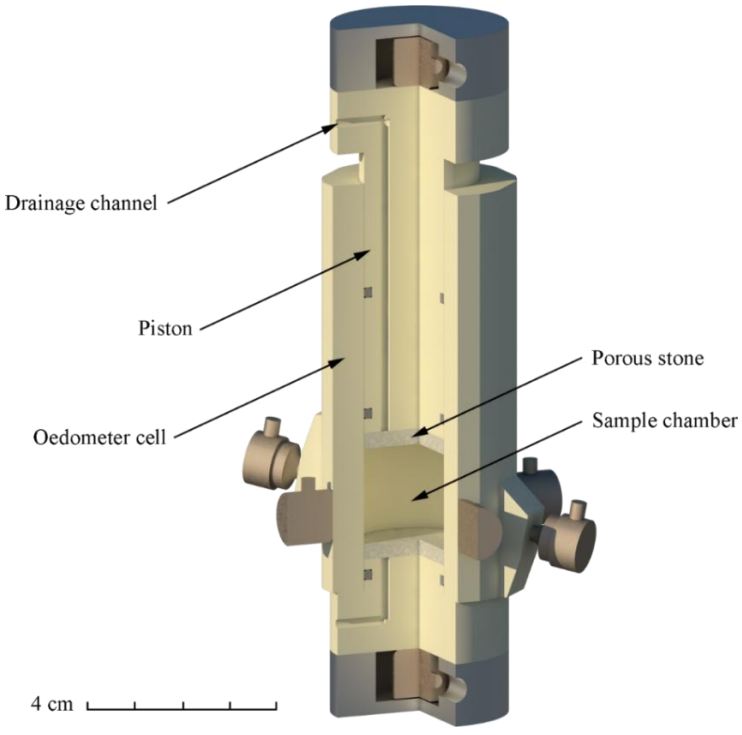

Source: modified from Beloborodov et al.(2017)

Figure 4. 1 Schematic of the mechanical compaction rig

Table 4. 1 Provenance and purity of chemicals used

Chemical name	Source of supply	State	Mass fraction
Montmorillonite	Ward's natural	Powder	≥ 0.950
Illite	Ward's natural	Powder	≥ 0.850
Kaolinite	Ward's natural	Powder	≥ 0.950
NaCl	Scharlab s.1.,	Powder	≥ 0.995
$CaCl_2$	Scharlab s.1.,	Powder	≥ 0.995
$MgCl_2$	Scharlab s.1.,	Powder	≥ 0.995
KCl	Scharlab s.1.,	Powder	≥ 0.995
CO_2	BOC, Australia	Gas	≥ 0.999
N_2	BOC, Australia	Gas	≥ 0.999
n-Decane	Sigma Aldrich	Liquid	≥ 0.999
DI water	David Gray's	Liquid	0.02 mS/cm*

*The conductivity of deionised water was measured with a Multiparameter (HI 9823) at T = 294 K at atmospheric pressure

4.3.2 Contact angle measurement

The contact angle measurements were conducted using the tilted plate technique (Lander et al., 1993) and a high temperature-high pressure goniometer method, as summarised in detail in (Yuan and Lee, 2013; Iglauer et al., 2015b). The schematic of the experimental setup is illustrated in Figure 4.2. The surface roughness of three prepared clay samples was measured with an atomic force microscope (AFM; instrument model DSE 95-200). The root mean square (RMS) surface roughness values were 180 nm, 310 nm and 740 nm for montmorillonite, kaolinite, and illite, respectively, as shown in Figure 4.3, the topography of the three clay surfaces imaged by AFM. Subsequently, the three samples were cleaned with air plasma for 5 minutes to eliminate any potential organic surface contamination (Love et al., 2005). The cleaning process is an essential step to help avoid introducing some possible bias in the results (Iglauer et al., 2015b).

The cleaned clay samples were then placed in the pressure chamber at a set temperature (308 K or 333 K). Using a high precision syringe pump (ISCO 500D; pressure

accuracy of 0.1 % FS), CO_2 was injected into the chamber, and the pressure was raised to prescribed values (5 MPa, 10 MPa, 15 MPa, or 20 MPa). After reaching the set pressure, a droplet (average volume of a single drop was ~6 μL ± 1 μL) of brine equilibrated with CO_2 by using a mixing reactor (El-Maghraby et al., 2012) was dispensed onto the tilted surface (tilting angle of 12^o) through a needle. However, the CO_2-brine equilibration does not affect contact angle measurements on quartz (Al-Yaseri et al., 2015). The whole process was recorded with a high resolution video camera (Basler scA (640-70) fm, pixel size = 7.4 μm; frame rate = 71 frames per second; Fujinon CCTV lens: HF35HA-1B; 1.6/35 mm). The contact angles were then measured on images extracted from the video records. The advancing water contact angle (θ_a) was measured at the leading edge of the droplet, immediately before the droplet started to move, while the receding contact angle (θ_r) was measured at the trailing end of the droplet.

Additional measurements were conducted for each clay sample at 333 K, and 10 and 15 MPa for N_2/brine and N_2/oil (n-decane), with N_2 injected into the cell, in place of CO_2, and the measurement was made through oil (n-decane), as a liquid phase, replacing the brine. The variation or error range in the reported contact angle is ~±3^o based on three (3) replicate measurements at experimental condition.

4.3.3 Zeta potential measurement

Zeta potential is an important technique of nanocrystal to assess the surface charge to understand the physical stability of nanoparticles in aqueous suspensions (Jiang et al., 2009). Zeta potential was measured by placing the clay dispersion into a folded capillary cell that is used in the Malvern NanoZS instrument at 25 °C. Clay dispersion

is controlled by the attractive and repulsive forces in the electrical double layer at the surface of charged colloids (Chorom and Rengasamy, 1995). Three replicates were measured, and the data are shown in Table 4.2.

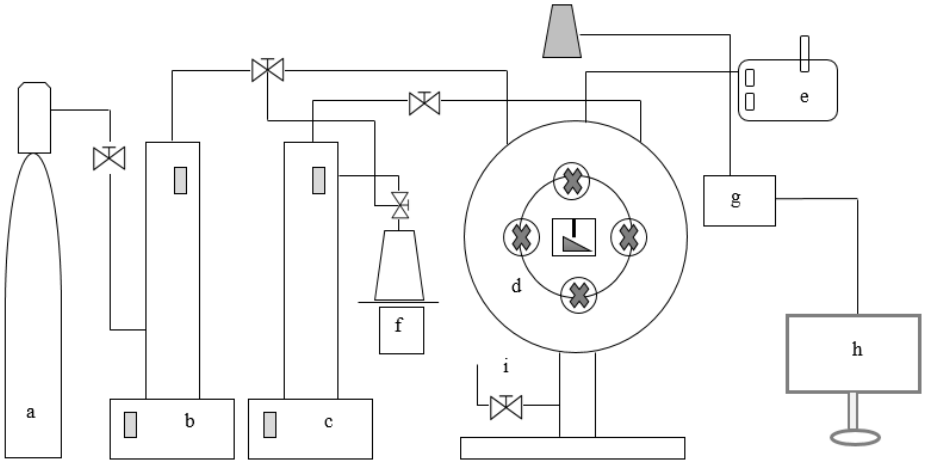

Sources: adapted from (Arif et al., 2017a)

Figure 4. 2 Schematic diagram of the contact angle setup

Note: The apparatus parts include (a) CO_2 cylinder (b) syringe pump-CO_2, (c) syringe pump-brine, (d) high pressure cell with substrate housed on a tilted plate inside, (e) heating unit, (f) liquid feed/drain system (reactor controller), (g) high resolution video camera, (h) image visualization and interpretation software, (i) pressure relief valve.

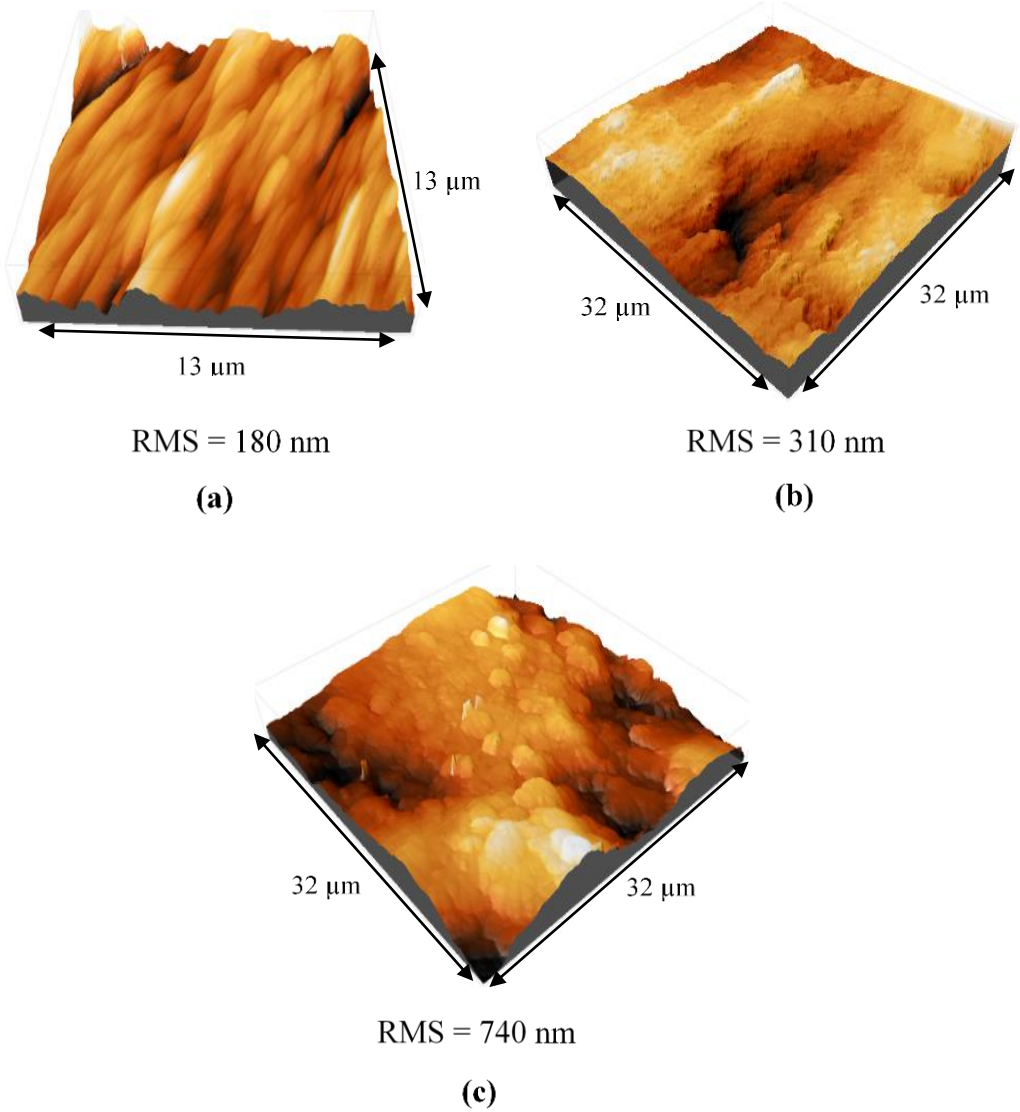

Figure 4. 3 3D topography of the three clay surfaces

Note: the three clay surfaces imaged by Atomic Force Microscopy; different heights are coloured differently. (a) Montmorillonite with RMS of 180 nm (black is 0 nm and white is 1600 nm), (b) Kaolinite with RMS of 310 nm (black is 0 nm and white is 2500 nm), (c) Illite with RMS of 740 nm (black is 0 nm and white is 4000 nm).

4.4. Results

Advancing (θ_a) and receding (θ_r) CO_2/brine contact angles (measured through water) increased with increasing pressure for all three clay types. For example, when the pressure was increased from 5 MPa to 20 MPa at 305 K, the advancing and receding water contact angles for montmorillonite increased from 77^o to 110^o and from 72^o to 105^o, respectively (Figure 4.4). This result is consistent with most of the literature data observed for contact angles of water/CO_2/mica (Chiquet et al., 2007; Arif et al., 2016a), water/CO_2/caprock (Roshan et al., 2016a; Iglauer et al., 2015a), water/CO_2/quartz (Al-Yaseri et al., 2015; Saraji et al., 2013; Sarmadivaleh et al., 2015; Al-Yaseri et al., 2016), water/CO_2/silica(Iglauer et al., 2015b; Jung and Wan, 2012), water/CO_2/feldspar (Farokhpoor et al., 2013), and water/CO_2/calcite (Broseta et al., 2012).

However, there was only a small reduction in advancing and receding contact angles with an increase in temperature. For instance, the advancing and receding contact angle for illite at 5 MPa dropped from 53 to 47° and 45 to 39°, respectively, when temperature increased from 305 K to 333 K (Figure 4.5). This result is also consistent with studies observed on water-wet mica surface (Arif et al., 2016a; Broseta et al., 2012; Wan et al., 2014), and on clean quartz and calcite surface (Bikkina, 2011; Saraji et al., 2013). Some studies, on the other hand, observed an increase in contact angles with the increase in temperature as measured on various surfaces such as shale rocks (Roshan et al., 2016a), feldspar (Farokhpoor et al., 2013), and quartz (Sarmadivaleh et al., 2015; Al-Yaseri et al., 2016).

Additional measurements were conducted for the nitrogen/brine and nitrogen/oil advancing and receding contact angles for each clay at 10 MPa and 15 MPa, at a constant temperature of 333 K (Figures 4.6 and 4.7), the same trend was observed for these systems. Zeta potentials of the clay slurry were also measured at atmospheric conditions (Figure 4.8 and Table 4.2) to investigate how the clay surface charge is related to the macroscopic contact angle, although the results can be different to CO_2 at storage conditions (Borysenko et al., 2009).

Table 4. 2 Zeta potential measured for each clay

Clay	Zeta Potential Value (mV)	Average (mV)
Montmorillonite	-9.01 -8.17 -12.3	-9.8 ± 2.5
Illite	-0.42 -3.69 -2.16	-2.1±1.6
Kaolinite	1.6 5.27 3.79	3.6 ± 2

*Measured in 4 wt% NaCl + 4 wt% $CaCl_2$ + 1 wt% $MgCl_2$ + 1 wt% KCl brine at 25^o C

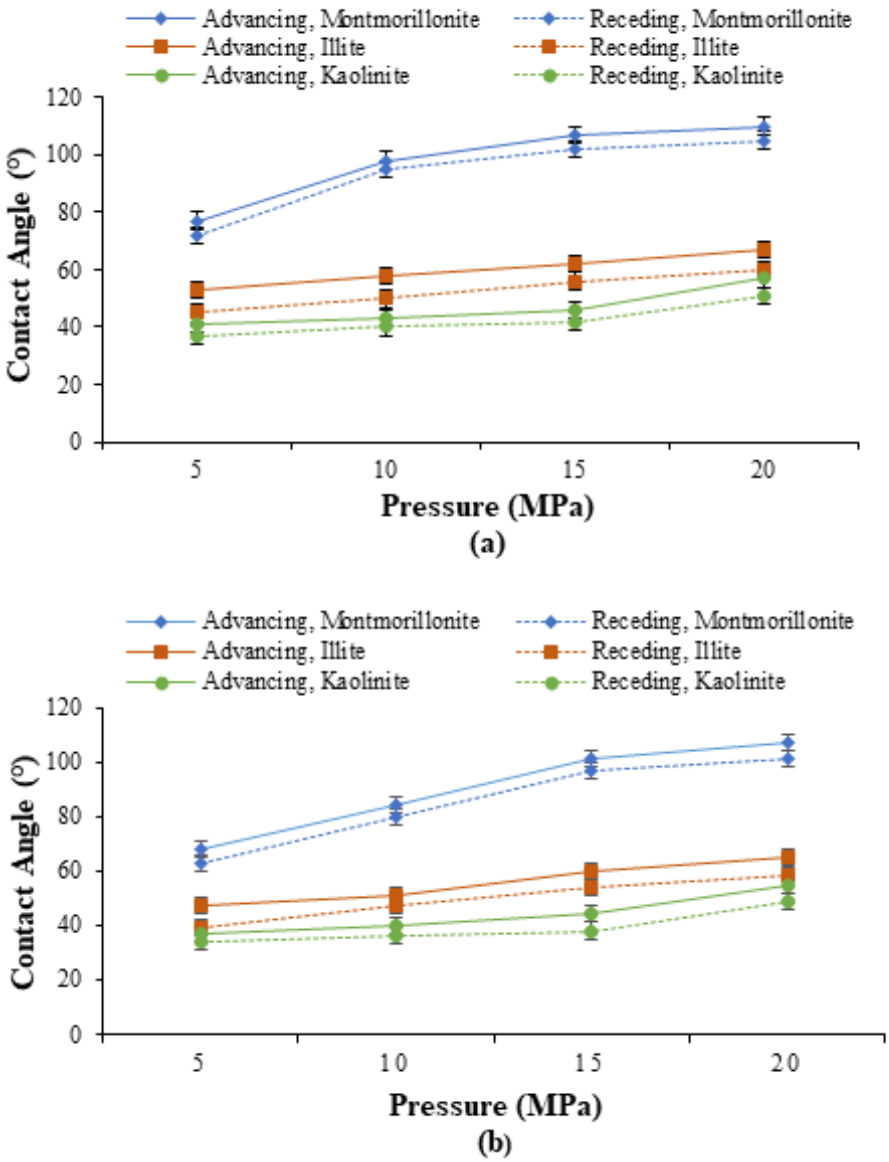

Figure 4. 4 θa and θr of the three clays as a function of pressure

Note: montmorillonite, illite and kaolinite were measured at (a) 305 K, and (b) 333 K

.

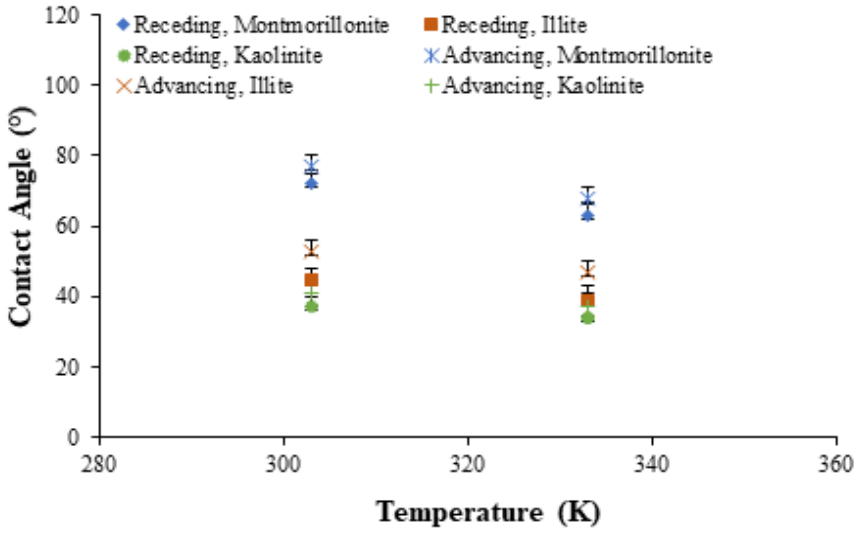

Figure 4. 5 Effect of temperature on θa and θr for CO_2/brine/clay system

Note: montmorillonite, illite and kaolinite were measured at 305 K and 333 K)

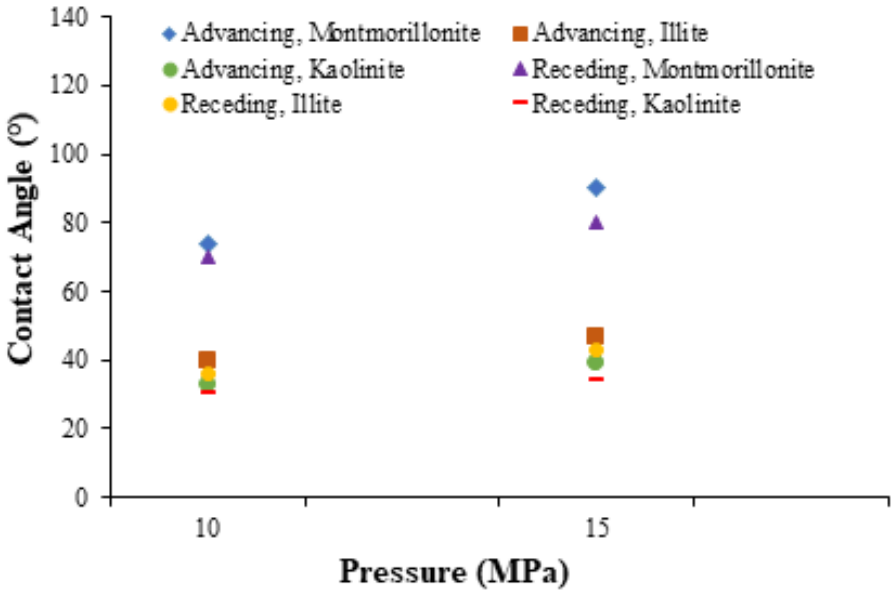

Figure 4. 6 θa and θr for the N_2/brine/clay systems

Note: montmorillonite, illite and kaolinite were measured at 333 K

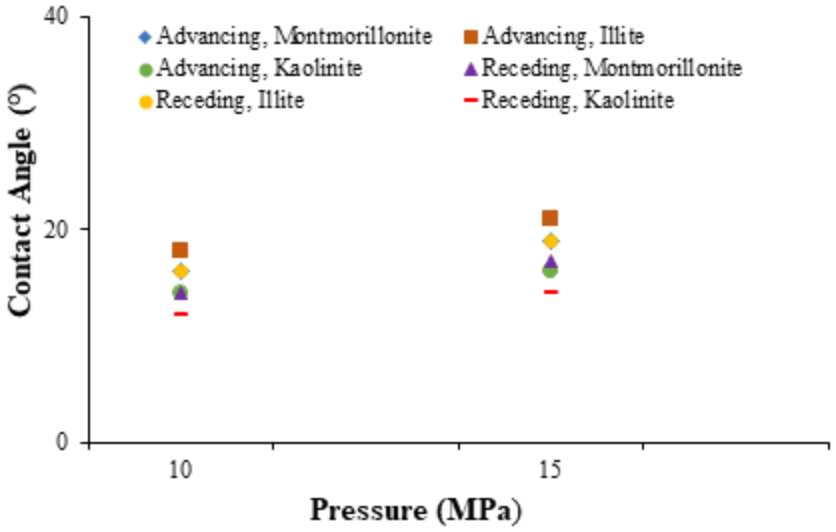

Figure 4. 7 θa and θr for the N_2/oil/clay systems

Note: montmorillonite, illite and kaolinite were measured at 10 MPa and 15 MPa, and 333 K)

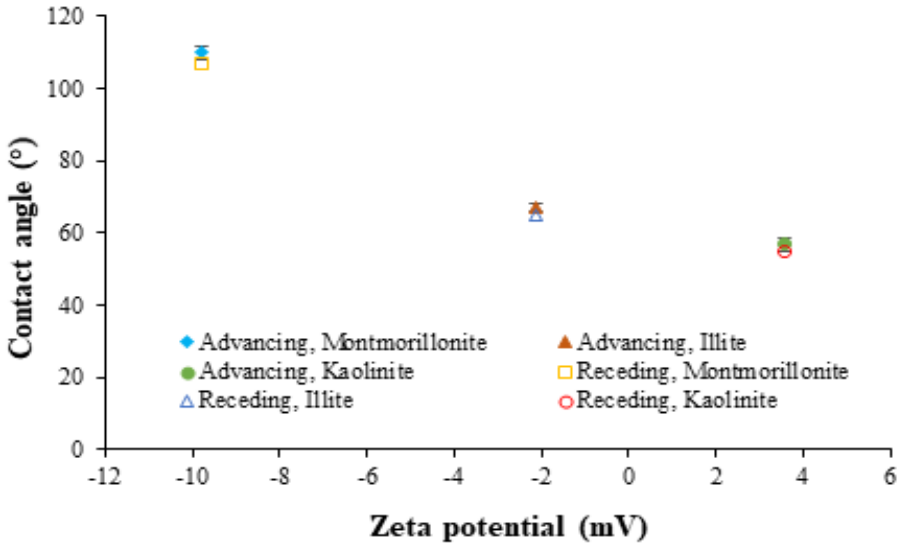

Figure 4. 8 θa and θr versus zeta potential

Note: montmorillonite, illite and kaolinite were measured at 305 K and 20 MPa

4.5. Discussion

Various parameters were examined in terms of how they affect the wettability, including pressure, temperature and clay type. The results of CO_2/brine wettability were then compared with N_2/brine and N_2/oil (n-decane) wettability measured at the same pressure and temperature. The findings are discussed in detail in the following sections.

4.5.1 Influence of pressure and temperature on brine/CO_2/clay wettability

The water contact angle was observed to increase with increase in pressure (Figure 4.4). It is related to the increasing CO_2 density, which strengthens the intermolecular interactions between CO_2 and the mineral, and therefore leads to de-wetting of the surface (Iglauer et al., 2012; Al-Yaseri et al., 2016). Furthermore, the effect of temperature on the contact angle measurement (Figure 4.5) is associated with fluid density and van der Waals forces. The legitimacy of this de-wetting observation has been strengthened by a previous study on hydrophilic versus hydrophobic surfaces of CO_2/brine/dolomite wettability (Al-Yaseri et al., 2017b). The reader is referred to this article for the theoretical details. This fact also has been formulated in detail in Al-Yaseri et al. (2016) for gas/brine/quartz systems in terms of fluid density. Clearly, there is a strong correlation between gas density and wettability. Likewise, the van der Waal potential on hydrophilic surfaces can significantly decrease with temperature, which can, in turn, increase in contact angle. The reason is that hydrophilic surfaces provide more effective van der Waals interactions between water molecules and the substrate surface, and hence a stronger function of temperature (Al-Yaseri et al., 2017b). Nevertheless, such interactions are weakly present on hydrophobic surfaces, and thus, the temperature dependency is weak. From the above observations and

discussions, it is apparent that hydrophobic surfaces are more likely to experience a decrease in contact angle with increasing temperature.

4.5.2 Influence of clay type

It is well defined that clay minerals often carry negative charges on their minerals surface due to their crystalline structure, thus increasing their wettability complexity (Grim, 1953; Brigatti et al., 2013). Montmorillonite has higher brine contact angle in the presence of CO_2 than illite and kaolinite (Figure 4.4). This behaviour can be attributed to the layered structure of the clay minerals formed by assemblages of hydroxide and crystalline silicate sheets (Bergaya and Lagaly, 2013).

Kaolinite is composed of one hydroxide and one silicate sheet (1:1 structure), and it has a weak negative charge on its basal planes, while it can be positively or negatively charged on its edges depending on the pH of the surrounding medium (Sposito et al., 1999). Kaolinite has the isoelectric point (pH value at which electrophoretic mobility is zero), as summarised by Schroth and Sposito (1997), of either 3.3, 4.6 (Parks, 1967), 5.0 (Ferris and Jepson, 1975), or 4.25 (Carroll-Webb and Walther, 1988), depending on the pre-treatment, which leads to varied silica-alumina ratios on the edges of the kaolinite crystal (Diz and Rand, 1989). Silicate surfaces in kaolinite have no isomorphism and a small surface charge density and therefore interact only weakly with water molecules. In contrast, the hydroxide surface interacts strongly with polar molecules, thus promoting water-wetness (Robin et al., 1995). Consequently, both polar and apolar attractions can be seen on kaolinite. On the other hand, the surface charge of 2:1 phyllosilicates such as illite (smectite) varies significantly, depending on the extent of isomorphous substitution in their crystalline structure and the nature of

the exchanged cations. Isomorphous substitution increases surface charge density and thus promotes water-wetness (Bergaya and Lagaly, 2013). However, when such substitutions are limited, resulting in a low surface charge density, the apolar component can interact with dispersed hydrated cations, thus resulting in oil-wet surfaces. The 2:1 clay minerals, with low surface charge density, are thus more likely to be oil-wet (e.g., montmorillonite) although this also depends on the nature of the exchangeable cations and their hydration enthalpy (Bergaya and Lagaly, 2013). This is consistent with the zeta potential measurements (Figure 4.8 and Table 4.2), which confirm that the test montmorillonite clay does not have high surface charge density in the test solution, and thus it is likely to be oil-wet, and that kaolinite and illite likely to be water-wet. However, it is worth noting that surface charge density alone (zeta potential) might not be an indicator of overall wetness (Bergaya and Lagaly, 2013).

4.5.3 Influence of pore systems on CO_2/brine/clay wettability

The pore system of reservoirs rock is also an important factor that impacts wettability. To take the porous character of the compressed clay samples into account, we refer to the study conducted by Alnali et al.(2018). This has been modelled with equation 4.2, below:

$$\gamma_{LG}\cos\theta = \gamma_{SG} - \gamma_{SL} - \frac{2\phi\gamma_{LG}\cos\theta}{r}h \qquad (4.2)$$

Where γ is the interfacial tension or surface free energy (S, G and L represent solid, gas and liquid phase, respectively), ϕ is the porosity, h is the average capillary rise (from a water droplet on the clay until it starts to migrate into the pores) in the pore system, and r is the average pore radius.

Furthermore, the Cassie-Baxter equation (Eq. 4.3, below) was applied to predict the trend of contact angle changes and to assess the accuracy of predicting the measured clay contact angle data.

$$cos\ \theta_c = f_i\ cos\ \theta - (1 - f_i) \tag{4.3}$$

Where θ_c is the predicted Cassie-Baxter contact angle, f_i is the fractional projected area of material (tested clay), θ is the smooth area contact angle, and $(1- f_i)$ describes the contribution of CO_2 remaining under the droplet (Milne and Amirfazli, 2012; Alnali et al., 2018).

Comparison of the equilibrium of the contact angle is obtained in this study through laboratory experiments, use of the Cassie-Baxter method and a new method, described in Alnali et al. (Eq. 4.2) (2018). The results are plotted in Figure 4.9. To this end, we used a porosity of 15 %, h = 0.5 mm, and the interfacial tension data given in (Arif et al., 2016b) for water-wet mica (muscovite), which serves as, a conservative proxy for illite. The results clearly show that the contact angles determined via the Cassie-Baxter equation and derived by Alnali's model for porous clay correction were systematically higher than those derived from the laboratory measurements. In this case, the number of surface pores (porosity fraction), pore throat diameter, and height of fluid infiltration play dominant roles in the magnitude and kinetics of contact angle variation on a porous surface. Therefore, the increase in contact angle due to the presence of pores was associated with the capillary-driven forces acting at the surface pore throat, which has been mathematically formulated earlier (Roshan et al., 2016b; Alnali et al., 2018). This has an impact on the effectiveness of CO_2 residual trapping during the

spontaneous imbibition for CO_2 geo-storage and enhanced oil recovery (Roshan et al., 2016b; Alnali et al., 2018; Strand et al., 2003)

4.5.4 Influence of surface roughness on CO_2/brine/clay wettability

The influence of surface roughness on contact angle has been long recognised, i.e Young's equation is only applicable to ideal (mathematically) flat surfaces (Marmur, 2006). The Wenzel equation (see Eq. 4.4 below) is used to account for the effect of surface roughness (Wenzel, 1936).

$$cos\ \theta_{rough} = r\ cos\ \theta_{smooth} \tag{4.4}$$

Where θ_{rough} is the contact angle on the rough surface (apparent) and θ_{smooth} is the Young's contact angle on an ideal surface; r is defined as the roughness ratio of the actual (measured) and the projected (ideal) solid surface. Thus, r is equal to 1 for an ideal surface and greater than 1 for a rough surface.

Note that wettability of the original surface is intensified by surface roughness (Seo et al., 2015); this effect is related to full infiltration of the wetting fluid into the roughness grooves, resulting in a homogeneous wetting regime (Marmur, 2006; Swain and Lipowsky, 1998). However, the Wenzel's equation is applicable only when the wetting droplet size is greater than the roughness scale by two to three orders of magnitude, as shown by molecular dynamics simulations (Marmur, 2006; Brandon et al., 2003).

In this study, surface roughness was measured by AFM, and r was quantified by dividing the actual length of the profile line (L_a from Figure 4.3) by the projected

profile line (L_i). The measurement was repeated for five different profile lines, and then the average *r* was calculated (Table 4.3). The roughness ratios lied between 1.003 and 1.010, with standard deviations of ± 0.0071, 0.0029 and 0.0026 for montmorillonite, illite and kaolinite, respectively.

The conversion results using the Wenzel equation showed that the θ_{smooth} values are slightly higher than θ_{rough} for the case of kaolinite and illite, but identical for montmorillonite. We note that additional factors such as surface sharpness, sorption on surfaces and associated energy dissipation can influence the contact angle on rough surfaces, and these are not considered in the Wenzel's equation (Butt et al., 2006).

4.5.5 N_2/brine, N_2/oil and converted brine/oil/clay wettability

Measuring brine/oil/clay contact angles at in situ conditions is a complex procedure. Therefore, N_2/brine/clay and N_2/oil/clay contact angles were measured (Figures 4.6 and 4.7) and then converted to brine/oil/clay contact angle, see below (Table 4.4). To convert nitrogen/brine/clay and nitrogen/oil/clay to brine/oil/clay contact angles, the equation 4.5 below, proposed by Siddiqui *et al*. (2018), was used. This equation was derived by extending Young's equation:

$$\theta_{OW} = cos^{-1}\left(\frac{\gamma_{SW} - \gamma_{SO}}{\gamma_{OW}}\right) = cos^{-1}\left(\frac{\gamma_{OA} cos\,\theta_{OA} - \gamma_{WA}\cos\theta_{WA}}{\gamma_{OW}}\right) \qquad (4.5)$$

Here γ is the interfacial tension, and θ is the water contact angle (where OW, SW, SO, OA and WA represent the oil/water, solid/water, solid/oil, oil/air and water/air interfaces). The oil/N_2, water/ N_2 and oil/water interfacial tension data was collected

from literature for each pressure and temperature (Jianhua et al., 1993; Wiegand and Franck, 1994; Yan et al., 2001). Advancing and receding contact angles were then converted to Young's equilibrium contact angles (Table 4.4), using (Chibowski and Terpilowski, 2008; Tadmor, 2004):

$$\theta_l = cos^{-1}\left(\frac{r_A cos\theta_A + r_R cos\theta_R}{r_A + r_R}\right) \tag{4.6}$$

with:

$$r_A = \left(\frac{sin^3\theta_A}{2 - 3cos\theta_A + cos^3\theta_A}\right)^{1/3}$$

and:

$$r_R = \left(\frac{sin^3\theta_R}{2 - 3cos\theta_R + cos^3\theta_R}\right)^{1/3}$$

The results of the conversion (shown in Table 4.4) show that montmorillonite is intermediate-wet to weakly oil-wet, depending on pressure, while illite and kaolinite are strongly water-wet. It is evident that increasing pressure renders the surface more hydrophobic. As discussed above, the 2:1 structured clays can be oil-wet if the surface charge density is low. This is, in fact, the case for the montmorillonite tested, as oil-wetness is observed. In contrast, the highly charged kaolinite is strongly water-wet, indicating a strong interaction between the surface hydroxyl groups with the polar water molecules (Barclay and Worden, 2009).

Table 4. 3 θa and θr on the rough and smooth surface at 20 MPa

Clay	RMS*(nm)	T (K)	θ_a rough (°)	θ_r rough (°)	r**	θ_a smooth*** (°)	θ_r smooth***(°)
Montmorillonite	180	303	110	105	1.003	109.9	105.0
		333	107	101		106.9	101.0
Illite	310	303	57	51	1.007	57.3	51.3
		333	55	49		55.3	49.3
Kaolinite	740	303	67	60	1.010	67.2	60.3
		333	65	58		65.3	58.4

* RMS = root-mean-square surface roughness

** r is roughness ratio

*** θ_a / θ_r smooth were predicted via the Wenzel equation

Table 4. 4 θ for N_2/oil/clay and N_2/brine/clay conversion to brine/oil/clay (Measured at 333 K)

Clay	Pressure (MPa)	Contact Angle (N_2+brine)		Contact Angle (N_2+oil)		Young brine/N_2	Young oil/N_2	Converted brine/oil
		Advancing	Receding	Advancing	Receding			
Montmorillonite	10	74	70	16	14	71.7	15.0	90.3
	15	90	84	19	17	89.9	18.0	116.9
Illite	10	40	36	18	16	38.0	17.0	46.2
	15	47	43	21	19	45.0	20.0	54.4
Kaolinite	10	33	30	14	12	31.5	13.0	38.9
	15	39	34	16	14	36.4	15.0	44.6

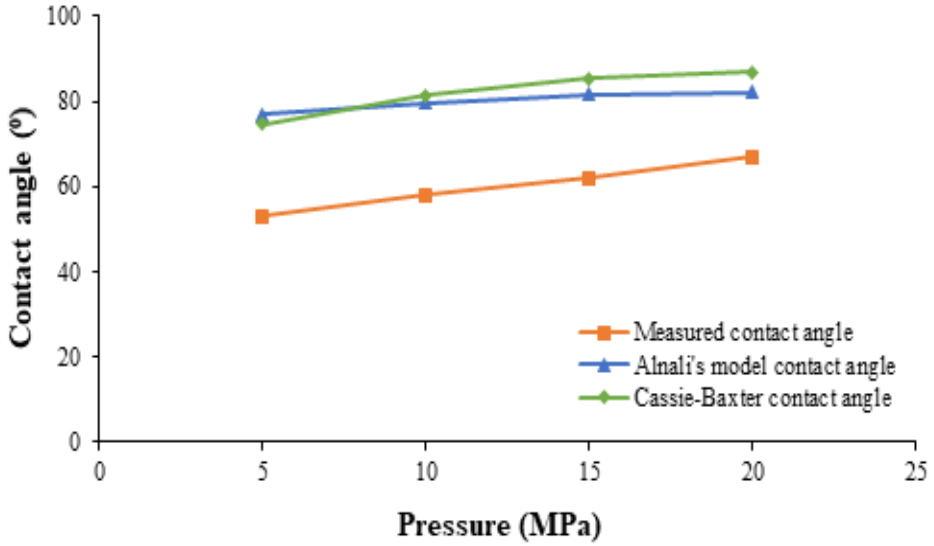

Figure 4. 9 Comparison of the equilibrium contact angles

Note: the equilibrium contact angles were obtained through the laboratory experiment, the Cassie-Baxter method and the Alnali's model (Alnali et al., 2018) (measured at 305 K for advancing Illite).

4.6. Conclusions

Carbon dioxide wettability of clay is poorly understood. This is despite its key role and importance in controlling the efficiency of carbon dioxide geo-storage trapping and methane recovery mechanisms. This complexity of understanding its wettability is further aggravated by the large variation in the composition of caprocks and storage rocks (Iglauer, 2017; Iglauer et al., 2015b). In this study, the wettability of montmorillonite, illite and kaolinite with carbon dioxide/brine, nitrogen/brine and nitrogen/oil were measured at elevated pressures and temperatures to assist in the understanding of fundamentally important issues.

The results demonstrated that montmorillonite has a higher water contact angle in the presence of carbon dioxide when compared to illite and kaolinite. The same trend was observed for nitrogen/brine and brine/oil systems. Moreover, the water contact angle increased with increase in pressure; consistent with most literature data observed for carbon dioxide-wettability of mica (Arif et al., 2016a; Chiquet et al., 2007), caprocks (Iglauer et al., 2015a; Roshan et al., 2016a), quartz (Al-Yaseri et al., 2015; Saraji et al., 2013; Sarmadivaleh et al., 2015; Al-Yaseri et al., 2016), silica (Iglauer et al., 2015b; Jung and Wan, 2012), feldspar (Farokhpoor et al., 2013), and calcite (Broseta et al., 2012). The explanation is that the increase in carbon dioxide density with pressure strengthens the intermolecular interactions between carbon dioxide and the mineral surface, and therefore leads to de-wetting of the surface (Iglauer et al., 2012; Al-Yaseri et al., 2016).

Furthermore, the contact angle slightly declined with increasing temperature for all clay samples. This is consistent with previous studies on other minerals; observed on water-wet mica (Arif et al., 2016a; Broseta et al., 2012; Wan et al., 2014) and clean quartz and calcite surfaces (Bikkina, 2011; Saraji et al., 2013), as well as with molecular dynamic simulations (Iglauer et al., 2012). However, it is inconsistent with observations on shale rocks (Roshan et al., 2016a), feldspar (Farokhpoor et al., 2013), and quartz (Sarmadivaleh et al., 2015; Al-Yaseri et al., 2016) by some researchers. This dissimilarities (of contact angle as a function of temperature) may be due to differences in, e.g. salt concentration, salt type or surface roughness (Al-Yaseri et al., 2016).

In summary, montmorillonite tends toward oil-wet, while illite and kaolinite are more water-wet. Montmorillonite, as a 2:1 structured clay can be oil-wet due to its lower surface charge density. Moreover, increasing pressure renders the surface more hydrophobic. In contrast, kaolinite is strongly water-wet, followed by illite, indicating a strong interaction between the surface hydroxyl groups with the polar water molecules (Barclay and Worden, 2009). Finally, this study concluded that montmorillonite is strongly oil-wet. Kaolinite and illite, however, are strongly water-wet at typical storage conditions (high pressure, elevated temperature). Some of the issues emerging from these findings relate specifically to the flow of carbon dioxide and its entrapment in the subsurface formations for carbon dioxide geo-storage, fluid spreading and the dynamics in the reservoir for carbon dioxide injection for methane recovery.

Chapter 5 Dependence of clay wettability on gas density

5.1 Summary

New correlations to predict the advancing and receding contact angles of three different clays (i.e. montmorillonite, Illite, and kaolinite) as a function of gas density have been developed. Advancing and receding contact angles of the three clays were measured for helium, nitrogen, argon, and carbon dioxide/brine systems at various pressures (5, 10, 15, and 20 MPa) and a constant temperature of 333 K. The statistical analysis shows that the developed correlations are capable of predicting the contact angles of the three clays with very high accuracy (i.e. $R > 0.95$, for all the newly developed correlations). The results also indicate than the wettability of these clays can be computed from knowledge of the gas densities, using these new empirical correlations. This work has important implications for improving wettability predictions, and thus reducing risks related to subsurface operations, such as carbon dioxide storage or hydrocarbon recovery.

5.2 Introduction

Mitigating global climate change requires immediate actions, to reduce atmospheric carbon dioxide (CO_2) emissions and evade the possibilities of upcoming devastating effects. Geological CO_2 sequestration (GCS) in deep saline reservoirs has received growing recognition to reach this goal (IPCC, 2005). In this process, CO_2 is extracted from stationary emission sources and locked in underground geological formations (Chalbaud et al., 2010; Lackner, 2003; IPCC, 2005). GCS storage efficiency and containment security depend on several CO_2 storage mechanisms, in which structural and residual CO_2 trapping are the main strorage mechanisms (Orr, 2009; IPCC, 2005).

These trapping mechanisms are affected by capillary forces, which exist in the rock pores. Capillarity controls the migration and distribution of CO_2, oil, methane and brine. Wettability is a key aspect determining residual saturations, capillary pressures and relative permeabilities (Anderson, 1986b; Morrow, 1990; Pentland et al., 2011a; Iglauer et al., 2011; Al-Khdheeawi et al., 2018). Thus, the process of CO_2 storage in underground geological formations is affected by rock, water/liquid and gas properties (Arendt et al., 2004; Chalbaud et al., 2009; Yang et al., 2008).

Studies have endeavoured to measure clay wettability through contact angle measurements and researchers have observed several inconsistencies. These studies observed CO_2 contact angles on pure clays (montmorillonite, illite and kaolinite) (Fauziah et al., 2019b), where the results show that montmorillonite is strongly oil-wet, while illite and kaolinite are water-wet. Studies on muscovite (mica) substrates (Chiquet et al., 2007; Farokhpoor et al., 2013; Arif et al., 2016a) show that the water contact angle increased with increasing pressure and salinity, and decreased with increasing temperature. Other studies examined CO_2 on organic shales (Barnet Shale) which mostly contained clay (Guiltinan et al., 2017; Pan et al., 2018; Arif et al., 2017d). In this case, the water contact angle decreased with pressure, and increased with temperature. The wettability of CH_4/brine/clay-coated quartz system has also been investigated, the results show that hydrophobicity increased with pressure (elevated pressure) for clean, kaolinite-coated, and montmorillonite-coated quartz (Pan et al., 2019a). In addition, clay-rich shale wettability has been tested by contact angle and spontaneous imbibition experiments, in which significant discrepancies have been observed for both measurement techniques (Borysenko et al., 2009; Siddiqui et al., 2019; Dehghanpour, 2013; Engelder et al., 2014). Contact angle

measurements are affected by several factors such as surface roughness and salinity, whereas the spontaneous imbibition is more relevant by heterogeneity, morphology of pore structure, and effect of clay minerals (Siddiqui et al., 2019). Prediction of molecular dynamic simulations show that Na-/Ca-montmorillonite is more hydrophobic when exposed to CO_2 at reservoir conditions (Myshakin et al., 2013), while kaolinite surfaces are more hydrophilic due to surface hydroxyl groups (Šolc et al., 2011). Gas densities has been previously shown to correlate with wettability on quartz surfaces (Pan et al., 2019b; Al-Yaseri et al., 2016). However, a similar correlation has yet to be examined on pure clays. In this study, we develop pseudo clay surfaces by compacting pure clay powder into a solid substrate.

To better understand the correlation between gas densities and wettability on pure clay, this research thoroughly analysed the wettability of various clays; montmorillonite, illite and kaolinite, through contact angle measurements. These three clays are important constituents of common rock-forming minerals present in reservoir and caprock lithologies (Iglauer et al., 2015b; Guidotti, 1984), which determine CO_2 sequestration. The measurements were performed for helium (He), nitrogen (N_2), argon (Ar), and carbon dioxide (CO_2)/brine system at various pressures (5 MPa, 10 MPa, 15 MPa and 20 MPa) and a constant temperature of 333 K. New mathematical models were developed from which advancing and receding contact angles can be predicted for montmorillonite, illite, and kaolinite as a function of pressure and gas density. These correlations can be implemented in reservoir simulation to improve CCS planning and operations.

5.3 Methodology

5.3.1 Sample preparation

Three clay powders (montmorillonite, illite, and kaolinite) were mechanically compacted to create solid samples. To eliminate the variabilities from natural sample (e.g., heterogeneities, discontinuities, etc.) and verify the repeatability of experimental results (Feng et al., 2019; Guo et al., 1993), synthetic sample was prepared and used in this study. The clay powders were initially mixed with formation brine (20 wt% NaCl / 1 wt% KCl in deionised water). This mixture was poured into a cylindrical steel cell (constructed inhouse, 10cm long and 3.8cm internal diameter) enclosed with a semi permeable, circular porous plate (porous alumina, 25% porosity, mean pore size < 2 µm). To simulate the natural sedimentary process, axial stress (10 MPa) was applied to the mixture using a high precision, 260D ISCO syringe pump series. Excess brine was expressed through a drainage tube. The compacted cylindrical samples (diameter of 3.8 cm and length of 1cm) were removed from the cell after one week and dried in an oven set at a temperature of 50 °C for 48 hours. All samples were compacted to the same porosity level of 15%. The grain size of montmorillonite, illite, and kaolinite was about 75 μm (Fauziah et al., 2019b). The size of individual clay particles is generally < 2 µm or < 4 µm (Bergaya and Lagaly, 2013; Weaver, 1989; Moore and Reynolds, 1997). The compaction apparatus used is illustrated in Figure 5.1 and details of the samples are provided in Table 5.1.

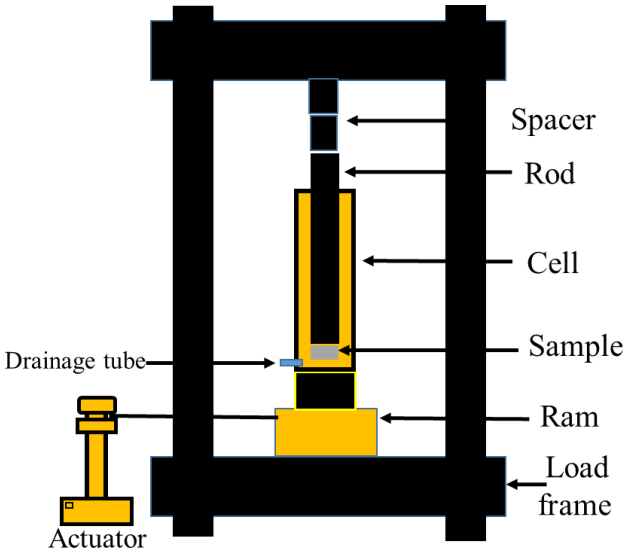

Figure 5. 1 Schematic of the mechanical compaction apparatus

5.3.2 Contact angle measurement

The compacted clay samples were placed into air plasma for 5 minutes to remove organic surface contamination (Love et al., 2005). This cleaning procedure is necessary to ensure accuracy of the results (Iglauer et al., 2014a; Bikkina, 2011). A tilted plate goniometric technique was used (Lander et al., 1993), and the setup comprised a cell designed to run at high temperature-high pressure settings. The detailed experimental setup has been described previously (Fauziah et al., 2019b; Fauziah et al., 2020). Brine (20 wt% NaCl and 1 wt% KCl, with mass fraction purities ≥ 0.99; see Table 5.1, in deionised water) was used for these measurements. The substrate was inserted inside the cell at a set temperature (333 K). He, N_2, Ar, and CO_2, all with mass fraction purities ≥ 0.99; (see Table 5.1), was then injected into the cell using a high precision syringe pump (ISCO 500D; pressure accuracy of 0.1 % FS), and the pressure was raised to pre-set values (5 MPa, 10 MPa, 15 MPa, or 20 MPa). Subsequently, an equilibrated brine droplet (average volume of a single drop was ~6 ± 1 μL) was released onto the surface of the substrate through a needle. The process

was filmed with a high-resolution video camera, and the images extracted from the files to acquire the advancing and receding water contact angle. The standard deviation associated with the contact angle measurements was ± 4°.

Table 5. 1 Provenance and purity of chemicals used

Chemical name	Source of supply	State	Mass fraction
Montmorillonite	Ward's natural	Powder	≥ 0.950
Illite	Ward's natural	Powder	≥ 0.850
Kaolinite	Ward's natural	Powder	≥ 0.950
NaCl	Scharlab s.1.,	Powder	≥ 0.995
KCl	Scharlab s.1.,	Powder	≥ 0.995
CO_2	BOC, Australia	Gas	≥ 0.999
N_2	BOC, Australia	Gas	≥ 0.999
Ar	BOC, Australia	Gas	≥ 0.999
He	BOC, Australia	Gas	≥ 0.999

5.4 Results and Discussion

In this section, new correlations were developed for predicting advancing and receding contact angles for the three different clays (i.e. montmorillonite, Illite, and kaolinite) as a function of gas density and reservoir pressure at an isothermal temperature of 333 K. The density of the four gases (i.e. He, N_2, Ar, and CO_2) was calculated using the Real Gas Equation of State (EOS; Eq 5.1) (Ahmed, 2018), plotted in Figure 5.2:

$$PV = ZnRT \tag{5.1}$$

Where P is the pressure (Pa), V is the volume (m^3), n is the number of moles of gas (mole), Z is the compressibility factor, R is the universal gas constant (8.314 m^3.Pa/K.mol), and T is the absolute temperature (K). In addition, n represents the ratio of weight of the gas (m) to its molecular weight (M), as described below:

$$n = \frac{m}{M} \tag{5.2}$$

Thus, the above EOS can be written as follows:

$$PV = Z\frac{m}{M}\mathrm{RT} \tag{5.3}$$

Where m is the weight of gas (lb), and M is molecular weight (lb/lb-mol).

Gas density (ρ) represents the ratio of gas mass to its volume. Thus, EOS can be rearranged in terms of gas density as follows:

$$\rho = \frac{m}{V} = \frac{P\,M}{Z\,R\,T} \tag{5.4}$$

Where ρ is the gas density (kg/m^3).

Importantly, the compressibility factor (Z) represents the ratio of the actual to the ideal volume of the gas.

$$Z = \frac{V_{Actual}}{V_{Ideal}} \tag{5.5}$$

Here, we used Standing and Katz's chart to calculate the compressibility factor for the used gases at various pressures (Ahmed, 2018).

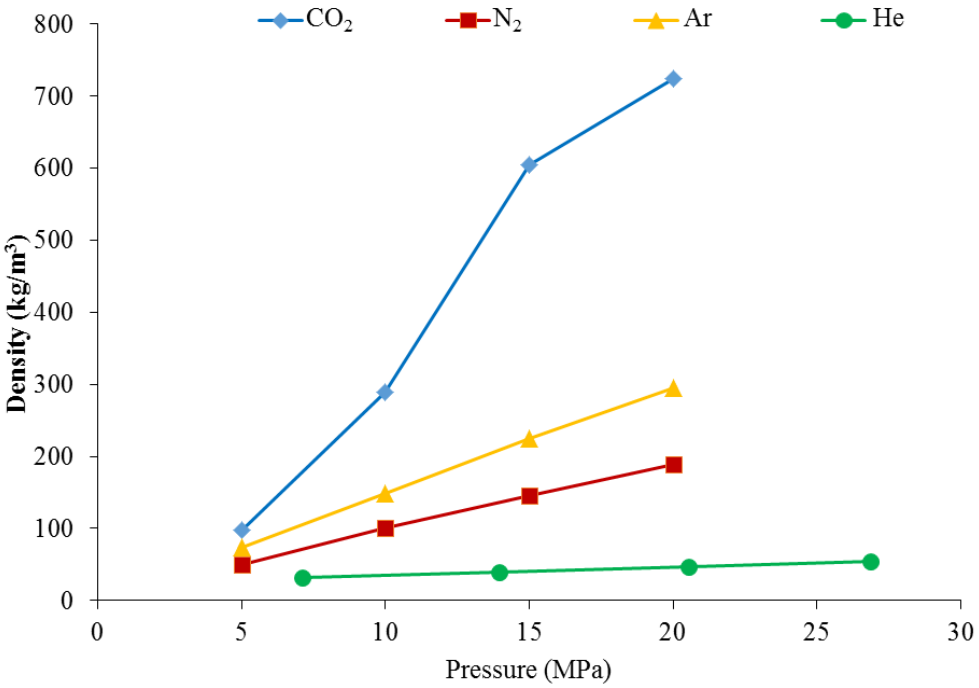

Figure 5. 2 Gas densities for CO_2, N_2, Ar, and He as a function of pressure

Note: the measurement was conducted at a constant temperature of 333 K)

Firstly, a pair of correlations for predicting advancing and receding contact angles for each clay as a function of the gas density only, at a constant temperature (333 K), was developed. The results indicate that the mathematical expressions, which were most representative of the relationships, were found to be the second degree polynomial form for montmorillonite, the logarithmic form for illite, and power form for kaolinite (Equations 5.6 to 5.11):

$$\theta_a\, montmorillonite = -6 \times 10^{-5}\rho^2 + 0.1359\,\rho + 42.256 \quad (5.6)$$

$$\theta_r\, montmorillonite = 7 \times 10^{-5}\rho^2 + 0.1349\,\rho + 39.039 \quad (5.7)$$

$$\theta_a\, illite = 7.2336\, ln\,(\rho) + 13.915 \quad (5.8)$$

$$\theta_r\, illite = 6.917\, ln\,(\rho) + 11.303 \quad (5.9)$$

$$\theta_a\ kaolinite = 17.07\ \rho^{0.1648} \quad (5.10)$$

$$\theta_r\ kaolinite = 15.738\ \rho^{0.1614} \quad (5.11)$$

Where θ_a and θ_r are the advancing and the receding contact angles, respectively; and ρ is the gas density (kg/m^3).

These correlations (Eq. 5.6 to 5.11) are able to predict the advancing and receding contact angles with acceptable accuracies, as indicated in Figures 5.3 and Table 5.2.

Table 5. 2 Statistical accuracy of the developed correlations

Correlation	Correlation Coefficient (R)	Average Absolute Error (%)
θ_a montmorillonite	0.95	8.99
θ_r montmorillonite	0.95	9.22
θ_a illite	0.87	9.32
θ_r illite	0.87	10.32
θ_a kaolinite	0.84	10.62
θ_r kaolinite	0.84	11.71

Note: the developed correlations of θ_a and θ_r as a function of gas density only

The average absolute error is a statistical parameter to measure the average value of the absolute relative deviation of the calculated contact angle from the measured contact angle. The percentage of the average absolute error can be calculated as follows:

$$\text{Average Absolute Error (\%)} = = \frac{1}{n_d} \sum_{i=1}^{n_d} |E_i| \quad (5.12)$$

E_i *is* the relative deviation of the calculated contact angle form measured contact angle:

$$E_i = \left[\frac{(\theta_{calculated} - \theta_{measured})^{x^2}}{\theta_{measured}}\right] \times 100 \qquad i = 1, 2, 3, \ldots n_d \qquad (5.13)$$

A lower value of Average Absolute Error indicates a better agreement between the calculated and measured contact angle.

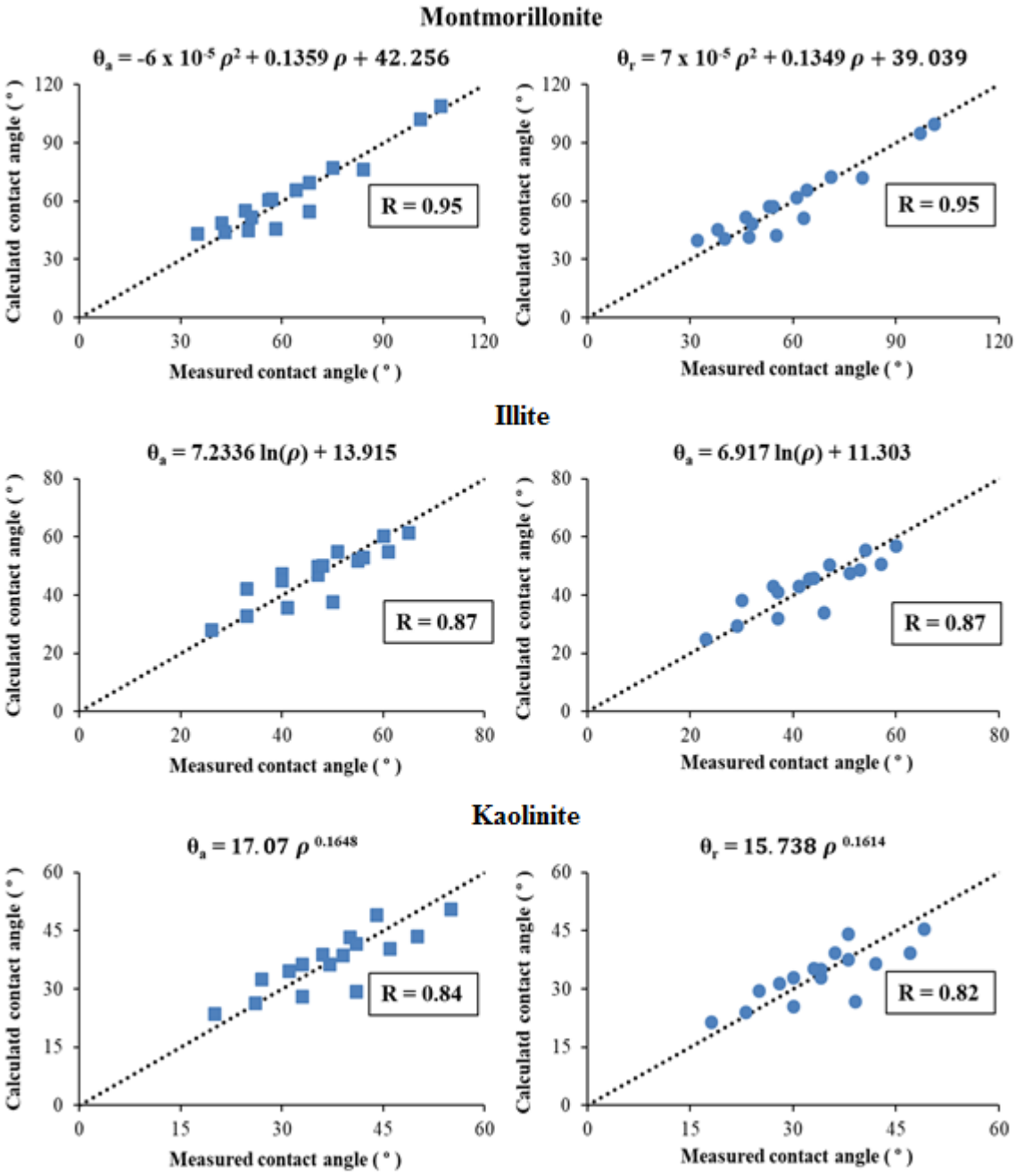

Figure 5. 3 Cross-plot of the experimental and predicted θa and θr

Note: the cross-plot obtained from the newly developed correlation

Subsequently, a pair of empirical correlations for predicting advancing and receding contact angles for each clay as a function of the pressure and gas density (at a constant temperature of 333 K) was developed. Non-linear multiple regression was used to obtain the best match for these data. The following correlations were identified between the two output parameters (advancing and receding contact angles) and the two input parameters (i.e. density and pressure):

$$\theta_a montmorillonite = 0.550812\ \rho^{0.728117} + 34.72902\ P^{0.063920} \quad (5.14)$$

$$\theta_r montmorillonite = 0.574271\ \rho^{0.715856} + 30.56862\ P^{0.084254} \quad (5.15)$$

$$\theta_a illite = 20.54697\ \rho^{0.144684} + 0.044753\ P^{1.908774} \quad (5.16)$$

$$\theta_r illite = 18.00631\ \rho^{0.150726} + 0.039616\ P^{1.947717} \quad (5.17)$$

$$\theta_a kaolinite = 17.37647\ \rho^{0.133958} + 0.001204\ P^{3.090959} \quad (5.18)$$

$$\theta_r kaolinite = 16.66928\ \rho^{0.123224} + 0.000151\ P^{3.771940} \quad (5.19)$$

where *P* is the pressure (MPa).

Ranges for the input and output variables that were used to develop the new correlations (Eq. 5.6 to 5.11 and Eq. 5.14 to 5.19) are summarized in Table 5.3. The correlations (Eq. 5.14 to 5.19) are able to predict the advancing and receding contact angles with an excellent accuracy (Figures 5.4 and 5.5) and Table 5.4. Importantly, Figures 5.4 and 5.5 and Table 5.4 indicate that by including the reservoir pressure in the correlations, improves the accuracy of the correlations of all tested clays.

Table 5. 3 Data ranges used for developing the new correlations

Characteristic	Minimum	Maximum	Mean
θ_a montmorillonite	35	107	63
θ_r montmorillonite	32	101	59.375
θ_a illite	26	65	47
θ_r illite	23	60	43
θ_a kaolinite	20	55	37
θ_r kaolinite	18	49	34
Pressure (MPa)	5	20	12.5
Density (kg/ m^3)	7.11	724.46	188.45

Table 5. 4 Statistical accuracy of the developed correlations

Correlation	Correlation Coefficient (R)	Average Absolute Error (%)
θ_a montmorillonite	0.951	8.44
θ_r montmorillonite	0.952	8.90
θ_a illite	0.966	5.25
θ_r illite	0.968	5.79
θ_a kaolinite	0.979	3.93
θ_r kaolinite	0.969	5.48

Note: the developed correlations of θ_a and θ_r as a function of gas density and reservoir pressure

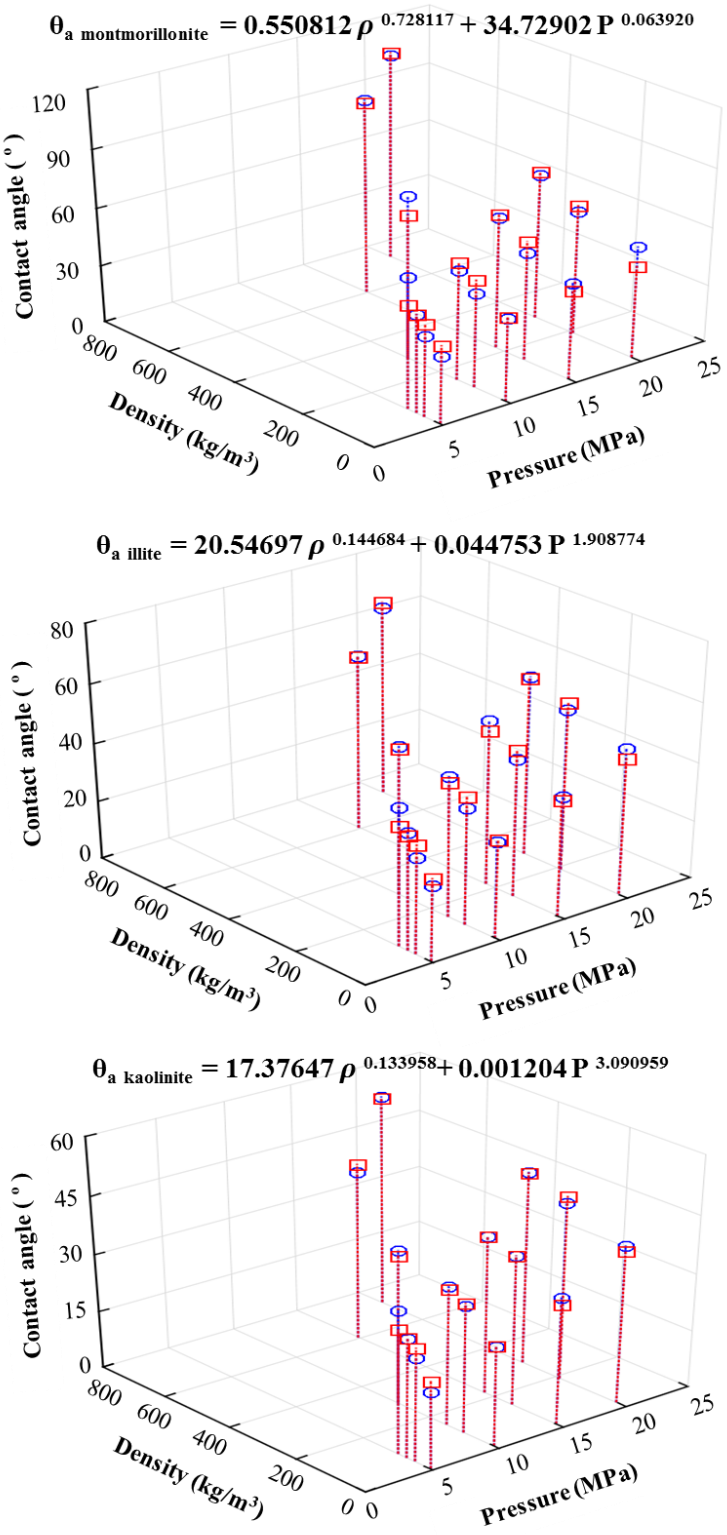

Figure 5. 4 3D scatter plots for the newly developed correlations for advancing contact angle

Note: the newly developed correlations of the θ_a of montmorillonite (top), illite (middle), and kaolinite (bottom) as a function of gas density and pressure

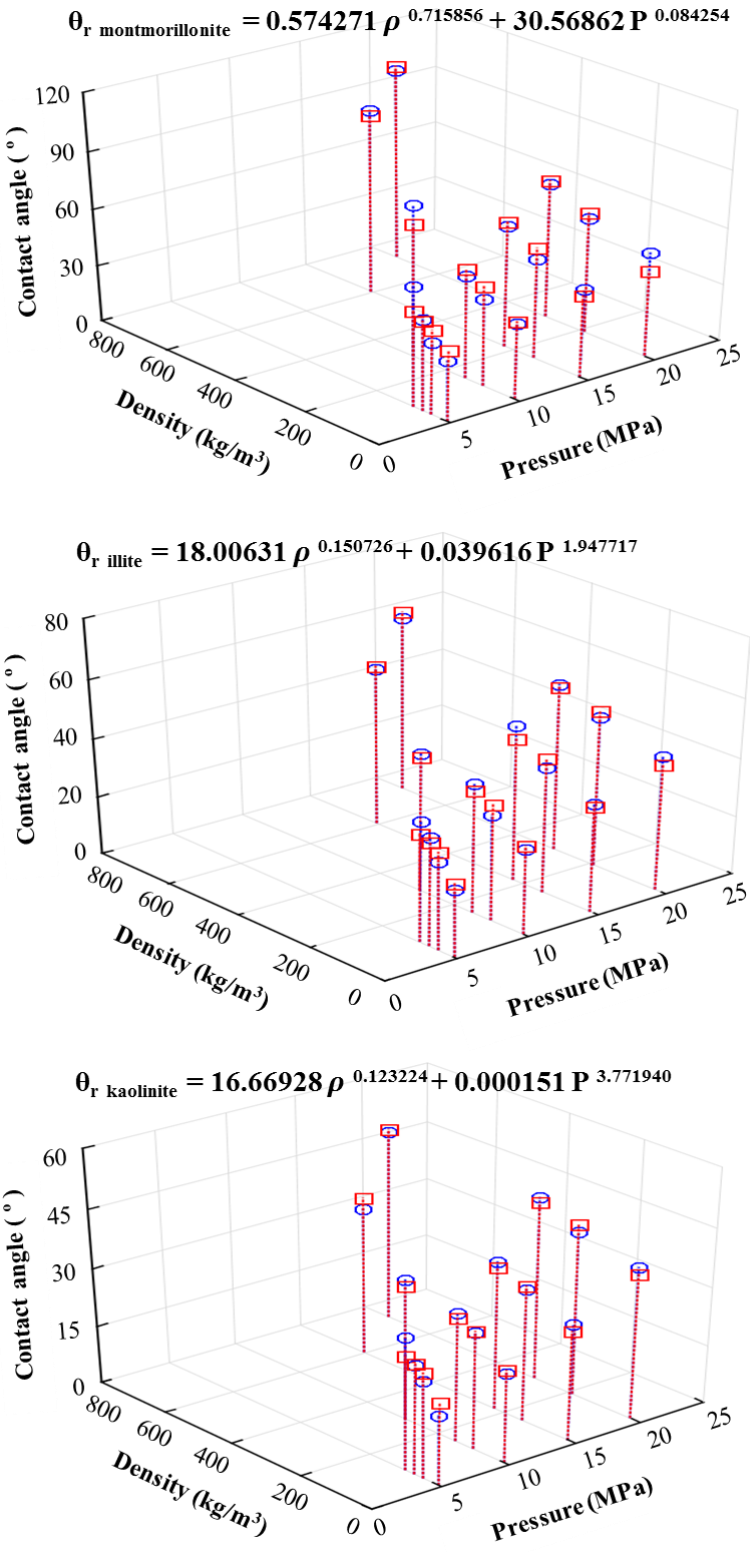

Figure 5. 5 3D scatter plots for the newly developed correlations for receding contact angles

Note: the newly developed correlations of the θ_r of montmorillonite (top), illite (middle), and kaolinite (bottom) as a function of gas density and pressure.

Figures 5.4 and 5.5 show that clay contact angle (i.e. clay wettability) is highly affected by gas density. Our results demonstrate that water gas wetness of clays increased with an increase in gas density (i.e. increasing gas density reduce the water wettability of clays). In addition, the results indicate that higher pressure leads to higher advancing and receding contact angles for all tested gases.

In summary, the results show that gas density and pressure influence montmorillonite, illite, and kaolinite wettability. Increasing pressure and gas density resulted in higher advancing and receding contact angles. These investigations determined that wettability could be successfully correlated to gas density and pressure. This output has important implication for improving the assessment of CO_2 geological sequestration and fluid flow in porous media.

5.5 Conclusions

Clay wettability is a key parameter which controls fluid movement through the porous medium and carbon dioxide storage efficiency. Wettability can be estimated by measuring the contact angle in the laboratory using different experimental methods such as tilted plate technique. However, this laboratory measurement is a time-consuming operation. In this research, six new mathematical models to predict advancing and receding contact angles for montmorillonite, illite, and kaolinite as a function of pressure and density at a constant temperature (333 K), were developed. 16 experimental data points were obtained from four different gases (i.e. helium, nitrogen, argon, and carbon dioxide and four pressures (5 MPa, 10 MPa, 15 MPa, and 20 MPa) for each clay and gas density between 7.11 and 724.46 kg/m^3. The calculated advancing and receding contact angles from the developed empirical correlation have

been compared with the measured contact angles from the laboratory. The results show that the correlation predictions have very high degrees of accuracy. The new correlations predict the contact angle with very high correlation coefficients (R is ranged from 0.951 to 0.979) and very low average absolute errors (AAE is ranged from 3.93% to 8.90%). It is therefore concluded that the newly developed correlations are able to be applied to predict the montmorillonite, illite, and kaolinite advancing and receding contact angles. This work will improve the estimation of clay contact angle and therefore assist with various wettability issues related to CO_2 geo-storage or hydrocarbon recovery.

Chapter 6 Carbon dioxide wettability of South West Hub sandstone, Western Australia: Implications for carbon geo-storage[2]

6.1 Summary

Wettability of carbon dioxide-brine-South West Hub sandstone (GSWA Harvey-1) was systematically analysed at various pressures (0.1 MPa, 5 MPa, 10 MPa, 15 MPa, and 20 MPa) and a temperature of 334 K. A new procedure based on organic carbon isotope tracking ($\delta^{13}C_{org}$) was proposed to eliminate the effect of artificial organic matter introduced by drilling mud penetration. The results indicate that the advancing (θ_a) and receding (θ_r) water contact angles for the carbon dioxide-brine-South West Hub sandstone system increased with increasing pressure (ranging from 71^o-118^o and 66^o-111^o). It can thus be suggested that the system was weakly water-wet to intermediate-wet. When the samples were treated with dichloromethane, a slight decline in organic content was observed leading to slight decrease in water contact angles. The wettability analyses demonstrate that: a) the contact angle is very sensitive to the amount of organic matter and therefore care should be taken to remove artificial organic matter from the sample, and b) this condition prevails in a real proposed carbon dioxide-storage site. These analyses thus have potentially important implications for assessing the feasibility of long-term carbon dioxide storage and enabling large-scale industrial carbon geological storage projects.

[2] *Reference: Fauziah, et al. 2020 in International Journal of Greenhouse Gas Control, 98, 103064. https://doi.org/10.1016/j.ijggc.2020.103064

6.2 Introduction

Carbon capture and storage (CCS) has been identified as a feasible technology to help in alleviating climate change effects by reducing carbon dioxide (CO_2) emissions (IPCC, 2005; Lackner, 2003; Chalbaud et al., 2009). In CCS, CO_2 is captured and collected from large gas emitters in power stations, filtered, concentrated, and then injected into deep geological rock formations for storage (IPCC, 2005). The potential for leakage of CO_2 from the storage reservoirs is a primary concern with CCS, since its density is lower than formation brine, resulting in CO_2 vertical migration. To prevent CO_2 leakage and mitigate CO_2 upward migration, various trapping mechanisms have been examined. These include *structural* (Jamaluddin et al., 1998; Iglauer et al., 2015a), *residual* (Hesse et al., 2008; Qi et al., 2009), *dissolution* (El-Maghraby et al., 2012; Riaz et al., 2006) and *mineral trapping* (Matter et al., 2016; Xu et al., 2003). *Adsorption trapping* in coal and shale such as clay-rich sandstone has been also suggested (Arif et al., 2017d; Busch et al., 2004). One of the key factors, which strongly affects storage capacity and containment security, is CO_2-rock wettability (Iglauer et al., 2015b; Iglauer, 2017). It is essential, therefore, that the science of wettability is characterised in detail. Rock wettability controls processes such as capillary pressure, residual saturation, and relative permeability, which dictates multiphase flow at reservoir-scale (Al-Khdheeawi et al., 2018).

Several studies have attempted to measure rock and mineral wettability through contact angle measurements. Researchers have observed several inconsistencies. For example, some studies reveal that with increasing pressure, the water contact angles increased (Alnali et al., 2018; Al-Yaseri et al., 2016; Fauziah et al., 2019b; Fauziah et al., 2019a; Saraji et al., 2013). However some other researchers did not observe such

increases (Espinoza and Santamarina, 2010; Farokhpoor et al., 2013; Wang et al., 2012a). Furthermore, the water contact angles were both observed to decrease (Bikkina, 2011; Saraji et al., 2013; Fauziah et al., 2019b), and increase with temperature (Alnali et al., 2018; Al-Yaseri et al., 2017b; Farokhpoor et al., 2013). Most importantly, hydrophobic surfaces can be CO_2-wet at high pressure (Iglauer, 2017), while variation in temperature induces different wetness (Al-Yaseri et al., 2017b). This is consistent with the observation that a high total organic content (TOC) leads to a high water contact angle and thus a decrease in water wettability (Arif et al., 2017d; Siddiqui et al., 2018; Yassin et al., 2017), although other studies found no influence of TOC (Guiltinan et al., 2017). More recently, it has been shown experimentally and theoretically that even minute concentrations of organics adsorbed on the mineral surface increases hydrophobicity significantly, and thus CO_2-wettability (Abramov et al., 2019). It is evident that increases in organic matter causes the rocks to be more hydrophobic (Siddiqui et al., 2018); while the distribution and connectivity of organic and inorganic matter control the precise wetting behaviour of the rock (Hu et al., 2016).

Despite these efforts, little is known how reservoir storage formations behave, and what wettability response might be expected if CO_2 is injected into the storage reservoir. In this work, an objective is to benchmark the wettability of a storage rock samples retrieved from a proposed storage site (SW Hub) (Saeedi et al., 2016a; Stalker et al., 2013a). The effect of organics, pressure, porosity and surface roughness were analysed, and the implications of the results on CO_2 geo-storage are discussed. In addition, a procedure to remove artificially introduced organic matter (from drilling mud) is presented to enable true contact angle measurements and improvements in the interpretations.

6.3 Experimental Methodology

6.3.1 Core samples

Four selected sandstone samples retrieved from GSWA Harvey-1 well were systematically analysed. GSWA Harvey-1 is a stratigraphic well located in the southern Perth Basin (the South West Hub), Western Australia, which has been proposed as a potential CO_2 storage site in the region near large-scale industrial emitters (Stalker et al., 2013a). The South West Hub area comprises the Triassic Lesueur Sandstone, which is divided into the upper Yalgorup (704-1380 m) and the lower Wonnerup Members (1380-2895 m) (Olierook et al., 2014). Harvey-1 well was drilled in 2012 by Geological Survey of Western Australia (GSWA) and reached a total depth of 2945 m (Olierook et al., 2014). The drilling fluid (or drilling mud) used to drill the Harvey-1 well was classified as a water-based mud, supplied by Newpark Drilling Fluid Australia. The mud formulation consisted of KCl (5 wt %) to control the clay swelling, barite (as required), and caustic soda (0.57 kg/m^3) to control mud weight, bentonite (40 kg/m^3) and xanthan gum (1.88 kg/m^3) to control rheology of the mud, rheopac LV (mixture of sodium carboxymethyl cellulose (> 88 wt%), sodium chloride (< 1.8 wt%), water (< 10 wt%), and sodium glycolate (< 0.7 wt%)) to control fluid loss along with soda ash (1.43 kg/m^3) (DMPWA, 2012). The well and material were substantially tested including petrography, wireline logging, coring, spectral analysis and core analysis (Millar and Reeve, 2014; Pevzner et al., 2013; Delle Piane et al., 2013; Saeedi et al., 2016b; Stalker et al., 2013a).

In this study, the tested core samples were retrieved from the Wonnerup member of the Triassic Lesueur sandstone, as reported in Table 6.1. The samples were thoroughly characterised with quantitative x-ray diffraction (XRD), atomic force microscope

(AFM), scanning electron microscopy-energy dispersive x-ray spectroscopy (SEM-EDX), total organic carbon (TOC) and organic carbon isotopic composition ($\delta^{13}C_{org}$) analyses. The samples mainly consisted of quartz, substantial amounts of feldspar/microcline, significant amounts of clay, and a small number of other minerals in low concentrations, Table 6.2.

Table 6. 1 Harvey core descriptions

Core ID	Sample Type	Core Description	Facies Type
Core A	Horizontal core plug	Coarse to gravelly sandstone, cross-bedded, clay-rich	Aii*
Core B	Horizontal core plug	Very coarse sandstone	Ai*
Core C	Horizontal core plug	Fine sandstone, cross-laminated	C**
Core D	Horizontal core plug	Fine to coarse sandstone, cross-bedded	Aii*

Source: (Delle Piane et al., 2013)

*Facies Ai, Aii to Aiii are coarse to very coarse grained sandstone
**Facies C is fine to medium grained sandstones

Table 6. 2 Harvey core characterisation and mineralogy

Core ID	Depth[a] (m)	Porosity[b] (%)	Permeability[c] (mD)	TOC[d] (%)	Surface Roughness[e] (nm)	Mineral Constituents[f]	
						Mineral	wt %
Core A	2520	10.7	2.37	0.015	520	Quartz	73.5
						Microcline	14.5
						Chlorite/Serp	6.2
						Kaolin	3.4
						Illite	1.9
						Anatase	0.5
Core B	2520.4	13.63	107.99	0.017	1100	Quartz	67.7
						Microcline	22.8
						Kaolin	7.3
						Illite	1.6
						Chlorite/Serp	0.5
						Anatase	0.1
Core C	2523.3	2.08	< 0.01	0.019	2300	Quartz	45.5
						Kaolin	33.2
						Microcline	9.3
						Illite	8.2
						Anatase	2.5
						Chlorite/Serp	1.3
Core D	2525.8	11.86	4.68	0.01	1200	Quartz	73.9
						Microcline	16.5
						Chlorite/Serp	5.3
						Kaolin	4
						Illite	0.3
						Anatase	0

[a,b,c]Data provided by Geotechnical Services Pty Ltd
[d]TOC was measured with FLASH 200 HT Elemental Analyzer
[e]Surface roughness was measured with Atomic Force Microscope-AFM DSE 95-200
[f]Mineral constituent of the samples were analysed with X-Ray Diffraction (XRD)-Bruker-AXS D9 Advance Diffractometer

6.3.2 Contact angle measurements

The rock samples were cut into smaller sample discs (5 mm thick, 38 mm in diameter) using a high-speed diamond blade. Each sample was then placed into air plasma for 5 minutes to remove surface contamination (Love et al., 2005). The cleaning procedure is a necessary phase to ensure accuracy of the results (Iglauer et al., 2014a; Bikkina, 2011). Prior to each measurement, the surface topography of each sample was measured with an AFM (Instrument model DSE 95-200), Figure 6.1. The advancing

(θ_a) and receding (θ_r) water contact angle were then measured using the tilted plate technique (Lander et al., 1993) and a high temperature-high pressure goniometer. For this experiment, the substrate was placed on the tilted surface with an inclination angle of $\alpha = 12^o$.

The measurements were conducted using brine with a salt concentration of 31,389 mg/L (~31,400 mg/L), which is representative of Harvey-1 conditions, by mixing $CaCl_2$, $MgSO_4.7H_2O$, KBr, NaCl, $NaHCO_3$, $SrCl_2$, and $CuSO_4.5H_2O$ (Saeedi et al., 2016b) (with mass fraction purity ≥ 0.99; see Tables 6.3). The cleaned samples were inserted in the pressure cell at a set temperature (334 K), representing Harvey-1 reservoir temperature at 2000 m depth. CO_2 was then injected into the cell by using a high precision syringe pump (ISCO 500D; pressure accuracy of 0.1 % FS), and the pressure was raised to pre-set values (0.1 MPa, 5 MPa, 10 MPa, 15 MPa, or 20 MPa). The schematic of the experimental setup is illustrated in Figure 6.2. Subsequently, an equilibrated brine droplet was released onto the surface of the substrate through a needle after the pressure attained the set pressure. It is noted that sufficiently large volume of CO_2 (> 200 ml) was injected into the cell from another pump and then left for interaction with brine in another pump at set temperature and pressure until no change in pump pressure, observed when the brine is equilibrated with CO_2 or when the brine is saturated by CO_2.

The whole process was recorded using a high-resolution video camera (Fauziah et al., 2019b). Thereafter, the contact angles were measured on the images extracted from the videos. The measurement of the advancing and receding water contact angles were

attained at the leading and trailing prior to the onset of the droplet movement; and the standard deviation associated with the contact angle measurements was ± 4º.

6.3.3 Dichloromethane (solvent) treatment

The samples' total organic content may have been affected by outside intrusion of organic matters from the drilling mud. It is possible to restore the original surface properties by cleaning with a particular solvent (Cuiec and Yahya, 1991). The samples were treated with dichloromethane (DCM, CH_2Cl_2, purity = 99.9 mol %) to remove this introduced organic matter (Muller et al., 2018; Thomazo et al., 2009; Wright et al., 1997).

To identify the source of organic content, the TOC and composition of organic carbon isotope ($\delta^{13}C_{org}$) were measured on the samples. The samples were dried in an oven at 50 ^{o} C overnight. Note that TOC is a key variable which determines the contact angle (Arif et al., 2017d; Al-Anssari et al., 2017). Precisely, the TOC content and $\delta^{13}C_{org}$ values were determined for DCM-treated and DCM-untreated aliquots (from powdered samples) using an elemental analyser-isotope ratio mass spectrometer (EA-IRMS). The TOC content and $\delta^{13}C_{org}$ values for the drilling mud were also measured in similar way as the untreated rock samples. Specifically, an aliquot of the rock samples was treated with 1M HCL solution to remove inorganic carbon and subsequently washed multiple times with Milli-Q (MQ) water and dried/ground before further analyses. Another aliquot of the sample was dried and ground before analyses. The samples were weighed into tin cups and analysed on the Thermo Flash 2000 Elemental Analyser with a thermal conductivity detector, which is connected to a Thermo MAT 253 isotope ratio mass spectrometer (IRMS). In the elemental analyser,

the sample was injected into an oxidation oven at 1000 °C and the carbon in the sample was converted to CO_2. A GC column separated the CO_2 from other produced gas which first pass through the thermal conductivity detector (TCD) and then to the isotope ratio mass spectrometer. The percent total carbon of the sample was determined by analysing the untreated aliquot with a calibrated elemental analyser, while the percent TOC was determined form the acid treated aliquot. The total inorganic carbon was that determined from subtracting the percent TOC from the total carbon. The CO_2 was subsequently analysed by the MAT 253 IRMS where the untreated sample reflected the $\delta^{13}C_{org}$ from the total carbon (TC) and the treated sample reflects the carbon isotopic value of the organic carbon in the sample. Delta notation (δ) and permil (‰) (relative to the Vienna Pee Dee Belemnite (VPDB) standard) are used here for the carbon isotopic composition (Muller et al., 2018). Additional contact angle measurements were subsequently performed on each DCM-treated sample.

Table 6. 3 Composition of brine used*

Chemical name	Chemical formula	Concentration, mg/L
Calcium chloride	$CaCl_2$	1200
Magnesium sulphate hydrated	$MgSO_4.7H_2O$	600
Potassium bromide	KBr	183
Sodium chloride	NaCl	26659
Sodium bicarbonate	$NaHCO_3$	125
Strontium chloride	$SrCl_2$	100
Copper (II) sulphate pentahydrate	$CuSO_4.5H_2O$	2522
Total dissolved solid (TDS)		31389

*The brine is representative the Harvey 1 reservoir conditions and data calculated as explained in detail in (Saeedi et al., 2016b)

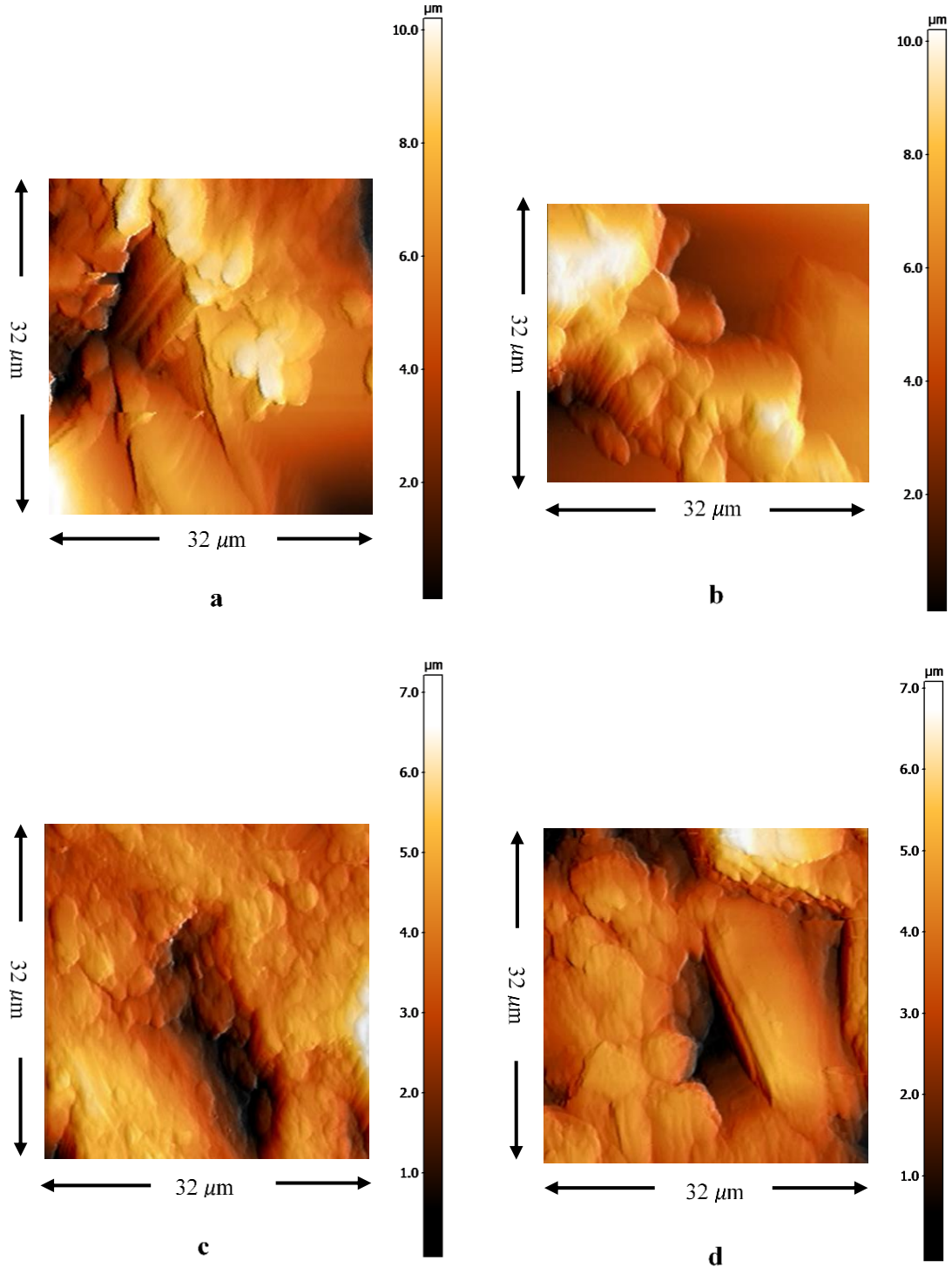

Figure 6. 1 Core surfaces imaged by Atomic Force Microscopy

Note: (a) Core A with root-mean-square (RMS) of 520 nm, (b) Core B with RMS of 2300 nm, (c) Core C with RMS of 1200 nm, (d) Core D with RMS of 1100 nm

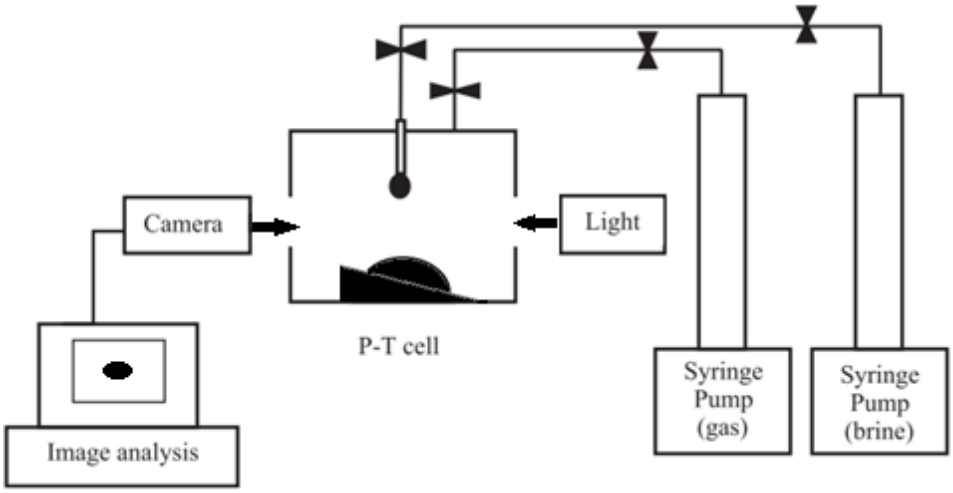

Source: adapted from Al-Yaseri et al.(2015)

Figure 6. 2 Schematic of the contact angle apparatus

6.4 Results and Discussion

Understanding CO_2-rock wettability is essential for CO_2 geo-storage planning, since wettability directly influences fluid flow, storage capacity and containment security (Al-Khdheeawi et al., 2018; Al-Anssari et al., 2017; Espinoza and Santamarina, 2010). However, wettability is a complex phenomenon which can be influenced by pressure, temperature, salinity, mineral type, pH, TOC, etc (Iglauer et al., 2015b; Arif et al., 2017d; Al-Yaseri et al., 2016). Additional complexity further arises when contact angles are measured on real rock substrates and not pure minerals and when the core sample is exposed to drilling fluids.

6.4.1 Effect of organic content on CO_2-rock wettability

The influence of organic content on CO_2 wettability has been recognised (Jha et al., 2019b; Abramov et al., 2019; Iglauer, 2017). Harvey sandstone substrates for a broad range of operating pressures (0.1-20 MPa) at 334 K were thus comprehensively examined. The results of θ_a and θ_r were shown to range between 71°-118° and 66°-

111°, respectively (Figure 6.3 (a) and 6.3(b)). Only a slight decline in organic content was observed when the samples were treated by DCM (see Table 6.4); this slight decline in organic content decreased θ_a and θ_r by 7° and 8°, respectively (Figure 6.3(c) and 6.3(d)). It is noted that the standard deviation from the replicate measurements is ± 4 degree that sits above measured contact angle values due to removal of organic matter.

It is noted that sample treatment with DCM lowered TOC by dissolution of an organic soluble fraction (Muller et al., 2018; Keshavarz et al., 2019). Such organic solvents (e.g. DCM) remove artificial organic fractions (associated with subsurface biological activity, groundwater penetration, drilling fluids, sampling and storage) (Brocks, 2011; Brocks et al., 2003; Muller et al., 2018; Gérard et al., 2009), but not all organic content in the samples can be extracted (e.g. kerogen). As the samples are sandstones and not source rocks, it is unlikely that they will contain significant volumes of organic matter except for some kerogen, originally. It is known that kerogen is not soluble in organic solvent such as DCM. From this study, it is evident from the values of TOC/$\delta^{13}C_{org}$ (Table 6.4) that this indigenous organic fraction relating to the host rock represents a significant natural organic fraction. TOC percent-change after solvent treatment remains fairly low, 29.5%, except for samples core C (having a large clay fraction that is prone to adsorb contaminants (Muller et al., 2018)), which is approximately 89.5%. Contact angle (both advancing and receding at any given pressure ≥ 5MPa) values range in value in the order sample C > sample B > sample D > sample A corresponding to kaolinite content 33.4%, 7.3%, 4%, and 3.4%, respectively for both solvent treated and untreated samples. Further to this, it is clearly evident that contact angles (both advancing and receding) also reduce due to treatment by solvent and the reduction in

TOC. However, this could not be compared quantitatively (in this work) with the TOC change due to the difference in measurement process since TOC measurements are performed for powdered samples. It is thus secure to assume that the organic matter removed was the contamination from other artificial organic fractions, and not the in situ kerogen, at least majority of it.

Note that such organic content in the samples was not as a result of contamination from the drilling mud. The drilling mud is high in organic content with a different isotopic composition (compare Table 6.4). It can be concluded that the samples contained no organic contamination from drilling mud. The extraction of small amounts of organic matter tends to decrease the contact angle. As an example, after treating Core C with DCM, TOC decreased from 0.019% to 0.003%, and the corresponding θ_a and θ_r decreased from 118^o and 111^o to 110^o and 104^o, respectively, at 20 MPa and 334 K. This implies that even smaller quantities of organic content result in intermediate-wet conditions, consistent with systematic experiments on pure calcite or quartz substrates (Abramov et al., 2019). As such, minute concentrations always prevalent in the subsurface (Jones et al., 2008; Bennett et al., 1993; Stalker et al., 2013b; Kharaka et al., 2009; Ni et al., 2015), intermediate-wet or weakly water-wet conditions can be expected in even deep saline aquifers.

Other studies have analysed the effect of TOC on CO_2 wettability and therefore on storage potential (Arif et al., 2017d; Guiltinan et al., 2017; Roshan et al., 2016a). The above-mentioned studies agreed that even minute amount of TOC strongly affect the reservoir storage capability and containment security. Other researchers (Pan et al., 2018; Siddiqui et al., 2018; Yassin et al., 2017) have investigated that there is a positive

correlation between contact angle and TOC, where generally, higher TOC result in higher contact angle. This is consistent with this study where the TOC values were very low.

6.4.2 Contact angles of Harvey sandstone as a function of pressure

Advancing (θ_a) and receding (θ_r) water contact angles were also evaluated at various pressures (0.1 MPa, 5 MPa, 10 MPa, 15 MPa and 20 MPa) at 334 K on the Harvey sandstone substrates. The contact angles for all tested sandstones increased with an increase in pressure; for instance, as the pressure increased from 5 MPa to 20 MPa at 334 K, the θ_a and θ_r for core A increased from 71^o to 92^o and from 66^o to 89^o, respectively (Figure 6.3(a) and 6.3(b)). This behaviour has been explained by other researchers as being related to increasing CO_2 density, which strengthens the CO_2 and mineral intermolecular interactions, and therefore leads to de-wetting of the surface (Roshan et al., 2016a; Arif et al., 2016b).

At any given temperature, CO_2 solubility in water as well as brine increases with increase in pressure, as does the density of CO_2-water (or brine) mixture (Li et al., 2004). In addition, at a given temperature, interfacial tension (IFT) between dissolved CO_2 + water (or brine) mixture and CO_2 decreases with increase in pressure (Bachu and Bennion, 2009; Chalbaud et al., 2009). Thus, we chose to calculate IFT between dissolved CO_2 + brine and CO_2 at 20 MPa (highest pressure) and 334 K in this work using pendant drop method (Jha et al., 2019a; Jha et al., 2019b) for its further use in the calculation of Bond number as suggested in the work of Kaveh et al. (2014). Theoretically, Bond number less than 1 implies dominating effect of interfacial tension (and not gravity or buoyancy) (Kaveh et al., 2014). The densities of dissolved CO_2 +

brine (this work) and CO_2 at 20 MPa and 334 K is approximately 1050 kg/m^3 (Li et al., 2004; Safarov et al., 2009) and 814 kg/m^3 (Müller and Gelb, 2003), respectively. The measured IFT is 28.74 mN/m which gives a reasonable match for similar system from the work of (Bachu and Bennion, 2009), and (Chalbaud et al., 2009). The characteristic length (drop diameter) calculated to be 3.31 mm (drop volume ~ 18.97 mm^3) which gives Bond number ~ 0.88, thus, indicating dominating effect of interfacial tension (and not gravity or buoyancy) (Kaveh et al., 2014).

The contact angle results obtained on dichloromethane treated samples to those of untreated samples were thus compared. The θ_a and θ_r after dichloromethane treatment decreased noticeably, Figure 6.3 (c) and 6.3(d). For example, θ_a for core A after treatment with dichloromethane at 5 MPa was 65^o, compared to the untreated core A, where θ_a was measured 71^o. The same trend shows that there was an increase in the water contact angles for all samples tested when the pressures increased. This is consistent with measurements reported in the literature for contact angles of water/CO_2/Warro sandstone (Alnali et al., 2018), water/CO_2/kaolinite (Fauziah et al., 2019b), water/CO_2/calcite (Saraji et al., 2013; Jung and Wan, 2012; Bikkina, 2011) and water/CO_2/quartz (Al-Yaseri et al., 2016; Saraji et al., 2013) systems.

In addition, Core C has higher contact angle than other samples, for example, θ_a for Core A at the pressures 15 MPa and 20 MPa were 86^o and 92^o, respectively, compare to Core C, where the θ_a at the same pressures was measured 112^o and 118^o, respectively. The difference is likely to be linked to the different composition of mineral constituent in particular the presence of clays in each sample, as shown in Table 6.1, i.e. Core C consisted of significant amounts of clay (kaolin 33.2%, illite 8.2%, and chlorite 1.3%).

Clay adsorbs organic contaminants by various mechanisms (such as ion exchange, protonation of organic molecules, ion dipole formation, hydrogen bonding, hydrophobic bonding, etc.) (Kowalska et al., 1994; Awad et al., 2019). The maximum change in TOC after DCM treatment has been observed for Core C due to high-adsorbed organic contaminants (attributed to high clay content).

Table 6. 4 TOC and $\delta^{13}C_{org}$ values measured for untreated and treated samples

	Untreated sample		Treated sample with DCM	
Sample	TOC (%)	$\delta^{13}C$ (‰)	TOC (%)	$\delta^{13}C$ (‰)
Core A	0.015	-27.2	0.012	-26.3
Core B	0.017	-26.7	0.012	-26.7
Core C	0.019	-26.4	0.003	-26
Core D	0.01	-34.3	0.008	-32.4
Drilling mud	2.51	11.64	-	-

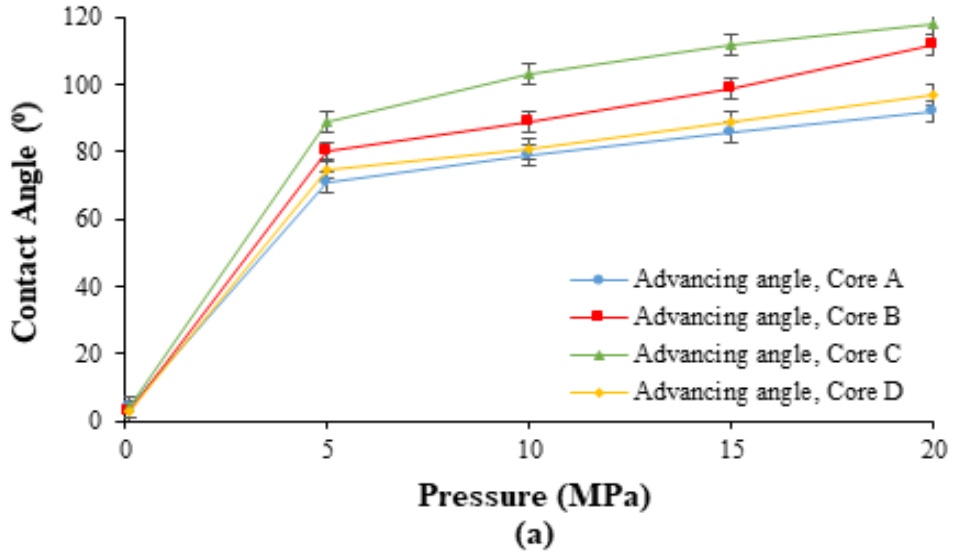
Contact Angle (º)
120
100
80
60
40
20
0
0
5
10
15
20
Pressure (MPa)
Advancing angle, Core A
Advancing angle, Core B
Advancing angle, Core C
Advancing angle, Core D

(a)

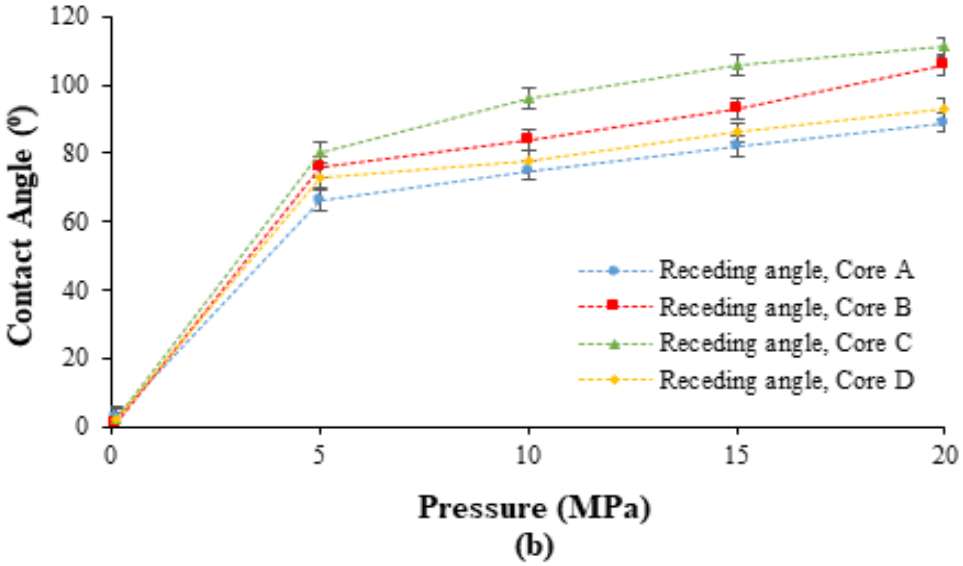
Contact Angle (º)
120
100
80
60
40
20
0
0
5
10
15
20
Pressure (MPa)
Receding angle, Core A
Receding angle, Core B
Receding angle, Core C
Receding angle, Core D

(b)

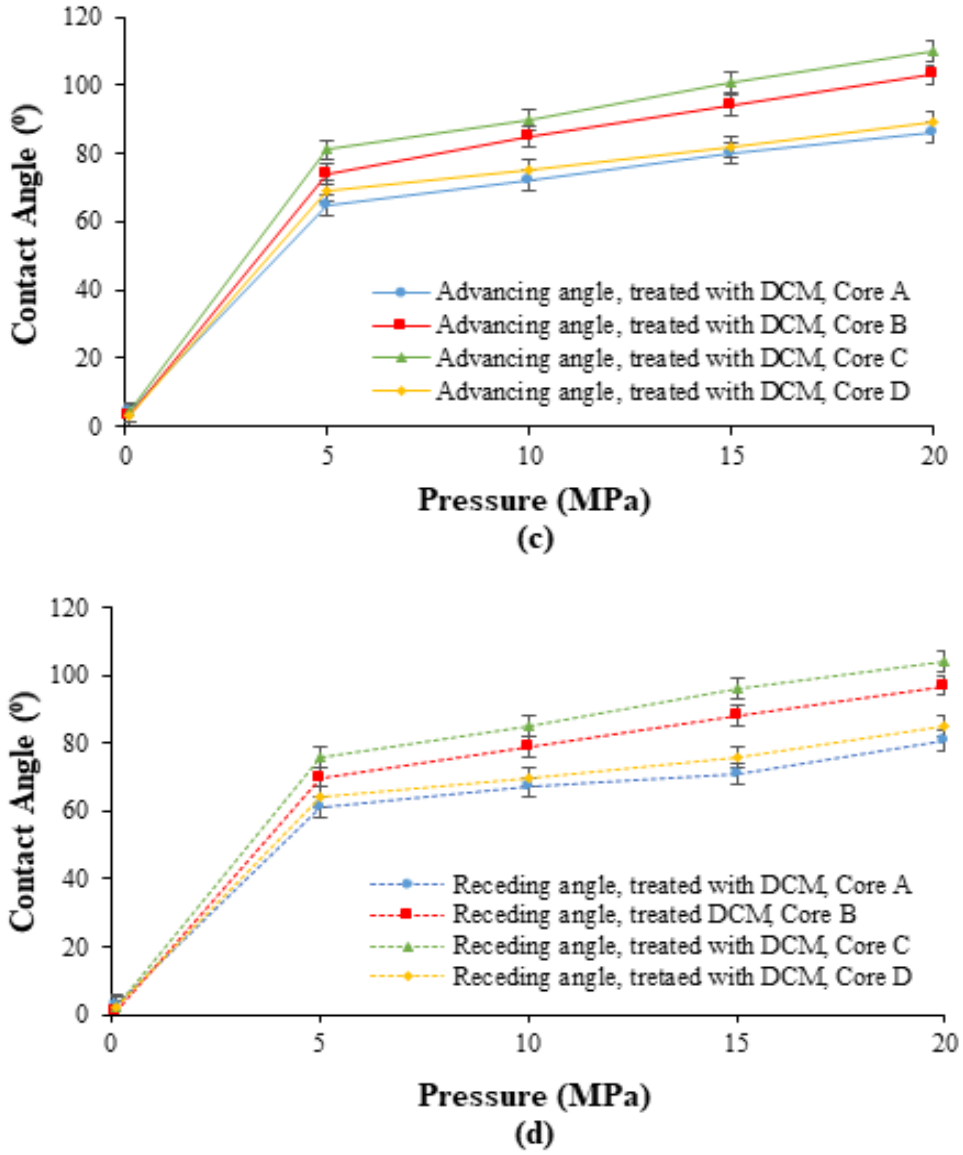

Figure 6. 3 θa (a&c) and θr (b&d) of Harvey cores as a function of pressure

Note: (a) and (b) untreated cores; (c) and (d) cores treated with dichloromethane (DCM), measured at 334 K for Harvey sandstones/CO_2/brine system

6.4.3 Influence of surface roughness and pores on contact angle measurements

Surface roughness influences the contact angle; therefore, the Wenzel equation was used to explain the effect of surface roughness (Wenzel, 1936).

$$cos\ \theta_{rough} = r\ cos\ \theta_{smooth} \tag{6.1}$$

where θ_{rough} is the contact angle measured on the rough surface and θ_{smooth} is the contact angle on an (imagined) ideal surface; r is the ratio of measured roughness and the projected (ideal) roughness of solid surface. Therefore, r is equal to 1 for an ideal surface and greater than 1 for a rough surface (Fauziah et al., 2019b). In this work, r was measured by AFM, Table 6.5: the actual length of the profile line (L_a) was divided by the projected length of profile line (L_i). The measurement was conducted repeatedly for five different profile lines. These measurements were averaged to obtain r. The results show that the θ_{smooth} values are considerably higher than θ_{rough}. Furthermore, the Harvey sandstone samples examined here were composed mainly of quartz, as shown in Table 6.1. The mathematical model below developed by Alnali et al. (2018) takes into consideration the presence of pores of the Harvey sandstone samples. The abbreviation γ denotes the interfacial tension for solid (S), gas (G) and liquid (L) phases; ϕ, h *and* r denote porosity, average capillary rise in the pore system, and average pore radius, respectively.

$$\gamma_{LG}\ cos\ \theta = \gamma_{SG} - \gamma_{SL} - \frac{2\phi\gamma_{LG} cos\ \theta}{r} h \tag{6.2}$$

Moreover, the Cassie-Baxter equation was considered to evaluate the accuracy of forecasting the measured contact angle data of the tested samples.

$$cos\ \theta_c = f_i\ cos\ \theta - (1 - f_i) \tag{6.3}$$

where θ_c is the predicted Cassie-Baxter contact angle, f_i is the fractional projected area of a material with smooth surface contact angle, θ, and $(1- f_i)$ and $(1- f_i)$ reflects the contribution of the remaining CO_2 under the drop (Milne and Amirfazli, 2012; Alnali et al., 2018).

The number of surface pores, pore throat diameter, and height of fluid infiltration, respectively significantly influences the magnitude and kinetics of contact angle variation on a porous surface (Roshan et al., 2016b; Strand et al., 2003). The new method described in Eq. 6.2 and Cassie-Baxter was applied to analyse the contact angle. The results are shown in Figure 6.4. For this the porosity data given in Table 6.2 was applied, h = 0.5 mm, and the interfacial tension obtained by interpolation data given in Arif et al. (2016b). Results indicate that the contact angles obtained using Cassie-Baxter equation, and derived by Alnali's model for porous rock, were systematically higher than the apparent ones measured in the laboratory. This could be due to the presence of pores in sandstone. Such an increase in contact angle due to the existence of pores was related to the capillary-driven forces acting at the pore throat surface, as mathematically formulated earlier (Alnali et al., 2018; Al-Yaseri et al., 2016).

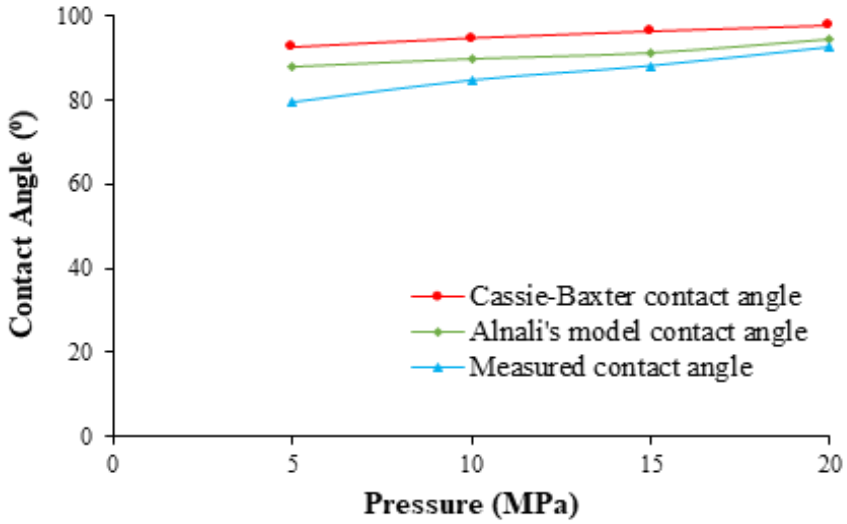

Figure 6. 4 Comparison of the equilibrium contact angles of Harvey sandstones

Note: comparison of the contact angles acquired through the laboratory experiments, the Cassie-Baxter model and Alnali's model (2018) at a temperature of 334 K for advancing water contact angle of core A.

Table 6. 5 θa and θr on the rough and smooth surface at 20 MPa and 343 K

Core ID	RMS*(nm)	T (K)	θ_a rough (°)	θ_r rough (°)	r**	θ_a smooth*** (°)	θ_r smooth***(°)
Core A	520	334	79	75	2.048	84.6	82.7
Core B	1100	334	89	84	2.131	89.5	87.2
Core C	2300	334	91	88	2.064	90.8	89.0
Core D	1200	334	81	78	2.011	85.5	84.1

*RMS = root-mean-square surface roughness
**r is roughness ratio
***θ_a / θ_r smooth were predicted via the Wenzel equation

6.5 Conclusions

It is evident CO_2 wettability of the storage and seal rock significantly can affect injectivity, CO_2 fluid dynamics, storage capacity, and containment security (Al-

Khdheeawi et al., 2018; Iglauer et al., 2015a; Iglauer, 2017), and thus the project economics and technical feasibility. Wettability of Harvey (Lesueur) sandstone retrieved from a proposed storage site, the South West Hub, Perth Basin, Western Australia at various pressures (0.1 MPa, 5 MPa, 10 MPa, 15 MPa, and 20 MPa) and temperature (334 K, representing Harvey 1 reservoir temperature at above 2000 m depth) were therefore measured. The organic carbon isotopic composition ($\delta^{13}C_{org}$) was also analysed to obtain information on the effect of drilling mud and original TOC on wettability.

This study found that the advancing (θ_a) and receding (θ_r) water contact angles increased with increase in pressure, θ ranged between 71°-118° and 66°-111°, respectively. These results imply that the wettability of the system changed from weakly water-wet to intermediate-wet at higher pressures. When the samples were treated with DCM, a slight decline in organic content was observed; this was associated with a slight decrease in advancing (θ_a) and receding (θ_r) water contact angles. The result implies that even minutes amounts of TOC, can affect the wettability. An increase in contact angle with pressure is also evident, which is caused by an increase in CO_2 density. The increase in CO_2 density results in higher the intermolecular interactions between CO_2 and mineral, and therefore resulting in de-wetting of the surface (Roshan et al., 2016a; Arif et al., 2016b; Al-Yaseri et al., 2016).

We thus conclude that even low TOC drastically increases CO_2 wettability, which may affect residual trapping capacities. It is evident that a detailed understanding of the organic matter concentration in a reservoir is vital for assessing the feasibility of long-

term geological CO_2 storage. This work will thus aid in planning and implementing large-scale industrial CO_2 geo-storage.

Chapter 7 Effect of CO_2 flooding on wettability evolution of sandstone

7.1 Summary

Contact angle of sandstones with varying clay content (Berea with low clay content and Bandera Gray with high clay content) was measured at different reservoir pressures of 10 MPa and 15 MPa and temperature of 323 K. The measurements were conducted for the samples before and after laboratory core flooding with carbonate water to characterise their wettability. The samples' microstructural changes were also assessed to investigate any potential alteration due to carbonated water exposure. The results indicate that Bandera Gray sandstone has a higher contact angle, i.e., it is more likely related to specific clay type in the sandstone samples. Besides, the sandstones turn slightly more hydrophobic after core flooding, indicating that the sandstones become more carbon dioxide-wet after carbon dioxide injection. This suggested that carbon dioxide flooding leads to an increase in the carbon dioxide-wettability of sandstone. This has important implications for carbon dioxide trapping capacity and containment security predictions. Such wettability changes caused by carbon dioxide flooding need to be taken into account to assist in process prediction more reliably.

7.2 Introduction

Carbon geological sequestration (CGS) has been proposed as an efficient method to reduce anthropogenic carbon dioxide (CO_2) emissions into the atmosphere and thus mitigate global climate change (IPCC, 2005). In essence, the technique involves capturing CO_2 from large stationary emission sources and locking it into some natural geological formations (e.g., deep saline aquifers, depleted oil fields, etc.) (IPCC, 2005;

Pacala and Socolow, 2004; Lackner and Sachs, 2005). However, the vertical migration of CO_2 is a primary concern involved in CO_2 storage due to the density differences between the brine and CO_2 (Deel et al., 2007; Li and Liu, 2016). Therefore, it is essential to assess and understand the different functional trapping mechanisms, which prevent or control the extent of upward migration of the buoyant CO_2 (IPCC, 2005).

CO_2 can be trapped in various ways in geological formations. These can be categorised as *structural trapping* (Iglauer et al., 2015a; Hesse and Woods, 2010), *capillary trapping* (Pentland et al., 2011b; Krevor et al., 2015; Ruprecht et al., 2014; Suekane et al., 2008), *solubility trapping* (Iglauer, 2011; Emami-Meybodi et al., 2015; Spycher et al., 2003), and *mineral trapping* (Bachu et al., 1994; Gaus, 2010; Matter et al., 2016).

In CGS, wettability is a crucial factor that significantly and directly influences containment security, injectivity, structural, dissolution, and residual trapping capacities (Broseta et al., 2012; Chiquet et al., 2007). Five different wettability states can be conceptualised in a real reservoir, i.e., strongly water-wet, weakly water-wet, intermediate-wet, weakly CO_2-wet, and strongly CO_2-wet, where complete wetting occurs for with approximate contact angles of 0°-50°, 50°-70°, 70°-110°, 110°-130°, 130°-180°, respectively (Iglauer et al., 2015b). These differences in wettability are caused by geological and chemical factors such as surface chemistry (e.g. organic content) (Ali et al., 2019; Abramov et al., 2019; Chen et al., 2015), reservoir pressure (increase in pressure leads to decrease in water wettability) (Niu et al., 2014; Wiegand and Franck, 1994; Broseta et al., 2012), reservoir temperature (Yang et al., 2008; Arif et al., 2016a; Farokhpoor et al., 2013), salinity and ion type (salinity increases, CO_2 wettability increases) (Broseta et al., 2012; Espinoza and Santamarina, 2010; Jha et

al., 2019b; Roshan et al., 2016a). Therefore, it is essential to understand the fluid-rock interaction as these clearly can affect the capillary pressure and aquifer permeability, hence, injectivity and storage capacities (Wiese et al., 2010; Ivanova et al., 2019).

Injected CO_2 forms carbonic acid in the brine phase (Carroll et al., 2011; Mohamed et al., 2012). It, in turn, interacts with rock minerals, which leads to mineral alterations and ion dissolution-precipitation (Worden and Smith, 2004). One of the potential candidates for CO_2 sequestration is deep saline sandstone reservoirs (IPCC, 2005). Sandstones generally consist of quartz (mostly) and siliceous minerals, clays, and various carbonates (Delle Piane et al., 2013). These minerals react differently to the changing environment when CO_2 is injected, e.g., calcite cement is highly reactive in an acidic environment (Carroll et al., 2011; Fischer et al., 2010; Lebedev et al., 2017). In fact, pH reduces to 3-4 when CO_2 mixes with brine at reservoir conditions (Jha et al., 2020), and such an acidic condition can considerably affect the permeability and pore morphology (Sigfusson et al., 2015). Alternatively, the unabsorbed CO_2 gas/super critical liquid phase can be trapped in the target reservoir's pore volume for hundreds or thousands of years due to the slow dissolution kinetics caused by partial mixing of CO_2 and brine (Ballentine et al., 2001).

Some studies have reported that water-CO_2-rock interactions could change the sandstone pore structures due to fines migration or reaction with sensitive materials (Yu et al., 2019; Berrezueta et al., 2013). Such changes potentially can strongly affect the rock porosity and permeability performance (Iglauer et al., 2014b; Mohamed et al., 2012; Lamy-Chappuis et al., 2014). The influence of temperature and injection rate on permeability reduction after CO_2 injection have been examined on the Berea sandstone

(Mohamed et al., 2012) and sandstones from the Pembina Cardium field, Canada (Sayegh et al., 1990). Other studies investigated factors controlling permeability changes in sandstone during core flooding (Al-Yaseri et al., 2017a). However, the effects of CO_2 injection on wettability have received less attention. Thus, in this study, how CO_2 injection can change wettability in sandstones was analysed. These changes are correlated with microstructural alteration in sandstones caused by CO_2 core flooding and explain how flooding can affect trapping capacities (i.e., residual and dissolution) and the amount of free CO_2 retained in saline aquifers (i.e., mobile CO_2).

7.3 Methodology

7.3.1 Materials

Two homogeneous Berea sandstone samples (low clay content) and two Bandera Gray (high clay content) were used in this study. The sandstones were thoroughly characterised by scanning electron microscopy (SEM) to measure the surface morphology and quantitative X-ray diffraction (XRD - Bruker-AXS D8) to measure the mineral composition before and after the flooding experiment. The samples' petrophysical properties, including porosity and permeability, were measured before and after flooding and are reported in Table 7.1.

Table 7. 1 Petrophysical and mineralogical sandstone properties

Sample	Porosity[a] (%)	Brine Permeability (mD)	Length (mm)	Diameter (mm)	Mineral Constituents[b]	
					Mineral	Wt %
Before flooding						
Berea	20	69	50.88	30.78	Quartz	84.3
					Kaolinite	4.1
					Illite	1.9
					Albite	4.2
Bandera Gray	19	9	60.32	30.80	Quartz	58.2
					Kaolinite	3.2
					Illite	3.6
					Albite	12.4
					Muscovite	1.6
After flooding						
Berea	22	80	50.88	30.78	Quartz	84.9
					Kaolinite	3.9
					Illite	1.8
					Albite	4.2
					Microcline	4.1
					Chlorite	1.1
Bandera Gray	20	7.3	60.32	30.80	Quartz	58.4
					Kaolinite	3.1
					Illite	3.2
					Albite	12.2
					Muscovite	3.1

[a]Porosity was measured with AP-608 Coretest Instrument
[b]Mineral composition of the samples was measured by X-Ray Diffraction (XRD)-Bruker-AXS D8

7.3.2 CO_2 core flooding experiment

The Berea and Bandera Gray core plugs were wrapped in polytetrafluoroethylene (PTFE) tape, aluminum foil, and PTFE tape. Subsequently, the samples were sealed with a PTFE heat-shrink sleeve and were placed in a rubber sleeve in a high-pressure and a high-temperature core holder (Figure 7.1). The samples were next placed under vacuum for more than 20 hours (Al-Yaseri et al., 2017a).

The samples were then saturated with dead brine (5 wt % NaCl and 1 wt% KCL) using a high-precision syringe pump (ISCO 500D). The dead brine was then displaced with 5 pore volumes of live brine (5 wt % NaCl and 1 wt% KCL equilibrated with CO_2) at 1 ml/min (El-Maghraby et al., 2012). The injection rate was reduced to 0.05 ml/min, and injection continues for 7 days at reservoir conditions (pore pressure of 10 MPa, confining pressure of 15 MPa, and temperature of 323 °K). This simulates CO_2-saturated brine at in situ reservoir conditions, i.e. dissolution trapping (Riaz et al., 2006; Frykman and Wessel-Berg, 2014; Emami-Meybodi et al., 2015). Finally, five-pore volumes of supercritical CO_2 ($scCO_2$) were injected to displace the live brine and to simulate CO_2 injection into the reservoir. Figure 7.1 presents a schematic of the core flooding apparatus used in this study.

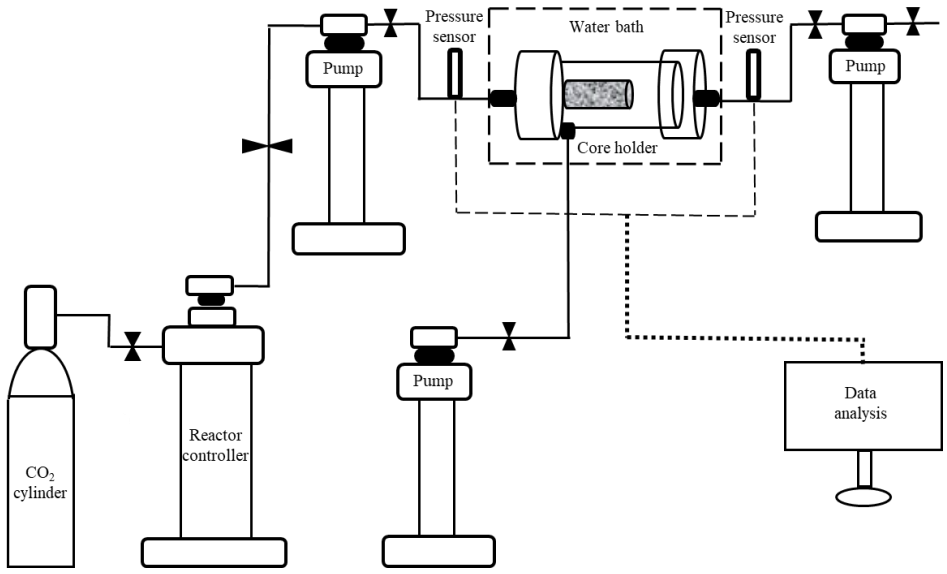

Source: modified from Al-Yaseri et al. (2017a)

Figure 7. 1 Schematic of the core flooding system

7.3.3 Contact angle measurements

For the CO_2 – wettability tests, the samples were cut with a high-speed diamond blade (to cuboids 5 mm thick, 38 mm diameter), and each sample was exposed to air plasma for 5 minutes to remove any potential organic surface contaminations (Love et al., 2005; Iglauer et al., 2014a). Subsequently, the contact angle was measured using the tilted plate method (as it can quantify simultaneously advancing and receding contact angle) (Lander et al., 1993) at reservoir storage conditions. For contact angle measurements, the sample was placed inside the pressure cell at a set temperature (323 °K). CO_2 pressure was raised to the desired pressure (10 MPa and 15 MPa). A droplet of the brine (5 wt% NaCl and 1 wt% KCl in deionized water) with an average volume of ~6 μL ± 1 μL was released onto the tilted (tilted angle of 12^o) sample (Berea and Bandera Gray) surface through a needle. The advancing and receding contact angles were then calculated at the leading and trailing edge. A high-resolution video camera recorded the whole process and images extracted from the video files to measure the

contact angles. The standard deviation in the contact angle result was determined as ±3° based on replicated measurements.

7.4 Results and Discussion

7.4.1 Controlling factors on sandstone wettability

The wettability of sandstone samples (Berea with low clay content and Bandera Gray with high clay content) was measured before and after CO_2 flooding at 10 and 15 MPa at a constant temperature of 323 K. The results clearly indicate that the contact angles after flooding were higher than before flooding for both samples. This shows that Berea and Bandera Gray sandstones became more CO_2 wet after CO_2 injection. The advancing and receding contact angles increased with increasing pressure for both Berea and Bandera Gray samples (Figure 7.2), which is consistent with literature data (Broseta et al., 2012; Fauziah et al., 2020; Arif et al., 2016b; Iglauer et al., 2015b). For example, the advancing contact angle of Bandera Gray before flooding increased from 86^o to 105^o at 323 K, for a pressure of 10 MPa and 15 MPa, respectively. The results also indicate that Bandera Gray has a higher contact angle, compared with Berea, for all test pressures and both before and after CO_2 flooding conditions.

Clay minerals can be distributed in different ways within the reservoirs, such as in the form of laminations between the grains (laminar clays), dispersed in the reservoir or structurally coating the grains (structural clays) (Al-Yaseri et al., 2017a; Siddiqui et al., 2019; Iqbal et al., 2019). Moreover, the specific clay type is also crucial in controlling the petrophysical properties of sandstone (Iqbal et al., 2019; Schrader and Yariv, 1990; Zhang et al., 2016a). The SEM and XRD analysis revealed that the Berea and Bandera Gray sandstones comprise different clay types and distributions. Clay

types present in both sandstone samples are shown in table 7.1. Studies by other researchers have also demonstrated that, besides smectite, all clay minerals can adsorb significant amounts of CO_2 (Busch et al., 2012). As seen from the SEM analysis, both sandstone samples contain the CO_2 adsorbing clays. Therefore, the high contact angle in Bandera Gray (CO_2-wet) can be attributed to the core's higher clay content.

Moreover, changes in albite and ankerite surfaces have been reported (Yu et al., 2016). Dissolution textures have been shown on the surfaces of detrital albite grains. Smooth surface and step-like structures of ankerite grains showed corrosion pits at grain boundaries post-experiment (Yu et al., 2016). Dissolution of illite and chlorite can also occur (Black and Haese, 2014), and chlorite dissolution following subsequent reaction with pre-existing calcite can lead to kaolinite and CO_2 rich ankerite production (Liu et al., 2019). The presence of calcite and its dissolution is a rate-limiting step of this reaction. Kaolinite and ankerite production and their precipitation will depend on the calcite content of the rock samples (Liu et al., 2019). Kaolinite precipitation was reported earlier (Yu et al., 2016) and evident in this work for both Berea and Bandera Grey samples (Figures 7.3 and 7.4). Kaolinite precipitation can also be due to interaction between CO_2 saturated brine and feldspar (k-feldspar, albite, microcline) present in the rock (Yu et al., 2016). Thus, it can be inferred that larger content of albite and ankerite in Bandera Gray samples are responsible for more significant interactions with CO_2 saturated brine. This phenomenon explains higher brine contact angle, thus higher CO_2 wetting, for Bandera Gray as compared to Berea sandstone at the same conditions.

XRD results (Figure 7.5) and XRD images (Figure 7.6) show no significant change in mineral composition before and after CO_2 flooding. This can be due to the dissolution of minerals corresponding to their stoichiometry, keeping the overall mineralogy unchanged (or insignificant change beyond the detection limit). The additional peak in the XRD results after the experiments corresponds to NaCl, and thus salt precipitation post drying cannot be ruled out.

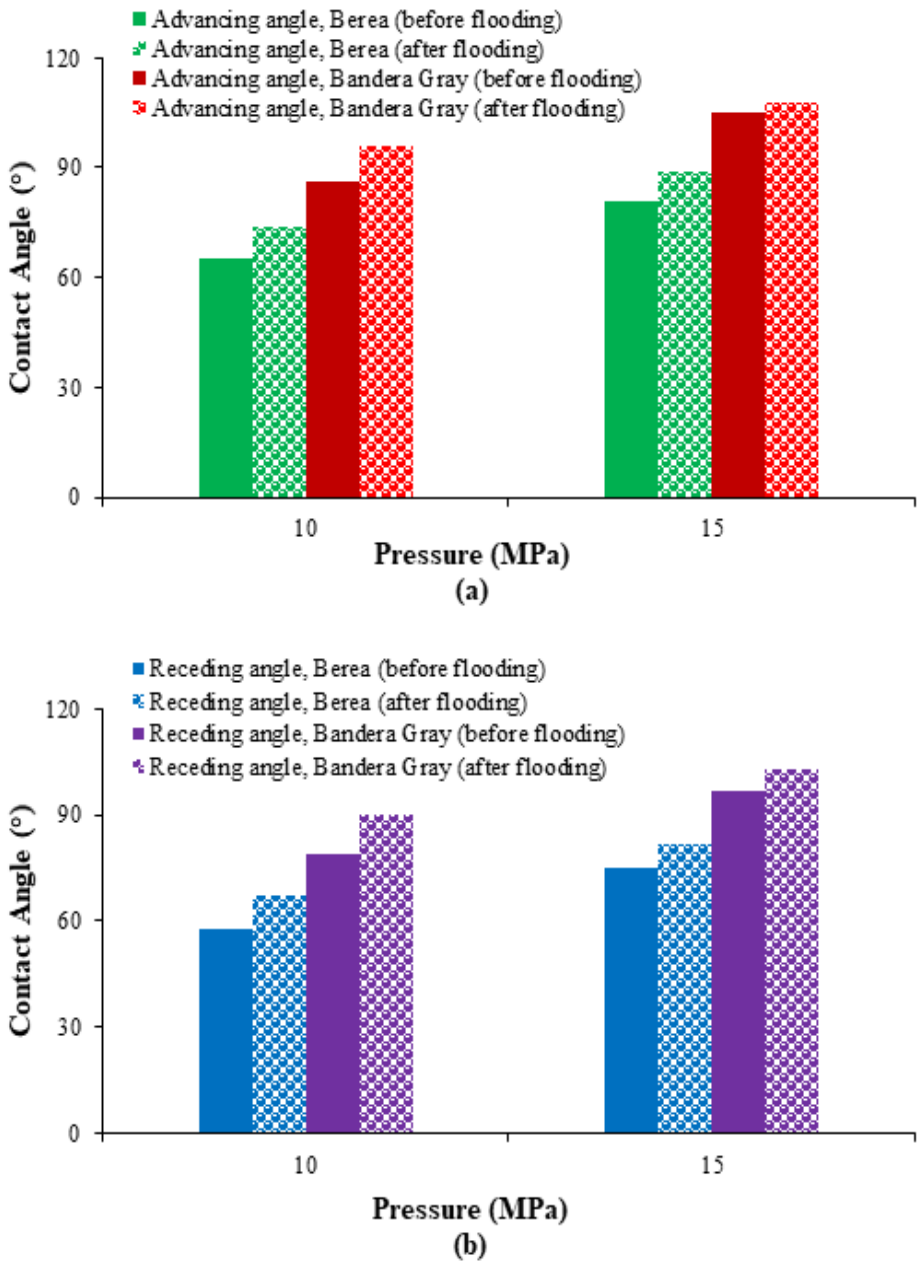

Figure 7. 2 Berea and Bandera Gray θa (a) and θr (b) as a function of pressure

Note: Berea and Bandera Gray were measured at 10 and 15 MPa, and 323 K

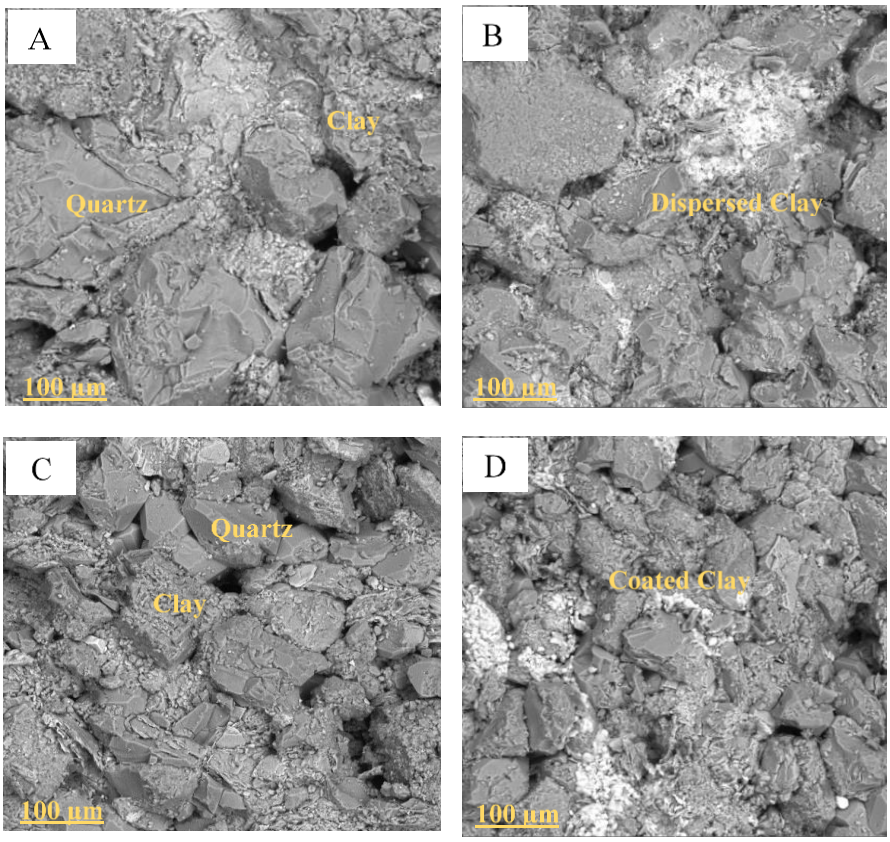

Figure 7. 3 SEM images of Berea and Bandera Gray (in 100 µm)

Note: SEM images of (A) Berea before flooding (B) Berea after flooding: pore filling dispersed clay (illite/kaolinite based on the XRD) (C) Bandera Gray before flooding (D) Bandera Gray after flooding, quartz grains coated structural clay (mostly chlorite based on the XRD)

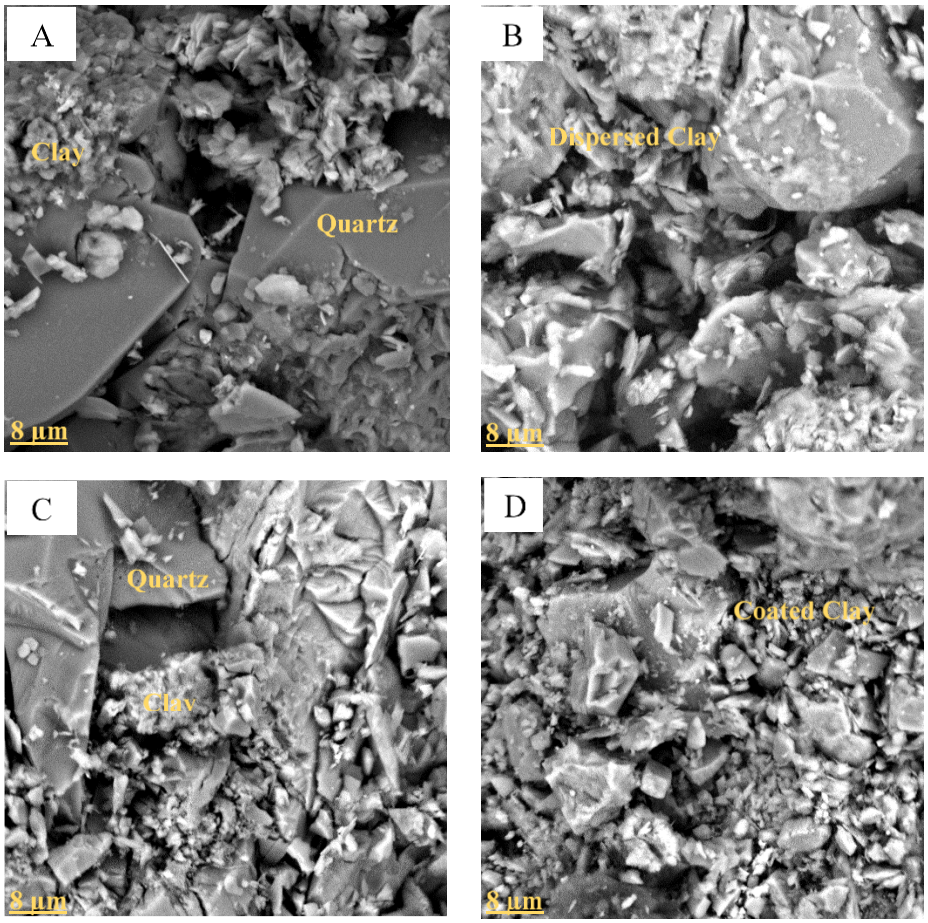

Figure 7. 4 SEM images of Berea and Bandera Gray (in 8 µm)

Note: SEM images of (A) Berea before flooding, smooth surface (B) Clutter Berea after flooding: pore filling dispersed clay (C) Bandera Gray before flooding (D) Clutter Bandera Gray after flooding, quartz grains coated structural clay.

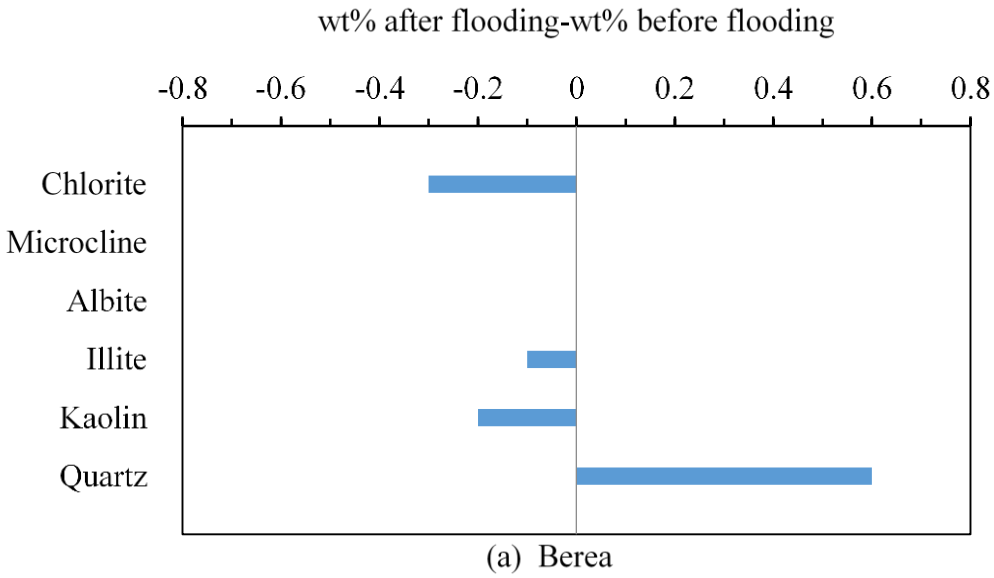

(a) Berea

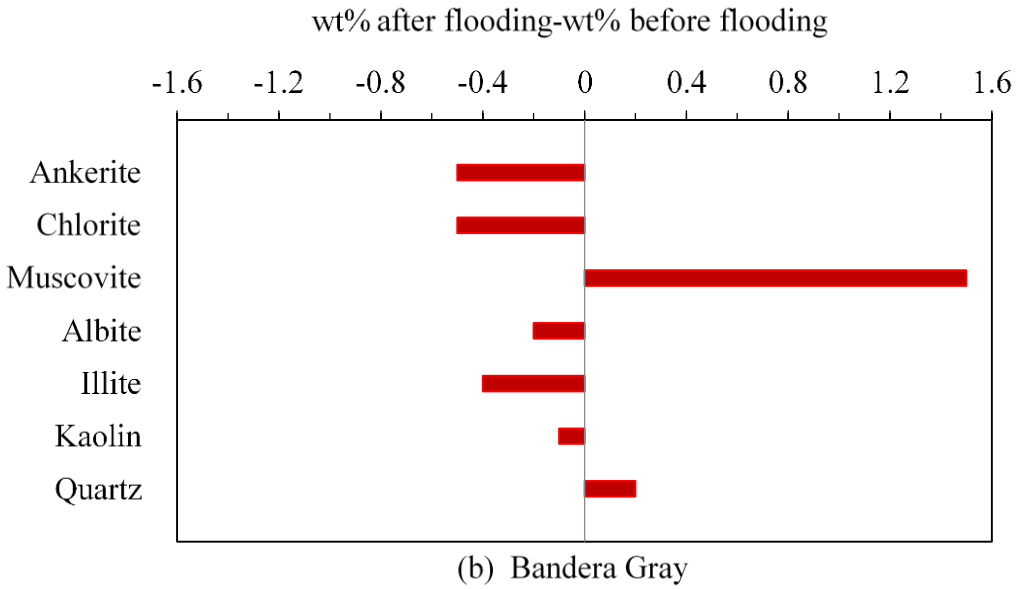

(b) Bandera Gray

Figure 7. 5 Differences in mineral compositions due to CO_2 flooding

Note: (a) Berea and (b) Bandera Gray

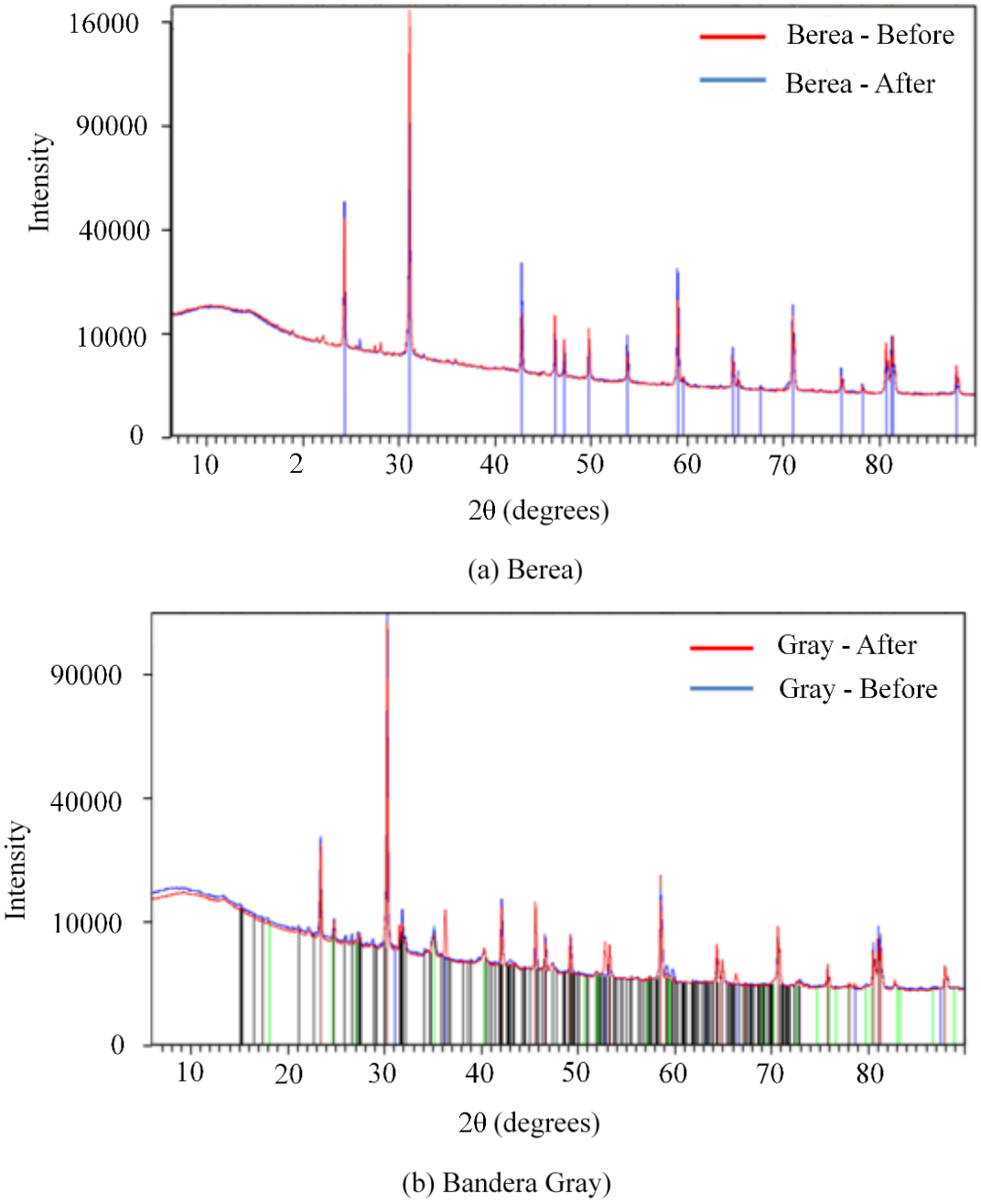

Figure 7. 6 XRD Images for Berea's mineralogical composition

Note: Berea (a) and Bandera Gray (b), before and after flooding

7.4.2 Effect of Clay Content on sandstone trapping capacity

Rock wettability affects significantly on CO_2 trapping capacities (Iglauer et al., 2015a; Krevor et al., 2015). A CO_2-wet rock has significantly higher CO_2 upwards mobility Al-Khdheeawi et al. (2017) and much lower residual trapping capacity (Al-Menhali et al., 2016; Krevor et al., 2015; Niu et al., 2014). The results presented in section (7.4.1) show that CO_2 flooding in sandstones with high clay content leads to the reservoir being CO_2-wet, which can cause the detrimental mobility and storage effects. For example, based on the previous simulation study by Al-Khdheeawi et al. (2017), the CO_2 mobility volume contribution is found to be 0.5% where dissolution trapping capacity is 18.3%, and residual trapping certain capacity is 81.2% in the storage capacity of strongly water-wet rocks. By contrast, the strongly CO_2-wet rocks have CO_2 mobility of 20.7%, dissolution trapping capacity of 28.6%, and residual trapping capacity of 50.7% after 10 years of storage (Figure 7.7).

On the contrary, in formations with low permeability where the biggest challenge is the injection of CO_2, enhanced CO_2 wetting of the rock's surface could be advantageous for pressure management provided a cap-rock that can make a good seal for containment security. The presence of high clay fractions in such low permeability formations will be beneficial for enhanced CO_2 storage capacity by increase in mobility, dissolution, and residual trapping.

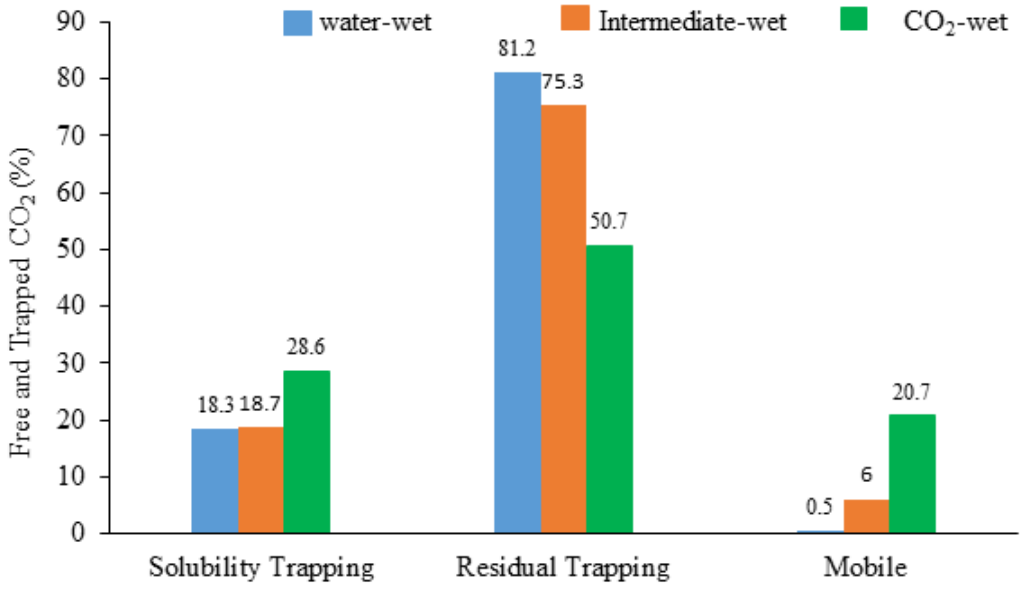

Figure 7. 7 Percentages of free and trapped CO_2 capacities

Note: percentages of free and trapped CO_2 capacities for strongly water-wet, intermediate-wet, and strongly CO_2- wet rocks (modified from Al-Khdheeawi et al. (2017)).

7.5 Conclusions

Rock wettability has a significant role in carbon geological sequestration (CGS) since fluid flow through porous media is strongly controlled by rock wettability. Despite previous research on the area, the parameters influencing the CO_2-brine-rock wettability variation are still not fully understood. This study systematically measured the contact angle (i.e. wettability) of two sandstones (i.e. low clay content (Berea) and high clay content (Bandera Gray)) before and after CO_2 flooding with brine (5 wt % NaCl + 1 wt % KCl in deionised water), CO_2-saturated (live) brine, and supercritical CO_2 ($scCO_2$); at 10 MPa and 15 MPa for a constant temperature (323 K). The results show that CO_2 flooding leads to an increase in the advancing and receding contact

angles of both Berea and Bandera Gray sandstones (i.e., CO_2 flooding leads to increase CO_2-sandstone wettability). These results also show that the CO_2-brine-rock contact angle increases with pressure increase, which is consistent with most literature data.

Overall, the measurements demonstrate, for all tested conditions (both before and after CO_2 flooding scenarios), that the Berea sandstone has lower contact angles (i.e., greater water wettability) than Bandera Gray (i.e., Bandera Gray tends to be more intermediate-wet to CO_2-wet), due to higher clay content of Bandera Gray. The SEM results show that the Bandera Gray sandstones, which became more CO_2-wet, contained high clay content. Published literature indicates that, except for smectites, all clays are CO_2 adsorbing. Hence, sandstones with high clay content become CO_2-wet when flooded with CO_2, which results in upward mobility of CO_2 in the reservoir and, consequently, reduced capillary trapping capacity. However, in the case of low permeability formations, with significant CO_2 injection pressure issues, CO_2-wetting of the reservoir rock surface, and adequate seal for containment security, could assist with pressure management. Therefore, high clay fractions in such formations can be advantageous in their enhancement of CO_2 storage capacity.

Chapter 8 Conclusions and Recommendations

This chapter introduces the overall conclusions drawn from the experiments performed in this research. The conclusions are summarised for each of the main chapters of the thesis and include recommendations for future work in advancing this research.

8.1 Conclusions

This study described the experimental wettability data of carbon dioxide (CO_2)-brine-rock-clay systems through contact angle measurements. Extensive range of experimental conditions were conducted to investigate the wettability of sandstone and clay, and how it evolves with CO_2 exposure. Various pressure values ranging from 0.1 MPa to 20 MPa and temperature values of 305 K, 323 K, 333 K and 334 K were investigated at a specific brine salinity. The effects of different parameters such as pressure, organic content, surface roughness, clay type, temperature, and pore system on wettability were addressed. Overall, the results of the study has led to an effective understanding of wettability and its implications for CO_2 geological sequestration, especially for the predictions of storage capacities and the integrity of containment. The major conclusions of the main thesis chapters are briefly summarised below:

8.1.1 Carbon dioxide/brine, nitrogen/brine and oil/brine wettability of montmorillonite, illite and kaolinite at elevated pressure and temperature

One of the key variables in the assessment of capacities and integrity of geological containments for CO_2 sequestration is the wettability of clay in CO_2-brine solution. However, limited information is available in the literature about this subject. Thus, the wettability of three different clays (montmorillonite, illite and kaolinite) was measured

for various fluid systems, such as CO_2/brine, N_2/brine and N_2/oil, at elevated pressures up to 20 MPa and temperatures of 305 K and 333 K to contribute to knowledge base in this subject area. The main findings of this chapter can be highlighted as follows:

- In comparison with illite and kaolinite, montmorillonite yielded higher contact angles for all three systems (CO_2/brine, N_2/brine and oil/brine). The measured contact angles were found to be positively related to pressure for all fluid/solid systems. This correlation with pressure could be attributed to the increased CO_2 density leading improved intermolecular interactions, between the gas molecules and the mineral surfaces and consequently, resulting in de-wetting of the surface.
- For all clays tested, the measured contact angle decreased slightly as temperature increased. This is in line with previous studies on water-wet mica, quartz, calcite surfaces.
- Based on its 2:1 structure and inherent lower surface charge density, montmorillonite was found to be oil-wet. On the contrary, due to their structural (surface) hydroxyl groups, kaolinite, followed by illite, was found to be strongly water-wet suggesting a strong bipolar interaction between the hydroxyl group and the water molecule.

8.1.2 Dependence of clay wettability on gas density

Contact angles of three different clays (i.e. montmorillonite, illite, and kaolinite) were measured for helium, nitrogen, argon, and carbon dioxide/brine systems for pressure ranging from 5 MPa to 20 MPa, and a single temperature value of 333 K. The following is the summary concluded from the obtained results:

- Six new mathematical models were developed to predict advancing and receding contact angles, as a function of the pressure and density at 333 K temperature, for each of montmorillonite, illite, and kaolinite.
- Increasing pressure and gas density resulted in higher advancing and receding contact angles.
- The measured contact angles were compared with those calculated using the empirical correlations, showing a good agreement with high correlation coefficients (R ranged from 0.951 to 0.979), and low average absolute errors (AAE is ranged from 3.93% to 8.90%).
- The correlations were able to predict the advancing and receding contact angles for all three clays to a high level of accuracy.

8.1.3 Carbon dioxide wettability of South West Hub sandstone, Western Australia: Implications for carbon geo-storage

Wettability of South West Hub sandstone (GSWA Harvey-1) was measured at various pressures ranging from 0.1 MPa to 20 MPa, and temperature of 334 K. To obtain information on the effect of drilling mud and original TOC on wettability, the organic carbon isotopic composition ($\delta^{13}C_{org}$) was also investigated. The key findings are as follows:

- Both advancing and receding water contact angles correlated positively with pressure, suggesting that the system's wettability changed from weakly water-wet to intermediate-wet at higher pressures.
- The samples were treated with dichloromethane (DCM) to remove artificial organic fractions. The results show that organic content slightly decreased for all

sample tested. This was associated with a slight decrease in advancing (θ_a) and receding (θ_r) water contact angles.

- These results indicate that even where minimal amounts of TOC are present, there was an evident increase of CO_2 wettability, which may affect a reservoir's residual trapping capacity.

8.1.4 Effect of CO_2 flooding on wettability evolution of sandstone

Wettability of two sandstones; low clay content (Berea) and high clay content (Bandera Gray), were measured at the pressure of 10 MPa and 15 MPa for a constant temperature of 323 K. The measurements were conducted on the samples before and after CO_2 flooding with brine (5 wt % NaCl + 1 wt % KCl in deionised water), CO_2-saturated (live) brine, and supercritical CO_2 ($scCO_2$); The key findings can be highlighted as follows:

- CO_2 flooding led to increased CO_2-sandstone wettability for both Berea and Bandera Gray sandstones, as shown by the increases in advancing and receding contact angles.
- The CO_2-brine-rock contact angle increased with pressure increased, which is in line with most literature data.
- Berea sandstone has lower contact angles (i.e., greater water wettability) than Bandera Gray (i.e., Bandera Gray tends to be more intermediate-wet to CO_2-wet), due to higher clay content of Bandera Gray. These results applied for all tested conditions (both before and after CO_2 flooding scenarios).
- When flooded with CO_2, the sandstones with high clay content became more CO_2-wet. This has the potential effect to facilitate the upward mobility of CO_2 in the reservoir, consequently reducing capillary trapping capacity. On the

other hand, in low permeability formations, CO_2-wetting of the reservoir rock surface, can provide advantages with injection pressure management issues.

8.2 Recommendations

Notwithstanding the wide range of wettability data for CO_2-brine-rock-clay systems, and the detailed analysis of the mechanisms of wettability variations, there are some research areas, in which this study was unable to cover. The following are some suggestions for future research to address other methods or important topics that were beyond the scope of this research:

- The presence of chemical reactions of CO_2 with clay and possibility of forming acid in presence of saline water needs to be addressed. These reactions could result in surface modification and wettability alteration of the clay surface.
- The wettability of CO_2-brine-rock/clay systems in this study was analysed through the sessile drop with a tilted plate technique. It is recommended similar studies be performed using other, relevant techniques to consolidate the validity of this studies' results or, conversely, assess possible disparities of such methods on contact angle measurements.
- The experimental works on the correlation of clay wettability on gas density was performed at a single temperature and one brine salinity value. Conducting similar experiments on a wider range of experimental conditions would assist with consolidating and improving the result of this study.
- It is recommended that more detailed investigations be carried out on zeta potential and surface charge determinations on clay wettability to better understand its link to macroscopic contact angle, surface chemistry and thus wettability.

- Further studies may be conducted to include tracking changes to aquifer pressure with time due to wettability alteration caused by supercritical CO_2 injection.

APPENDIX A Official Permissions and Copyrights

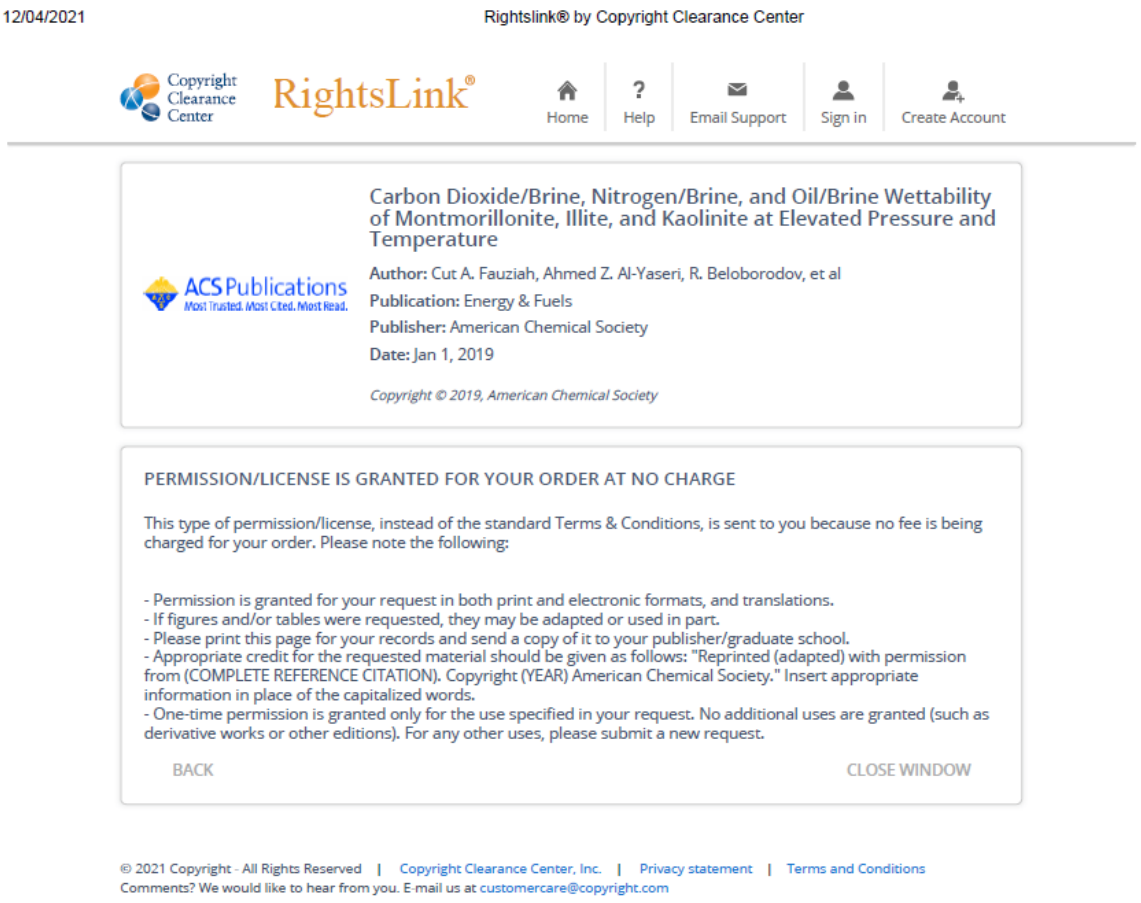

12/04/2021 Rightslink® by Copyright Clearance Center

Copyright Clearance Center RightsLink® Home Help Email Support Sign in Create Account

ACS Publications Most Trusted. Most Cited. Most Read.

Carbon Dioxide/Brine, Nitrogen/Brine, and Oil/Brine Wettability of Montmorillonite, Illite, and Kaolinite at Elevated Pressure and Temperature

Author: Cut A. Fauziah, Ahmed Z. Al-Yaseri, R. Beloborodov, et al
Publication: Energy & Fuels
Publisher: American Chemical Society
Date: Jan 1, 2019

Copyright © 2019, American Chemical Society

PERMISSION/LICENSE IS GRANTED FOR YOUR ORDER AT NO CHARGE

This type of permission/license, instead of the standard Terms & Conditions, is sent to you because no fee is being charged for your order. Please note the following:

- Permission is granted for your request in both print and electronic formats, and translations.
- If figures and/or tables were requested, they may be adapted or used in part.
- Please print this page for your records and send a copy of it to your publisher/graduate school.
- Appropriate credit for the requested material should be given as follows: "Reprinted (adapted) with permission from (COMPLETE REFERENCE CITATION). Copyright (YEAR) American Chemical Society." Insert appropriate information in place of the capitalized words.
- One-time permission is granted only for the use specified in your request. No additional uses are granted (such as derivative works or other editions). For any other uses, please submit a new request.

BACK CLOSE WINDOW

© 2021 Copyright - All Rights Reserved | Copyright Clearance Center, Inc. | Privacy statement | Terms and Conditions
Comments? We would like to hear from you. E-mail us at customercare@copyright.com

Carbon dioxide wettability of South West Hub sandstone, Western Australia: Implications for carbon geo-storage

Author:
Cut Aja Fauziah,Ahmed Z. Al-Yaseri,Nilesh Kumar Jha,Christopher Lagat,Hamid Roshan,Ahmed Barifcani,Stefan Iglauer

Publication: International Journal of Greenhouse Gas Control

Publisher: Elsevier

Date: July 2020

Permission to use Figure 2.9. The schematic of clay layers

ELSEVIER ORDER DETAILS
Apr 12, 2021

Order Number	501646592
Order date	Apr 12, 2021
Licensed Content Publisher	Elsevier
Licensed Content Publication	Elsevier Books
Licensed Content Title	Developments in Clay Science
Licensed Content Author	F. Bergaya,G. Lagaly
Licensed Content Date	2013
Licensed Content Volume	5
Licensed Content Issue	n/a
Licensed Content Pages	19
Start Page	1
End Page	19
Type of Use	reuse in a thesis/dissertation
Portion	figures/tables/illustrations
Number of figures/tables/illustrations	1
Format	both print and electronic
Are you the author of this Elsevier chapter?	No
Will you be translating?	No
Title	Evaluation of the Wettability Characteristics of CO2-Brine-Rock-Clay Mineral Systems: Implications for CO2 Sequestration
Institution name	Curtin University
Expected presentation date	Apr 2021
Order reference number	02
Portions	Figure 1.1
Requestor Location	Fauziah Unit 1/25 Lawson Street Bentley, WA 6102 Australia Attn: Fauziah
Publisher Tax ID	GB 494 6272 12
Total	Not Available

Permission to use Figure 2.10. The atomic structures of layered clay minerals

ELSEVIER LICENSE
TERMS AND CONDITIONS

Apr 18, 2021

This Agreement between Fauziah ("You") and Elsevier ("Elsevier") consists of your license details and the terms and conditions provided by Elsevier and Copyright Clearance Center.

License Number	5046380055812
License date	Apr 12, 2021
Licensed Content Publisher	Elsevier
Licensed Content Publication	Advances in Colloid and Interface Science
Licensed Content Title	A review on clay wettability: From experimental investigations to molecular dynamics simulations
Licensed Content Author	Bin Pan,Xia Yin,Stefan Iglauer
Licensed Content Date	Nov 1, 2020
Licensed Content Volume	285
Licensed Content Issue	n/a
Licensed Content Pages	1
Start Page	102266
End Page	0
Type of Use	reuse in a thesis/dissertation
Portion	figures/tables/illustrations

Number of figures/tables/illustrations	1
Format	both print and electronic
Are you the author of this Elsevier article?	No
Will you be translating?	No
Title	Evaluation of the Wettability Characteristics of CO2-Brine-Rock-Clay Mineral Systems: Implications for CO2 Sequestration
Institution name	Curtin University
Expected presentation date	Apr 2021
Order reference number	01
Portions	Figure 1
Requestor Location	Fauziah Unit 1/25 Lawson Street Bentley, WA 6102 Australia Attn: Fauziah
Publisher Tax ID	GB 494 6272 12
Total	0.00 USD
Terms and Conditions	

Permission to use Figure 4.2. Schematic diagram of the contact angle setup

ELSEVIER LICENSE
TERMS AND CONDITIONS

Apr 16, 2021

This Agreement between Fauziah ("You") and Elsevier ("Elsevier") consists of your license details and the terms and conditions provided by Elsevier and Copyright Clearance Center.

License Number	5050590486635
License date	Apr 16, 2021
Licensed Content Publisher	Elsevier
Licensed Content Publication	International Journal of Greenhouse Gas Control
Licensed Content Title	Electrochemical investigation of the effect of temperature, salinity and salt type on brine/mineral interfacial properties
Licensed Content Author	Muhammad Arif,Franca Jones,Ahmed Barifcani,Stefan Iglauer
Licensed Content Date	Apr 1, 2017
Licensed Content Volume	59
Licensed Content Issue	n/a
Licensed Content Pages	12
Start Page	136
End Page	147
Type of Use	reuse in a thesis/dissertation
Portion	figures/tables/illustrations

Number of figures/tables/illustrations	1
Format	both print and electronic
Are you the author of this Elsevier article?	No
Will you be translating?	No
Title	Evaluation of the Wettability Characteristics of CO2-Brine-Rock-Clay Mineral Systems: Implications for CO2 Sequestration
Institution name	Curtin University
Expected presentation date	Apr 2021
Order reference number	03
Portions	Figure 1
Requestor Location	Fauziah Unit 1/25 Lawson Street Bentley, WA 6102 Australia Attn: Fauziah
Publisher Tax ID	GB 494 6272 12
Total	0.00 USD

Permission to use Figure 6.2. Schematic of the contact angle apparatus

ELSEVIER LICENSE
TERMS AND CONDITIONS

Apr 16, 2021

This Agreement between Fauziah ("You") and Elsevier ("Elsevier") consists of your license details and the terms and conditions provided by Elsevier and Copyright Clearance Center.

License Number	5050591045866
License date	Apr 16, 2021
Licensed Content Publisher	Elsevier
Licensed Content Publication	Journal of Petroleum Science and Engineering
Licensed Content Title	N2+CO2+NaCl brine interfacial tensions and contact angles on quartz at CO2 storage site conditions in the Gippsland basin, Victoria/Australia
Licensed Content Author	Ahmed Al-Yaseri,Mohammad Sarmadivaleh,Ali Saeedi,Maxim Lebedev,Ahmed Barifcani,Stefan Iglauer
Licensed Content Date	May 1, 2015
Licensed Content Volume	129
Licensed Content Issue	n/a
Licensed Content Pages	5
Start Page	58
End Page	62
Type of Use	reuse in a thesis/dissertation

Portion	figures/tables/illustrations
Number of figures/tables/illustrations	1
Format	both print and electronic
Are you the author of this Elsevier article?	No
Will you be translating?	No
Title	Evaluation of the Wettability Characteristics of CO2-Brine-Rock-Clay Mineral Systems: Implications for CO2 Sequestration
Institution name	Curtin University
Expected presentation date	Apr 2021
Order reference number	04
Portions	Figure 2
Requestor Location	Fauziah Unit 1/25 Lawson Street Bentley, WA 6102 Australia Attn: Fauziah
Publisher Tax ID	GB 494 6272 12
Total	0.00 USD
Terms and Conditions	

APPENDIX B Attribution of Authorship

"Carbon dioxide/brine, nitrogen/brine and oil/brine wettability of montmorillonite, illite and kaolinite at elevated pressure and temperature"
Energy & Fuels, 2019, 33 (1), 441-448

Cut Aja Fauziah[a], Ahmed Z. Al-Yaseri[a], Roman Beloborodov[a,b], Mohammed A. Q. Siddiqui[c], Maxim Lebedev[a], Drew. Parsons[d], Hamid Roshan[c], Ahmed Barifcani[a], Stefan Iglauer[c,a]

[a] WASM: Minerals, Energy and Chemical Engineering, Curtin University, 6151 Kensington, Western Australia
[b] CSIRO, Deep Earth Imaging Future Science Platform, 26 Dick Perry Avenue, 6151 Kensington, Western Australia, Australia
[c] University of New South Wales, School of Petroleum Engineering,2052 Kensington, Sydney, Australia
[d] Murdoch University, School of Engineering & IT, 6150 Murdoch, Western Australia, Australia
[f] Edith Cowan University, School of Engineering, 6027 Joondalup, Western Australia, Australia

Name	Conception and design	Manuscript preparation	Acquisition of data and method	Analysis and statistical method	Interpretation and discussion	Final approval
Ahmed Z. Al-Yaseri	x			x	x	

I acknowledge that these represent my contributions to the above research output.

Signature:

"Carbon dioxide/brine, nitrogen/brine and oil/brine wettability of montmorillonite, illite and kaolinite at elevated pressure and temperature"
Energy & Fuels, 2019, 33 (1), 441-448

Cut Aja Fauziah[a], Ahmed Z. Al-Yaseri[a], Roman Beloborodov[a,b], Mohammed A. Q. Siddiqui[c], Maxim Lebedev[a], Drew. Parsons[d], Hamid Roshan[c], Ahmed Barifcani[a], Stefan Iglauer[e,a]

[a] WASM: Minerals, Energy and Chemical Engineering, Curtin University, 6151 Kensington, Western Australia
[b] CSIRO, Deep Earth Imaging Future Science Platform, 26 Dick Perry Avenue, 6151 Kensington, Western Australia, Australia
[c] University of New South Wales, School of Petroleum Engineering,2052 Kensington, Sydney, Australia
[d] Murdoch University, School of Engineering & IT, 6150 Murdoch, Western Australia, Australia
[f] Edith Cowan University, School of Engineering, 6027 Joondalup, Western Australia, Australia

Name	Conception and design	Manuscript preparation	Acquisition of data and method	Analysis and statistical method	Interpretation and discussion	Final approval
Roman Beloborodov			x		x	

I acknowledge that these represent my contributions to the above research output.

Signature:

"Carbon dioxide/brine, nitrogen/brine and oil/brine wettability of montmorillonite, illite and kaolinite at elevated pressure and temperature"
Energy & Fuels, 2019, 33 (1), 441-448

Cut Aja Fauziah[a], Ahmed Z. Al-Yaseri[a], Roman Beloborodov[a,b], Mohammed A. Q. Siddiqui[c], Maxim Lebedev[a], Drew. Parsons[d], Hamid Roshan[c], Ahmed Barifcani[a], Stefan Iglauer[e,a]

[a] WASM: Minerals, Energy and Chemical Engineering, Curtin University, 6151 Kensington, Western Australia
[b] CSIRO, Deep Earth Imaging Future Science Platform, 26 Dick Perry Avenue, 6151 Kensington, Western Australia, Australia
[c] University of New South Wales, School of Petroleum Engineering,2052 Kensington, Sydney, Australia
[d] Murdoch University, School of Engineering & IT, 6150 Murdoch, Western Australia, Australia
[f] Edith Cowan University, School of Engineering, 6027 Joondalup, Western Australia, Australia

Name	Conception and design	Manuscript preparation	Acquisition of data and method	Analysis and statistical method	Interpretation and discussion	Final approval
Mohammed A.Q. Siddiqui			x		x	

I acknowledge that these represent my contributions to the above research output.

Signature:

"Carbon dioxide/brine, nitrogen/brine and oil/brine wettability of montmorillonite, illite and kaolinite at elevated pressure and temperature"
Energy & Fuels, 2019, 33 (1), 441-448

Cut Aja Fauziah[a], Ahmed Z. Al-Yaseri[a], Roman Beloborodov[a,b], Mohammed A. Q. Siddiqui[c], Maxim Lebedev[a], Drew. Parsons[d], Hamid Roshan[c], Ahmed Barifcani[a], Stefan Iglauer[e,a]

[a] WASM: Minerals, Energy and Chemical Engineering, Curtin University, 6151 Kensington, Western Australia
[b] CSIRO, Deep Earth Imaging Future Science Platform, 26 Dick Perry Avenue, 6151 Kensington, Western Australia, Australia
[c] University of New South Wales, School of Petroleum Engineering,2052 Kensington, Sydney, Australia
[d] Murdoch University, School of Engineering & IT, 6150 Murdoch, Western Australia, Australia
[f] Edith Cowan University, School of Engineering, 6027 Joondalup, Western Australia, Australia

Name	Conception and design	Manuscript preparation	Acquisition of data and method	Analysis and statistical method	Interpretation and discussion	Final approval
Maxim Lebedev			x	x		

I acknowledge that these represent my contributions to the above research output.

Signature:

"Carbon dioxide/brine, nitrogen/brine and oil/brine wettability of montmorillonite, illite and kaolinite at elevated pressure and temperature"
Energy & Fuels, 2019, 33 (1), 441-448

Cut Aja Fauziah[a], Ahmed Z. Al-Yaseri[a], Roman Beloborodov[a,b], Mohammed A. Q. Siddiqui[c], Maxim Lebedev[a], Drew. Parsons[d], Hamid Roshan[c], Ahmed Barifcani[a], Stefan Iglauer[e,a]

[a] WASM: Minerals, Energy and Chemical Engineering, Curtin University, 6151 Kensington, Western Australia
[b] CSIRO, Deep Earth Imaging Future Science Platform, 26 Dick Perry Avenue, 6151 Kensington, Western Australia, Australia
[c] University of New South Wales, School of Petroleum Engineering,2052 Kensington, Sydney, Australia
[d] Murdoch University, School of Engineering & IT, 6150 Murdoch, Western Australia, Australia
[f] Edith Cowan University, School of Engineering, 6027 Joondalup, Western Australia, Australia

Name	Conception and design	Manuscript preparation	Acquisition of data and method	Analysis and statistical method	Interpretation and discussion	Final approval
Drew Parsons				x	x	

I acknowledge that these represent my contributions to the above research output.

Signature:

"Carbon dioxide/brine, nitrogen/brine and oil/brine wettability of montmorillonite, illite and kaolinite at elevated pressure and temperature"
Energy & Fuels, 2019, 33 (1), 441-448

Cut Aja Fauziah[a], Ahmed Z. Al-Yaseri[a], Roman Beloborodov[a,b], Mohammed A. Q. Siddiqui[c], Maxim Lebedev[a], Drew. Parsons[d], Hamid Roshan[c], Ahmed Barifcani[a], Stefan Iglauer[e,a]

[a] WASM: Minerals, Energy and Chemical Engineering, Curtin University, 6151 Kensington, Western Australia
[b] CSIRO, Deep Earth Imaging Future Science Platform, 26 Dick Perry Avenue, 6151 Kensington, Western Australia, Australia
[c] University of New South Wales, School of Petroleum Engineering,2052 Kensington, Sydney, Australia
[d] Murdoch University, School of Engineering & IT, 6150 Murdoch, Western Australia, Australia
[f] Edith Cowan University, School of Engineering, 6027 Joondalup, Western Australia, Australia

Name	Conception and design	Manuscript preparation	Acquisition of data and method	Analysis and statistical method	Interpretation and discussion	Final approval
Hamid Roshan	x			x	x	x

I acknowledge that these represent my contributions to the above research output.

Signature:

"Carbon dioxide/brine, nitrogen/brine and oil/brine wettability of montmorillonite, illite and kaolinite at elevated pressure and temperature"
Energy & Fuels, 2019, 33 (1), 441-448

Cut Aja Fauziah[a], Ahmed Z. Al-Yaseri[a], Roman Beloborodov[a,b], Mohammed A. Q. Siddiqui[c], Maxim Lebedev[a], Drew. Parsons[d], Hamid Roshan[c], Ahmed Barifcani[a], Stefan Iglauer[e,a]

[a] WASM: Minerals, Energy and Chemical Engineering, Curtin University, 6151 Kensington, Western Australia
[b] CSIRO, Deep Earth Imaging Future Science Platform, 26 Dick Perry Avenue, 6151 Kensington, Western Australia, Australia
[c] University of New South Wales, School of Petroleum Engineering,2052 Kensington, Sydney, Australia
[d] Murdoch University, School of Engineering & IT, 6150 Murdoch, Western Australia, Australia
[f] Edith Cowan University, School of Engineering, 6027 Joondalup, Western Australia, Australia

Name	Conception and design	Manuscript preparation	Acquisition of data and method	Analysis and statistical method	Interpretation and discussion	Final approval
Ahmed Barifcani					x	x

I acknowledge that these represent my contributions to the above research output.

Signature:

"Carbon dioxide/brine, nitrogen/brine and oil/brine wettability of montmorillonite, illite and kaolinite at elevated pressure and temperature"
Energy & Fuels, 2019, 33 (1), 441-448

Cut Aja Fauziah[a], Ahmed Z. Al-Yaseri[a], Roman Beloborodov[a,b], Mohammed A. Q. Siddiqui[c], Maxim Lebedev[a], Drew. Parsons[d], Hamid Roshan[c], Ahmed Barifcani[a], Stefan Iglauer[e,a]

[a] WASM: Minerals, Energy and Chemical Engineering, Curtin University, 6151 Kensington, Western Australia
[b] CSIRO, Deep Earth Imaging Future Science Platform, 26 Dick Perry Avenue, 6151 Kensington, Western Australia, Australia
[c] University of New South Wales, School of Petroleum Engineering,2052 Kensington, Sydney, Australia
[d] Murdoch University, School of Engineering & IT, 6150 Murdoch, Western Australia, Australia
[f] Edith Cowan University, School of Engineering, 6027 Joondalup, Western Australia, Australia

Name	Conception and design	Manuscript preparation	Acquisition of data and method	Analysis and statistical method	Interpretation and discussion	Final approval
Stefan Iglauer	x			x	x	x

I acknowledge that these represent my contributions to the above research output.

Signature:

"Carbon dioxide wettability of South West Hub sandstone, Western Australia: Implications for carbon geo-storage"
International Journal of Greenhouse Gas Control, 2020, 98, 103064

Cut Aja Fauziah[a], Ahmed Z. Al-Yaseri[d], Nilesh Kumar Jha[a,b], Christopher Lagat[a], Hamid Roshan[c], Stefan Iglauer[d], Ahmed Barifcani[a]

[a] WASM: Minerals, Energy and Chemical Engineering, Curtin University, 6151 Kensington, Western Australia
[b] Indian Institute of Technology Madras, Petroleum Engineering Program, Department of Ocean Engineering, Chennai, 600036 Tamil Nadu, India
[c] University of New South Wales, School of Petroleum Engineering,2052 Kensington, Sydney, Australia
[d] Edith Cowan University, School of Engineering, 6027 Joondalup, Western Australia, Australia

Name	Conception and design	Manuscript preparation	Acquisition of data and method	Analysis and statistical method	Interpretation and discussion	Final approval
Ahmed Z. Al-Yaseri	x			x	x	

I acknowledge that these represent my contributions to the above research output.

Signature:

"Carbon dioxide wettability of South West Hub sandstone, Western Australia: Implications for carbon geo-storage"
International Journal of Greenhouse Gas Control, 2020, 98, 103064

Cut Aja Fauziah[a], Ahmed Z. Al-Yaseri[d], Nilesh Kumar Jha[a,b], Christopher Lagat[a], Hamid Roshan[c], Stefan Iglauer[d], Ahmed Barifcani[a]

[a] WASM: Minerals, Energy and Chemical Engineering, Curtin University, 6151 Kensington, Western Australia
[b] Indian Institute of Technology Madras, Petroleum Engineering Program, Department of Ocean Engineering, Chennai, 600036 Tamil Nadu, India
[c] University of New South Wales, School of Petroleum Engineering, 2052 Kensington, Sydney, Australia
[d] Edith Cowan University, School of Engineering, 6027 Joondalup, Western Australia, Australia

Name	Conception and design	Manuscript preparation	Acquisition of data and method	Analysis and statistical method	Interpretation and discussion	Final approval
Nilesh Kumar Jha			x	x	x	

I acknowledge that these represent my contributions to the above research output.

Signature

"Carbon dioxide wettability of South West Hub sandstone, Western Australia: Implications for carbon geo-storage"
International Journal of Greenhouse Gas Control, 2020, 98, 103064

Cut Aja Fauziah[a], Ahmed Z. Al-Yaseri[d], Nilesh Kumar Jha[a,b], Christopher Lagat[a], Hamid Roshan[c], Stefan Iglauer[d], Ahmed Barifcani[a]

[a] WASM: Minerals, Energy and Chemical Engineering, Curtin University, 6151 Kensington, Western Australia
[b] Indian Institute of Technology Madras, Petroleum Engineering Program, Department of Ocean Engineering, Chennai, 600036 Tamil Nadu, India
[c] University of New South Wales, School of Petroleum Engineering,2052 Kensington, Sydney, Australia
[d] Edith Cowan University, School of Engineering, 6027 Joondalup, Western Australia, Australia

Name	Conception and design	Manuscript preparation	Acquisition of data and method	Analysis and statistical method	Interpretation and discussion	Final approval
Christopher Lagat					x	x

I acknowledge that these represent my contributions to the above research output.

Signature:

"Carbon dioxide wettability of South West Hub sandstone, Western Australia: Implications for carbon geo-storage"
International Journal of Greenhouse Gas Control, 2020, 98, 103064

Cut Aja Fauziah[a], Ahmed Z. Al-Yaseri[d], Nilesh Kumar Jha[a,b], Christopher Lagat[a], Hamid Roshan[c], Stefan Iglauer[d], Ahmed Barifcani[a]

[a] WASM: Minerals, Energy and Chemical Engineering, Curtin University, 6151 Kensington, Western Australia
[b] Indian Institute of Technology Madras, Petroleum Engineering Program, Department of Ocean Engineering, Chennai, 600036 Tamil Nadu, India
[c] University of New South Wales, School of Petroleum Engineering,2052 Kensington, Sydney, Australia
[d] Edith Cowan University, School of Engineering, 6027 Joondalup, Western Australia, Australia

Name	Conception and design	Manuscript preparation	Acquisition of data and method	Analysis and statistical method	Interpretation and discussion	Final approval
Hamid Roshan					x	x

I acknowledge that these represent my contributions to the above research output.

Signature:

"Carbon dioxide wettability of South West Hub sandstone, Western Australia: Implications for carbon geo-storage"
International Journal of Greenhouse Gas Control, 2020, 98, 103064

Cut Aja Fauziah[a], Ahmed Z. Al-Yaseri[d], Nilesh Kumar Jha[a,b], Christopher Lagat[a], Hamid Roshan[c], Stefan Iglauer[d], Ahmed Barifcani[a]

[a] WASM: Minerals, Energy and Chemical Engineering, Curtin University, 6151 Kensington, Western Australia
[b] Indian Institute of Technology Madras, Petroleum Engineering Program, Department of Ocean Engineering, Chennai, 600036 Tamil Nadu, India
[c] University of New South Wales, School of Petroleum Engineering,2052 Kensington, Sydney, Australia
[d] Edith Cowan University, School of Engineering, 6027 Joondalup, Western Australia, Australia

Name	Conception and design	Manuscript preparation	Acquisition of data and method	Analysis and statistical method	Interpretation and discussion	Final approval
Ahmed Barifcani					x	x

I acknowledge that these represent my contributions to the above research output.

Signature:

"Carbon dioxide wettability of South West Hub sandstone, Western Australia: Implications for carbon geo-storage"
International Journal of Greenhouse Gas Control, 2020, 98, 103064

Cut Aja Fauziah[a], Ahmed Z. Al-Yaseri[d], Nilesh Kumar Jha[a,b], Christopher Lagat[a], Hamid Roshan[c], Stefan Iglauer[d], Ahmed Barifcani[a]

[a] WASM: Minerals, Energy and Chemical Engineering, Curtin University, 6151 Kensington, Western Australia
[b] Indian Institute of Technology Madras, Petroleum Engineering Program, Department of Ocean Engineering, Chennai, 600036 Tamil Nadu, India
[c] University of New South Wales, School of Petroleum Engineering,2052 Kensington, Sydney, Australia
[d] Edith Cowan University, School of Engineering, 6027 Joondalup, Western Australia, Australia

Name	Conception and design	Manuscript preparation	Acquisition of data and method	Analysis and statistical method	Interpretation and discussion	Final approval
Stefan Iglauer	x			x	x	x

I acknowledge that these represent my contributions to the above research output.

Signature:

References

Abramov, A., Iglauer, S. & Keshavarz, A. 2019. Wettability of fully hydroxylated and alkylated (001) alpha-quartz surface in carbon dioxide atmosphere. *The Journal of Physical Chemistry C,* 123**,** 9027–9040. https://doi.org/10.1021/acs.jpcc.9b00263

Ahmed, T. 2018. *Reservoir engineering handbook,* Gulf professional publishing.

Ahr, W. M. 2011. *Geology of Carbonate Reservoirs: The Identification, Description and Characterization of Hydrocarbon Reservoirs in Carbonate Rocks*, John Wiley & Sons.

Al-Anssari, S., Arif, M., Wang, S., Barifcani, A., Lebedev, M. & Iglauer, S. 2017. Wettability of nano-treated calcite/CO_2/brine systems: Implication for enhanced CO_2 storage potential. *International Journal of Greenhouse Gas Control,* 66**,** 97-105. https://doi.org/10.1016/j.ijggc.2017.09.008

Al-Khdheeawi, E. A., Vialle, S., Barifcani, A., Sarmadivaleh, M. & Iglauer, S. 2017. Impact of reservoir wettability and heterogeneity on CO_2-plume migration and trapping capacity. *International Journal of Greenhouse Gas Control,* 58**,** 142-158. https://doi.org/10.1016/j.ijggc.2017.01.012

Al-Khdheeawi, E. A., Vialle, S., Barifcani, A., Sarmadivaleh, M. & Iglauer, S. 2018. Effect of wettability heterogeneity and reservoir temperature on CO_2 storage efficiency in deep saline aquifers. *International Journal of Greenhouse Gas Control,* 68**,** 216-229. https://doi.org/10.1016/j.ijggc.2017.11.016

Al-Menhali, A., Niu, B. & Krevor, S. 2015. Capillarity and wetting of carbon dioxide and brine during drainage in Berea sandstone at reservoir conditions. *Water Resources Research,* 51(10)**,** 7895-7914. https://doi.org/10.1002/2015WR016947

Al-Menhali, A. S., Menke, H. P., Blunt, M. J. & Krevor, S. C. 2016. Pore scale observations of trapped CO_2 in mixed-wet carbonate rock: applications to storage in oil fields. *Environmental Science & Technology,* 50(18)**,** 10282-10290. https://doi.org/10.1021/acs.est.6b03111

Al-Yaseri, A., Zhang, Y., Ghasemiziarani, M., Sarmadivaleh, M., Lebedev, M., Roshan, H. & Iglauer, S. 2017a. Permeability evolution in sandstone due to CO_2 injection. *Energy & Fuels,* 31(11)**,** 12390-12398. https://doi.org/10.1021/acs.energyfuels.7b01701

Al-Yaseri, A. Z., Lebedev, M., Barifcani, A. & Iglauer, S. 2016. Receding and advancing (CO_2+ brine+ quartz) contact angles as a function of pressure, temperature, surface roughness, salt type and salinity. *Journal of Chemical Thermodynamics,* 93**,** 416-423. https://doi.org/10.1016/j.jct.2015.07.031

Al-Yaseri, A. Z., Roshan, H., Zhang, Y., Rahman, T., Lebedev, M., Barifcani, A. & Iglauer, S. 2017b. Effect of the temperature on CO_2/brine/dolomite wettability: Hydrophilic versus hydrophobic surfaces. *Energy & Fuels,* 31(6)**,** 6329-6333. https://doi.org/10.1021/acs.energyfuels.7b00745

Al-Yaseri, A. Z., Sarmadivaleh, M., Saidi, A., Lebedev, M., Barifcani, A. & Iglauer, S. 2015. N_2 + CO_2+ NaCl brine interfacial tensions and contact angles on quartz at CO_2 storage site conditions in the Gippsland basin, Victoria/Australia. *Journal of Petroleum Science and Engineering,* 129**,** 58-62. https://doi.org/10.1016/j.petrol.2015.01.026

Al-Khdheeawi, E. A., Vialle, S., Barifcani, A., Sarmadivaleh, M. & Iglauer, S. 2017. Influence of CO_2-wettability on CO_2 migration and trapping capacity in deep saline aquifers. *Greenhouse Gases: Science and Technology,* 7(2)**,** 328-338. https://doi.org/10.1002/ghg.1648

Al-Yaseri, A. Z., Roshan, H., Lebedev, M., Barifcani, A. & Iglauer, S. 2016. Dependence of quartz wettability on fluid density. *Geophysical Research Letters,* 43(8)**,** 3771-3776. https://doi.org/10.1002/2016GL068278

Ali, M., Arif, M., Sahito, M. F., Al-Anssari, S., Keshavarz, A., Barifcani, A., Stalker, L., Sarmadivaleh, M. & Iglauer, S. 2019. CO_2-wettability of sandstones exposed to traces of organic acids: Implications for CO_2 geo-storage. *International Journal of Greenhouse Gas Control,* 83**,** 61-68. https://doi.org/10.1016/j.ijggc.2019.02.002

Alnali, F., Al-Yaseri, A. Z., Roshan, H., Rahman, T., Verall, M., Lebedev, M., Sarmadivaleh, M., Iglauer, S. & Barifcani, A. 2018. Carbon dioxide/brine wettability of porous sandstone versus solid quartz: An experimental and theoretical investigation. *Journal of Colloid and Interface Science,* 524**,** 188-194. https://doi.org/10.1016/j.jcis.2018.04.029

Anderson, W. 1986a. Wettability literature survey- Part 2: Wettability measurement. *Journal of Petroleum Technology,* 38(11)**,** 1246-1262. https://doi.org/10.2118/13933-pa

Anderson, W. G. 1986b. Wettability literature survey- Part 1: Rock/oil/brine interactions and the effects of core handling on wettability. *Society of Petroleum Engineers,* SPE-13932-PA. https://doi.org/10.2118/13932-PA

Arendt, B., Dittmar, D. & Eggers, R. 2004. Interaction of interfacial convection and mass transfer effects in the system CO2–water. *International Journal of Heat and Mass Transfer,* 47(17)**,** 3649-3657. https://doi.org/https://doi.org/10.1016/j.ijheatmasstransfer.2004.04.011

Arif, M., Abu-Khamsin, S. A. & Iglauer, S. 2019. Wettability of rock/CO_2/brine and rock/oil/CO_2-enriched-brine systems: Critical parametric analysis and future outlook. *Advances in Colloid and Interface Science,* 268**,** 91-113. https://doi.org/10.1016/j.cis.2019.03.009

Arif, M., Al-Yaseri, A. Z., Barifcani, A., Lebedev, M. & Iglauer, S. 2016a. Impact of pressure and temperature on CO_2–brine–mica contact angles and CO_2–brine interfacial tension: Implications for carbon geo-sequestration. *Journal of Colloid and Interface Science,* 462**,** 208-215. https://doi.org/10.1016/j.jcis.2015.09.076

Arif, M., Barifcani, A. & Iglauer, S. 2016b. Solid/CO_2 and solid/water interfacial tensions as a function of pressure, temperature, salinity and mineral type: Implications for CO_2-wettability and CO_2 geo-storage. *International Journal of Greenhouse Gas Control* 53**,** 263-273. https://doi.org/10.1016/j.ijggc.2016.08.020

Arif, M., Jones, F., Barifcani, A. & Iglauer, S. 2017a. Electrochemical investigation of the effect of temperature, salinity and salt type on brine/mineral interfacial properties. *International Journal of Greenhouse Gas Control,* 59**,** 136-147. https://doi.org/10.1016/j.ijggc.2017.02.013

Arif, M., Jones, F., Barifcani, A. & Iglauer, S. 2017b. Influence of surface chemistry on interfacial properties of low to high rank coal seams. *Fuel,* 194**,** 211-221. https://doi.org/10.1016/j.fuel.2017.01.027

Arif, M., Lebedev, M., Barifcani, A. & Iglauer, S. 2017c. CO_2 storage in carbonates: Wettability of calcite. *International Journal of Greenhouse Gas Control,* 62**,** 113-121. https://doi.org/10.1016/j.ijggc.2017.04.014

Arif, M., Lebedev, M., Barifcani, A. & Iglauer, S. 2017d. Influence of shale-total organic content on CO_2 geo-storage potential. *Geophysical Research Letters,* 44(17)**,** 8769-8775. https://doi.org/10.1002/2017GL073532

Awad, A. M., Shaikh, S. M. R., Jalab, R., Gulied, M. H., Nasser, M. S., Benamor, A. & Adham, S. 2019. Adsorption of organic pollutants by natural and modified clays: A comprehensive review. *Separation and Purification Technology,* 228**,** 115719. https://doi.org/10.1016/j.seppur.2019.115719

Bachu, S. & Bennion, D. B. 2009. Interfacial tension between CO_2, freshwater, and brine in the range of pressure from (2 to 27) MPa, temperature from (20 to 125) ^{0}C, and water salinity from (0 to 334 000) mg· L^{-1}. *Journal of Chemical & Engineering Data,* 54(3)**,** 765-775. https://doi.org/10.1021/je800529x

Bachu, S., Bonijoly, D., Bradshaw, J., Burruss, R., Holloway, S., Christensen, N. P. & Mathiassen, O. M. 2007. CO_2 storage capacity estimation: Methodology and gaps. *International Journal of Greenhouse Gas Control,* 1(4)**,** 430-443. https://doi.org/10.1016/S1750-5836(07)00086-2

Bachu, S., Gunter, W. & Perkins, E. 1994. Aquifer disposal of CO_2: Hydrodynamic and mineral trapping. *Energy Conversion and Management,* 35(4)**,** 269-279. https://doi.org/10.1016/0196-8904(94)90060-4

Bae, J.-S. & Bhatia, S. K. 2006. High-pressure adsorption of methane and carbon dioxide on coal. *Energy & Fuels,* 20(6)**,** 2599-2607. https://doi.org/10.1021/ef060318y

Ballah, J., Chamerois, M., Durand-Vidal, S., Malikova, N., Levitz, P. & Michot, L. J. 2016. Effect of chemical and geometrical parameters influencing the wettability of smectite clay films. *Colloids and Surface A: Physicochemical and Engineering Aspects,* 511**,** 255. https://doi.org/10.1016/j.colsurfa.2016.10.002

Ballentine, C. J., Schoell, M., Coleman, D. & Cain, B. A. 2001. 300-Myr-old magmatic CO_2 in natural gas reservoirs of the west Texas Permian basin. *Nature,* 409**,** 327-331. https://doi.org/10.1038/35053046

Barclay, S. A. & Worden, R. H. 2009. Effects of reservoir wettability on quartz cementation in oil fields. *In: Worden R.H & Morad S. (Eds) Quartz Cementation in Sandstones. Special Publication.* Vol. 29, pp. 103-117. Blackwell. https://doi.org/10.1002/9781444304237.ch8

Beloborodov, R., Pervukhina, M. & Lebedev, M. 2017. Compaction trends of full stiffness tensor and fluid permeability in artificial shales. *Geophysical Journal International,* 212(3)**,** 1687-1693. https://doi.org/10.1093/gji/ggx510

Beloborodov, R., Pervukhina, M., Luzin, V., Piane, C. D., Clennell, M. B., Zandi, S. & Lebedev, M. 2016. Compaction of quartz-kaolinite mixtures: The influence of the pore fluid composition on the development of their microstructure and elastic anisotropy. *Marine and Petroleum Geology,* 78**,** 426-438. https://doi.org/10.1016/j.marpetgeo.2016.09.030

Bennett, P., Siegel, D., Baedecker, M. & Hult, M. 1993. Crude oil in a shallow sand and gravel aquifer—I. Hydrogeology and inorganic geochemistry. *Applied Geochemistry,* 8(6)**,** 529-549. https://doi.org/10.1016/0883-2927(93)90012-6

Bergaya, F. & Lagaly, G. 2013. General introduction: Clays, clay minerals, and clay science. *In: Bergaya F., Theng B.K.G and Lagaly G. (Eds) Handbook of Clay Science.* Vol. Development in Clay Science, Vol. 5, pp. 1-19. Amsterdam: Elsevier. https://doi.org/10.1016/B978-0-08-098258-8.00001-8

Berrezueta, E., González-Menéndez, L., Breitner, D. & Luquot, L. 2013. Pore system changes during experimental CO_2 injection into detritic rocks: Studies of potential storage rocks from some sedimentary basins of Spain. *International Journal of Greenhouse Gas Control,* 17**,** 411-422. https://doi.org/10.1016/j.ijggc.2013.05.023

Bikkina, P. K. 2011. Contact angle measurements of CO_2–water–quartz/calcite systems in the perspective of carbon sequestration. *International Journal of Greenhouse Gas Control,* 5(5)**,** 1259-1271. https://doi.org/10.1016/j.ijggc.2011.07.001

Black, J. R. & Haese, R. R. 2014. Batch Reactor experimental Results for GaMin'11: Reactivity of Siderite/Ankerite, Labradorite, Illite and Chlorite Under CO_2 Saturated Conditions. *Energy Procedia,* 63**,** 5443-5449. https://doi.org/10.1016/j.egypro.2014.11.575

Borysenko, A., Clennell, B., Sedev, R., Burgar, I., Ralston, J., Raven, M., Dewhurst, D. & Liu, K. 2009. Experimental investigations of the wettability of clays and shales. *Journal of Geophysical Research Solid Earth,* 114(B7). https://doi.org/10.1029/2008JB005928

Botto, J., Fuchs, S. J., Fouke, B. W., Clarens, A. F., Freiburg, J. T., Berger, P. M. & Werth, C. J. 2017. Effects of mineral surface properties on supercritical CO_2 wettability in a siliciclastic reservoir. *Energy & Fuels,* 31(5)**,** 5275-5285. https://doi.org/10.1021/acs.energyfuels.6b03336

Brandon, S., Haimovich, N., Yeger, E. & Marmur, A. 2003. Partial wetting of chemically patterned surfaces: The effect of drop size. *Journal of Colloid and Interface Science,* 263(1)**,** 237-243. https://doi.org/10.1016/S0021-9797(03)00285-6

Brigatti, M. F., Galán, E. & Theng, B. K. G. 2013. Structure and mineralogy of clay minerals. *In: Bergaya F., Theng B.K.G and Lagaly G. (Eds) Handbook of Clay Science.* Vol. Development in Clay Science Vol. 5, pp. 21-81. Elsevier. https://doi.org/10.1016/B978-0-08-098258-8.00002-X

Brocks, J. J. 2011. Millimeter-scale concentration gradients of hydrocarbons in Archean shales: Live-oil escape or fingerprint of contamination? *Geochimica et Cosmochimica Acta,* 75(11)**,** 3196-3213. https://doi.org/10.1016/j.gca.2011.03.014

Brocks, J. J., Buick, R., Summons, R. E. & Logan, G. A. 2003. A reconstruction of Archean biological diversity based on molecular fossils from the 2.78 to 2.45 billion-year-old Mount Bruce Supergroup, Hamersley Basin, Western Australia. *Geochimica et Cosmochimica Acta,* 67(22)**,** 4321-4335. https://doi.org/10.1016/S0016-7037(03)00209-6

Broseta, D., Tonnet, N. & Shah, V. 2012. Are rocks still water-wet in the presence of dense CO_2 or H_2S? *Geofluids,* 12(4)**,** 280-294. https://doi.org/10.1111/j.1468-8123.2012.00369.x

Bryant, S. & Blunt, M. 1992. Prediction of relative permeability in simple porous media. *Physical review A,* 46(4)**,** 2004. https://doi.org/10.1103/PhysRevA.46.2004

Bryant, S. L., Lakshminarasimhan, S. & Pope, G. A. 2008. Buoyancy-dominated multiphase flow and its effect on geological sequestration of CO_2. *SPE Journal,* 13(04)**,** 447-454. https://doi.org/10.2118/99938-pa

Burchette, T. P. 2012. Carbonate rocks and petroleum reservoirs: A geological perspective from the industry. *Geological Society of London, Special Publications,* 370(1)**,** 17-37. https://doi.org/10.1144/SP370.14

Burnside, N. & Naylor, M. 2011. Evaluation of CO_2 storage actuarial risk: Defining an evidence base. DEVEX, 12th May. *School of Geoscience, University of Edinburgh.*

Busch, A., Alles, S., Gensterblum, Y., Prinz, D., Dewhurst, D. N., Raven, M. D., Stanjek, H. & Krooss, B. M. 2008. Carbon dioxide storage potential of shales. *International Journal of Greenhouse Gas Control,* 2(3)**,** 297-308. https://doi.org/10.1016/j.ijggc.2008.03.003

Busch, A., Bertier, P., Gensterblum, Y., Giesting, P., Guggenheim, S., Koster van Groos, A. & Weniger, P.Clay/CO_2 Interactions in the Context of Geological Storage of Carbon Dioxide. 3rd EAGE Shale Workshop - Shale Physics and Shale Chemistry. *European Association of Geoscientists & Engineers*. 2012. https://doi.org/10.3997/2214-4609.20143935

Busch, A., Gensterblum, Y., Krooss, B. M. & Littke, R. 2004. Methane and carbon dioxide adsorption–diffusion experiments on coal: Upscaling and modeling.

International Journal Coal Geology, 60(2)**,** 151-168. https://doi.org/10.1016/j.coal.2004.05.002

Bustin, R. M. & Clarkson, C. R. 1998. Geological controls on coalbed methane reservoir capacity and gas content. *International Journal of Coal Geology,* 38(1)**,** 3-26. https://doi.org/10.1016/S0166-5162(98)00030-5

Butt, H. J., Graf, K. & Kappl, M. 2006. *Physics and Chemistry of Interfaces,* Weinheim, Wiley-VCH GmbH & Co. KGaA.

Carroll-Webb, S. A. & Walther, J. V. 1988. A surface complex reaction model for the pH-dependence of corundum and kaolinite dissolution rates. *Geochimica et Cosmochimica Acta,* 52(11)**,** 2609-2623. https://doi.org/10.1016/0016-7037(88)90030-0

Carroll, S. A., McNab, W. W. & Torres, S. C. 2011. Experimental study of cement-sandstone/shale-brine-CO_2 interactions. *Geochemical Transactions,* 12(9)**,** 1-19. https://doi.org/10.1186/1467-4866-12-9

Cassie, A. B. D. & Baxter, S. 1944. Wettability of porous surfaces. *Transaction of the Faraday Society,* 40**,** 546-551.

CCSBrowser. 2020. *A guide to CO_2 capture and storage* [Online]. Available: https://www.ccsbrowser.com [Accessed 13 February 2021].

Chalbaud, C., Robin, M., Lombard, J.-M., Bertin, H. & Egermann, P. 2010. Brine/CO_2 interfacial properties and effects on CO_2 storage in deep saline aquifers. *Oil & Gas Science and Technology–Revue de l'Institut Français du Pétrole,* 65(4)**,** 541-555. https://doi.org/10.2516/ogst/2009061

Chalbaud, C., Robin, M., Lombard, J. M., Martin, F., Egermann, P. & Bertin, H. 2009. Interfacial tension measurements and wettability evaluation for geological CO_2 storage. *Advances in Water Resources,* 32(1)**,** 98-109. https://doi.org/10.1016/j.advwatres.2008.10.012

Chau, T. T., Bruckard, W. J., Koh, P. T. L. & Nguyen, A. V. 2009. A review of factors that affect contact angle and implications for flotation practice. *Advances in Colloid and Interface Science,* 150(2)**,** 106-115. https://doi.org/10.1016/j.cis.2009.07.003

Chaudhary, K., Bayani Cardenas, M., Wolfe, W. W., Maisano, J. A., Ketcham, R. A. & Bennett, P. C. 2013. Pore-scale trapping of supercritical CO_2 and the role of

grain wettability and shape. *Geophysical Research Letters,* 40(15)**,** 3878-3882. https://doi.org/10.1002/grl.50658

Chen, C., Wan, J., Li, W. & Song, Y. 2015. Water contact angles on quartz surfaces under supercritical CO_2 sequestration conditions: Experimental and molecular dynamics simulation studies. *International Journal of Greenhouse Gas Control,* 42**,** 655-665. https://doi.org/10.1016/j.ijggc.2015.09.019

Chibowski, E. & Terpilowski, K. 2008. Surface free energy of sulfur—Revisited: I. Yellow and orange samples solidified against glass surface. *Journal of Colloid and Interface Science,* 319(2)**,** 505-513. https://doi.org/10.1016/j.jcis.2007.10.059

Chiquet, P., Broseta, D. & Thibeau, S. 2007. Wettability alteration of caprock minerals by carbon dioxide. *Geofluids,* 7(2)**,** 112-122. https://doi.org/10.1111/j.1468-8123.2007.00168.x

Chorom, M. & Rengasamy, P. 1995. Dispersion and zeta potential of pure clays as related to net particle charge under varying pH, electrolyte concentration and cation type. *European Journal of Soil Science,* 46(4)**,** 657-665. https://doi.org/10.1111/j.1365-2389.1995.tb01362.x

Clarkson, C. R. & Bustin, R. M. 2000. Binary gas adsorption/desorption isotherms: Effect of moisture and coal composition upon carbon dioxide selectivity over methane. *International Journal of Coal Geology,* 42(4)**,** 241-271. https://doi.org/10.1016/S0166-5162(99)00032-4

Craig, F. F. 1971. *The Reservoir Engineering Aspects of Waterflooding*, HL Doherty Memorial Fund of AIME New York.

Cuéllar-Franca, R. M. & Azapagic, A. 2015. Carbon capture, storage and utilisation technologies: A critical analysis and comparison of their life cycle environmental impacts. *Journal of CO_2 Utilization,* 9**,** 82-102. https://doi.org/10.1016/j.jcou.2014.12.001

Cuiec, L. & Yahya, F. A. 1991. Wettability of Asab Reservoir Rock: Comparison of Various Evaluation Methods, Role of Lithology. *SCA Conference Paper Number 9109*.

Dake, L. P. 1978. *Fundamentals of Reservoir Engineering*, Elsevier, Amsterdam.

Deel, D., Mahajan, K., Mahoney, C. R., McIlvried, H. G. & Srivastava, R. D. 2007. Risk assessment and management for long-term storage of CO_2 in geologic formations-United States Department of Energy R&D. *Systemics, Cybernetics and Informatics,* 5(1)**,** 79-84.

Dehghanpour, H., Q. Lan., Y. Saeed., H. Fei, and Z. Qi 2013. Spontaneous imbibition of brine and oil in gas shales: effect of water adsorption and resulting microfractures. *Energy & Fuels,* 27(6)**,** 3039-3049. https://doi.org/10.1021/ef4002814

Delle Piane, C., Timms, N. E., Saeedi, A., Rezaee, M. R., Mikhaltsevitch, V., Lebedev, M. & Olierook, H. 2013. Facies-based rock properties distribution along the Harvey 1 stratigraphic well. *CSIRO Report Number EP133710*.

Diz, H. M. M. & Rand, B. 1989. Variable nature of the isoelectric point of the edge surface of kaolinite. *British Ceramic Transactions and Journal,* 88(5)**,** 162-166.

DMPWA 2012. Drilling Fluid Summary (Well: Harvey 1-Western Australia). https://wapims.dmp.wa.gov.au/WAPIMS/Search/WellDetails#.

Durand, C. & Rosenberg, E. 1998. Fluid distribution in kaolinite- or illite-bearing cores: Cryo-SEM observations versus bulk measurements. *Journal of Petroleum Science and Engineering,* 19(1)**,** 65-72. https://doi.org/10.1016/S0920-4105(97)00036-3

El-Maghraby, R. M., Pentland, C. H., Iglauer, S. & Blunt, M. J. 2012. A fast method to equilibrate carbon dioxide with brine at high pressure and elevated temperature including solubility measurements. *The Journal of Supercritical Fluids,* 62**,** 55-59. https://doi.org/10.1016/j.supflu.2011.11.002

Emami-Meybodi, H., Hassanzadeh, H., Green, C. P. & Ennis-King, J. 2015. Convective dissolution of CO_2 in saline aquifers: Progress in modeling and experiments. *International Journal of Greenhouse Gas Control,* 40**,** 238-266. https://doi.org/10.1016/j.ijggc.2015.04.003

Emami-Meybodi, H., Hassanzadeh, H. & Ennis-King, J. 2015. CO2 dissolution in the presence of background flow of deep saline aquifers. *Water Resources Research,* 51(4)**,** 2595-2615. https://doi.org/10.1002/2014WR016659

Engelder, T., Cathles, L. M. & Bryndzia, L. T. 2014. The fate of residual treatment water in gas shale. *Journal of Unconventional Oil and Gas Resources,* 7**,** 33-48. https://doi.org/http://dx.doi.org/10.1016/j.juogr.2014.03.002

Ennis-King, J. & Paterson, L.Role of convective mixing in the long-term storage of carbon dioxide in deep saline formations. SPE Annual Technical Conference and Exhibition. 2003. SPE-84344-MS. https://doi.org/10.2118/84344-ms

Eshkalak, M. O., Al-Shalabi, E. W., Sanaei, A., Aybar, U. & Sepehrnoori, K. 2014. Simulation study on the CO_2-driven enhanced gas recovery with sequestration versus the re-fracturing treatment of horizontal wells in the U.S. unconventional shale reservoirs. *Journal of Natural Gas Science and Engineering,* 21**,** 1015-1024. https://doi.org/10.1016/j.jngse.2014.10.013

Espinoza, D. N. & Santamarina, J. C. 2010. Water-CO_2-mineral systems: Interfacial tension, contact angle, and diffusion—Implications to CO_2 geological storage. *Water Resources Research,* 46(7). https://doi.org/10.1029/2009WR008634

Espinoza, D. N. & Santamarina, J. C. 2012. Clay interaction with liquid and supercritical CO_2: The relevance of electrical and capillary forces. *International Journal of Greenhouse Gas Control,* 10**,** 351-362. https://doi.org/10.1016/j.ijggc.2012.06.020

Farokhpoor, R., Bjørkvik, B. J. A., Lindeberg, E. & Torsæter, O. 2013. Wettability behaviour of CO_2 at storage conditions. *International Journal of Greenhouse Gas Control,* 12**,** 18-25. https://doi.org/10.1016/j.ijggc.2012.11.003

Fauziah, C. A., Al-Khdheeawi, E. A., Barifcani, A. & Iglauer, S.Wettability Measurements of Mixed Clay Minerals at Elevated Temperature and Pressure: Implications for CO Geo-Storage. SPE Gas & Oil Technology Showcase and Conference. 2019a. Dubai. *Society of Petroleum Engineers*. https://doi.org/10.2118/198591-MS

Fauziah, C. A., Al-Yaseri, A. Z., Beloborodov, R., Siddiqui, M. A., Lebedev, M., Parsons, D. F., Roshan, H., Barifcani, A. & Iglauer, P. S. 2019b. Carbon dioxide/brine, nitrogen/brine and oil/brine wettability of montmorillonite, illite and kaolinite at elevated pressure and temperature. *Energy & Fuels,* 33(1)**,** 441-448. https://doi.org/10.1021/acs.energyfuels.8b02845

Fauziah, C. A., Al-Yaseri, A. Z., Jha, N. K., Lagat, C., Roshan, H., Barifcani, A. & Iglauer, S. 2020. Carbon dioxide wettability of South West Hub sandstone, Western Australia: Implications for carbon geo-storage. *International Journal of Greenhouse Gas Control,* 98**,** 103064. https://doi.org/10.1016/j.ijggc.2020.103064

Feng, R., Zhang, Y., Rezagholilou, A., Roshan, H. & Sarmadivaleh, M. 2019. Brittleness Index: From Conventional to Hydraulic Fracturing Energy Model.

Rock Mechanics and Rock Engineering. https://doi.org/10.1007/s00603-019-01942-1

Fernø, M. A., Hauge, L. P., Uno Rognmo, A., Gauteplass, J. & Graue, A. 2015. Flow visualization of CO_2 in tight shale formations at reservoir conditions. *Geophysical Research Letters,* 42(18)**,** 7414-7419. https://doi.org/10.1002/2015GL065100

Ferris, A. P. & Jepson, W. B. 1975. The exchange capacities of kaolinite and the preparation of homoionic clays. *Journal of Colloid and Interface Science,* 51(2)**,** 245-259. https://doi.org/10.1016/0021-9797(75)90110-1

Fischer, S., Liebscher, A., Wandrey, M. & Group, C. S. 2010. CO_2–brine–rock interaction—First results of long-term exposure experiments at in situ P–T conditions of the Ketzin CO_2 reservoir. *Chemie der Erde-Geochemistry,* 70**,** 155-164. https://doi.org/10.1016/j.chemer.2010.06.001

Flett, M., Gurton, R. & Weir, G. 2007. Heterogeneous saline formations for carbon dioxide disposal: Impact of varying heterogeneity on containment and trapping. *Journal of Petroleum Science and Engineering,* 57(1)**,** 106-118. https://doi.org/10.1016/j.petrol.2006.08.016

Frykman, P. & Wessel-Berg, D. 2014. Dissolution trapping-convection enhancement limited by geology. *Energy Procedia,* 63**,** 5467-5478. https://doi.org/10.1016/j.egypro.2014.11.578

Gaus, I. 2010. Role and impact of CO_2–rock interactions during CO_2 storage in sedimentary rocks. *International Journal of Greenhouse Gas Control,* 4(1)**,** 73-89. https://doi.org/10.1016/j.ijggc.2009.09.015

Ge, H.-K., Yang, L., Shen, Y.-H., Ren, K., Meng, F.-B., Ji, W.-M. & Wu, S. 2015. Experimental investigation of shale imbibition capacity and the factors influencing loss of hydraulic fracturing fluids. *Petroleum Science,* 12(4)**,** 636-650. https://doi.org/10.1007/s12182-015-0049-2

Gérard, E., Moreira, D., Philippot, P., Van Kranendonk, M. J. & López-García, P. 2009. Modern Subsurface Bacteria in Pristine 2.7 Ga-Old Fossil Stromatolite Drillcore Samples from the Fortescue Group, Western Australia. *PLOS ONE,* 4(4)**,** e5298. https://doi.org/10.1371/journal.pone.0005298

Gershenzon, N. I., Ritzi Jr, R. W., Dominic, D. F., Soltanian, M., Mehnert, E. & Okwen, R. T. 2015. Influence of small-scale fluvial architecture on CO_2 trapping processes in deep brine reservoirs. *Water Resources Research,* 51(10)**,** 8240-8256. https://doi.org/10.1002/2015WR017638

Gharbi, O. & Blunt, M. J. 2012. The impact of wettability and connectivity on relative permeability in carbonates: A pore network modeling analysis. *Water Resources Research,* 48(12). https://doi.org/10.1029/2012WR011877

Gibbins, J. & Chalmers, H. 2008. Carbon capture and storage. *Energy Policy,* 36(12)**,** 4317-4322. https://doi.org/10.1016/j.enpol.2008.09.058

Giraldo, J., Benjumea, P., Lopera, S., Cortés, F. B. & Ruiz, M. A. 2013. Wettability alteration of sandstone cores by alumina-based nanofluids. *Energy & Fuels,* 27(7)**,** 3659-3665. https://doi.org/10.1021/ef4002956

Golding, S. D., Uysal, I. T., Boreham, C. J., Kirste, D., Baublys, K. A. & Esterle, J. S. 2011. Adsorption and mineral trapping dominate CO_2 storage in coal systems. *Energy Procedia,* 4**,** 3131-3138. https://doi.org/10.1016/j.egypro.2011.02.227

Gray, I. 1987. Reservoir engineering in coal seams: Part 1-The physical process of gas storage and movement in coal seams. *SPE Reservoir Engineering,* 2(01)**,** 28-34. https://doi.org/10.2118/12514-pa

Grim, R. E. 1953. *Clay Mineralogy,* New York, McGraw-Hill Book Company, Inc.

Grundke, K., Bogumil, T., Gietzelt, T., Jacobasch, H.-J., Kwok, D. & Neumann, A. 1996. Wetting measurements on smooth, rough and porous solid surfaces. *Interfaces, Surfactants and Colloids in Engineering.* pp. 58-68. Springer. https://doi.org/10.1007/BFb0114445

Guggenheim, S. & Martin, R. 1995. Definition of clay and clay mineral: Joint report of the AIPEA nomenclature and CMS nomenclature committees. *Clays and clay minerals,* 43(2)**,** 255-256.

Guidotti, C. V. 1984. Micas in metamorphic rocks. *Reviews in Mineralogy and Geochemistry,* 13(1)**,** 357-467.

Guiltinan, E. J., Cardenas, M. B., Bennett, P. C., Zhang, T. & Espinoza, D. N. 2017. The effect of organic matter and thermal maturity on the wettability of supercritical CO_2 on organic shales. *International Journal of Greenhouse Gas Control,* 65**,** 15-22. https://doi.org/10.1016/j.ijggc.2017.08.006

Gunter, W. D., Perkins, E. H. & McCann, T. J. 1993. Aquifer disposal of CO_2-rich gases: Reaction design for added capacity. *Energy Conversion and Management,* 34(9)**,** 941-948. https://doi.org/10.1016/0196-8904(93)90040-H

Guo, F., Morgenstern, N. & Scott, J. 1993. An experimental investigation into hydraulic fracture propagation—Part 1. Experimental facilities. *International Journal of Rock Mechanics and Mining Sciences & Geomechanics Abstracts* 30(3)**,** 177-188. https://doi.org/10.1016/0148-9062(93)92722-3

Hesse, M. A., Orr, F. M. & Tchelepi, H. A. 2008. Gravity currents with residual trapping. *Journal of Fluid Mechanics,* 611**,** 35-60. https://doi.org/10.1016/j.egypro.2009.02.113

Hesse, M. A. & Woods, A. 2010. Buoyant dispersal of CO_2 during geological storage. *Geophysical Research Letters,* 37(1). https://doi.org/10.1029/2009GL041128

Hirasaki, G. 1991. Wettability: Fundamentals and surface forces. *SPE Formation Evaluation,* 6(02)**,** 217-226. https://doi.org/10.2118/17367-PA

Hu, Y., Devegowda, D. & Sigal, R. 2016. A microscopic characterization of wettability in shale kerogen with varying maturity levels. *Journal of Natural Gas Science and Engineering,* 33**,** 1078-1086. https://doi.org/10.1016/j.jngse.2016.06.014

Hu, Y., Liu, X. & Xu, Z. 2003. Role of crystal structure in flotation separation of diaspore from kaolinite, pyrophyllite and illite. *Minerals Engineering,* 16(3)**,** 219-227. https://doi.org/10.1016/S0892-6875(02)00368-0

Ide, S. T., Jessen, K. & Orr Jr, F. M. 2007. Storage of CO_2 in saline aquifers: Effects of gravity, viscous, and capillary forces on amount and timing of trapping. *International Journal of Greenhouse Gas Control,* 1(4)**,** 481-491. https://doi.org/10.1016/S1750-5836(07)00091-6

IEA 2015. World Energy Outlook 2015. https://www.iea.org/reports/world-energy-outlook-2015: International Energy Agency, Paris France.

Iglauer, S. 2011. Dissolution trapping of carbon dioxide in reservoir formation brine – A carbon storage mechanism. *In: Nakajima H. (Eds) Mass Transfer Advanced Aspects.* pp. 233-262. InTechOpen. https://doi.org/10.5772/1432

Iglauer, S. 2017. CO_2–water–rock wettability: Variability, influencing factors, and implications for CO_2 geostorage. *Accounts of Chemical Research,* 50(5)**,** 1134-1142. https://doi.org/10.1021/acs.accounts.6b00602

Iglauer, S., Al-Yaseri, A. Z., Rezaee, R. & Lebedev, M. 2015a. CO_2 wettability of caprocks: Implications for structural storage capacity and containment

security. *Geophysical Research Letters,* 42(21)**,** 9279-9284. https://doi.org/10.1002/2015GL065787

Iglauer, S., Mathew, M. S. & Bresme, F. 2012. Molecular dynamics computations of brine–CO_2 interfacial tensions and brine–CO_2–quartz contact angles and their effects on structural and residual trapping mechanisms in carbon geo-sequestration. *Journal of Colloid and Interface Science,* 386(1)**,** 405-414. https://doi.org/10.1016/j.jcis.2012.06.052

Iglauer, S., Paluszny, A., Pentland, C. H. & Blunt, M. J. 2011. Residual CO_2 imaged with X-ray micro-tomography. *Geophysical Research Letters,* 38(21). https://doi.org/10.1029/2011GL049680

Iglauer, S., Pentland, C. H. & Busch, A. 2015b. CO_2 wettability of seal and reservoir rocks and the implications for carbon geo-sequestration. *Water Resources Research,* 51(1)**,** 729-774. https://doi.org/10.1002/2014WR015553

Iglauer, S., Salamah, A., Sarmadivaleh, M., Liu, K. & Phan, C. 2014a. Contamination of silica surfaces: Impact on water–CO_2–quartz and glass contact angle measurements. *International Journal of Greenhouse Gas Control,* 22**,** 325-328. https://doi.org/10.1016/j.ijggc.2014.01.006

Iglauer, S., Sarmadivaleh, M., Al-Yaseri, A. & Lebedev, M. 2014b. Permeability evolution in sandstone due to injection of CO_2-saturated brine or supercritical CO_2 at reservoir conditions. *Energy Procedia,* 63**,** 3051-3059. https://doi.org/10.1016/j.egypro.2014.11.328

IPCC 2005. Special report on carbon dioxide capture and storage. *In: Metz B., Davidson O., Coninck H.d., Loos M and Meyer L. (Eds) Working Group III of the Intergovernmental Panel on Climate Change.* Cambridge University Press, Cambridge, United Kingdom and New York, USA.

IPCC 2014. Climate change 2014: Mitigation of climate change *In: Edenhofer O., Pichs-Madruga R., Sokona Y., Farahani E., Kadner S., Seyboth K., Adler A., Baum I., Brunner S., Eickemeier P., Kriemann B., Savolaine J., Schlömer S., von Stechow C., Zwickel T and Minx J.C. (Eds) Contribution of Working Group III to the Fifth Assessment Report of the Intergovernmental Panel on Climate Change.* Cambridge University Press, Cambridge, United Kingdom and New York, USA.

Iqbal, M. A., Salim, A. M. A., Baioumy, H., Gaafar, G. R. & Wahid, A. 2019. Identification and characterization of low resistivity low contrast zones in a clastic outcrop from Sarawak, Malaysia. *Journal of Applied Geophysics,* 160**,** 207-217. https://doi.org/10.1016/j.jappgeo.2018.11.013

Ivanova, A., Mitiurev, N., Cheremisin, A., Orekhov, A., Kamyshinsky, R. & Vasiliev, A. 2019. Characterization of organic layer in oil carbonate reservoir rcks and its efect on mcroscale wtting properties. *Scientific reports,* 9(1)**,** 1-10. https://doi.org/10.1038/s41598-019-47139-y

Jamaluddin, A. K. M., Bennion, D. B., Thomas, F. B. & Clark, M. A.Acid/sour gas management in the petroleum industry. Abu Dhabi International Petroleum Exhibition and Conference. 1998. *Society of Petroleum Engineers* 49522, 584-598. https://doi.org/10.2118/49522-MS

Jeon, P. R., Kim, D.-W. & Lee, C.-H. 2018. Dissolution and reaction in a CO2-brine-clay mineral particle system under geological CO2 sequestration from subcritical to supercritical conditions. *Chemical Engineering Journal,* 347**,** 1-11. https://doi.org/https://doi.org/10.1016/j.cej.2018.04.052

Jha, N. K., Ali, M., Iglauer, S., Lebedev, M., Roshan, H., Barifcani, A., Sangwai, J. S. & Sarmadivaleh, M. 2019a. Wettability Alteration of Quartz Surface by Low-Salinity Surfactant Nanofluids at High-Pressure and High-Temperature Conditions. *Energy & Fuels,* 33(8)**,** 7062-7068. https://doi.org/10.1021/acs.energyfuels.9b01102

Jha, N. K., Iglauer, S., Barifcani, A., Sarmadivaleh, M. & Sangwai, J. S. 2019b. Low-salinity surfactant nanofluid formulations for wettability alteration of sandstone: Role of the SiO_2 nanoparticle concentration and divalent cation/SO_4^{2-} ratio. *Energy & Fuels*. https://doi.org/10.1021/acs.energyfuels.8b03406

Jha, N. K., Ivanova, A., Lebedev, M., Barifcani, A., Cheremisin, A., Iglauer, S., Sangwai, J. S. & Sarmadivaleh, M. 2020. Interaction of low salinity surfactant nanofluids with carbonate surfaces and molecular level dynamics at fluid-fluid interface at $ScCO_2$ loading. *Journal of Colloid and Interface Science*. https://doi.org/10.1016/j.jcis.2020.10.095

Jiang, J., Oberdörster, G. & Biswas, P. 2009. Characterization of size, surface charge, and agglomeration state of nanoparticle dispersions for toxicological studies. *Journal of Nanoparticle Research,* 11(1)**,** 77-89. https://doi.org/10.1007/s11051-008-9446-4

Jianhua, T., Satherley, J. & Schiffrin, D. J. 1993. Density and interfacial tension of nitrogen-hydrocarbon systems at elevated pressures. *Chinese Journal of Chemical Engineering* 1(4)**,** 223-231.

Johnson Jr, R. E. & Dettre, R. H. 1964. Contact angle hysteresis. III. Study of an idealized heterogeneous surface. *The journal of physical chemistry,* 68(7)**,** 1744-1750.

Jones, D., Head, I., Gray, N., Adams, J., Rowan, A., Aitken, C., Bennett, B., Huang, H., Brown, A. & Bowler, B. 2008. Crude-oil biodegradation via methanogenesis in subsurface petroleum reservoirs. *Nature,* 451(7175)**,** 176. https://doi.org/10.1038/nature06484

Juanes, R., Spiteri, E., Orr Jr, F. & Blunt, M. 2006. Impact of relative permeability hysteresis on geological CO_2 storage. *Water resources research,* 42(12). https://doi.org/10.1029/2005WR004806

Jung, J. W. & Wan, J. 2012. Supercritical CO_2 and ionic strength effects on wettability of silica surfaces: Equilibrium contact angle measurements. *Energy & Fuels,* 26(9)**,** 6053-6059. https://doi.org/10.1021/ef300913t

Kaveh, N. S., Barnhoorn, A. & Wolf, K. H. 2016. Wettability evaluation of silty shale caprocks for CO_2 storage. *International Journal of Greenhouse Gas Control,* 49**,** 425-435. https://doi.org/10.1016/j.ijggc.2016.04.003

Kaveh, N. S., Rudolph, E., Van Hemert, P., Rossen, W. & Wolf, K.-H. 2014. Wettability evaluation of a CO_2/water/bentheimer sandstone system: contact angle, dissolution, and bubble size. *Energy & Fuels,* 28(6)**,** 4002-4020. https://doi.org/10.1021/ef500034j

Kaveh, N. S., Wolf, K. H., Ashrafizadeh, S. N. & Rudolph, E. S. J. 2012. Effect of coal petrology and pressure on wetting properties of wet coal for CO_2 and flue gas storage. *International Journal of Greenhouse Gas Control,* 11**,** S91-S101. https://doi.org/10.1016/j.ijggc.2012.09.009

Keshavarz, V., Khosravanian, R., Taheri-Shakib, J., Salimidelshad, Y. & Hosseini, S. A. 2019. Chemical removal of organic precipitates deposition from porous media: Characterizing adsorption and surface properties. *Journal of Petroleum Science and Engineering,* 175**,** 200-214. https://doi.org/10.1016/j.petrol.2018.12.021

Kharaka, Y. K., Thordsen, J. J., Hovorka, S. D., Seay Nance, H., Cole, D. R., Phelps, T. J. & Knauss, K. G. 2009. Potential environmental issues of CO_2 storage in deep saline aquifers: Geochemical results from the Frio-I Brine Pilot test, Texas, USA. *Applied Geochemistry,* 24(6)**,** 1106-1112. https://doi.org/10.1016/j.apgeochem.2009.02.010

Kowalska, M., Güler, H. & Cocke, D. L. 1994. Interactions of clay minerals with organic pollutants. *Science of the total environment,* 141(1-3)**,** 223-240. https://doi.org/10.1016/0048-9697(94)90030-2

Krevor, S., Blunt, M. J., Benson, S. M., Pentland, C. H., Reynolds, C., Al-Menhali, A. & Niu, B. 2015. Capillary trapping for geologic carbon dioxide storage – From pore scale physics to field scale implications. *International Journal of Greenhouse Gas Control,* 40**,** 221-237. https://doi.org/10.1016/j.ijggc.2015.04.006

Krooss, B. M., van Bergen, F., Gensterblum, Y., Siemons, N., Pagnier, H. J. M. & David, P. 2002. High-pressure methane and carbon dioxide adsorption on dry and moisture-equilibrated Pennsylvanian coals. *International Journal of Coal Geology,* 51(2)**,** 69-92. https://doi.org/10.1016/S0166-5162(02)00078-2

Kumar, A., Noh, M., Pope, G. A., Sepehrnoori, K., Bryant, S. & Lake, L. W.Reservoir simulation of CO_2 storage in deep saline aquifers. SPE/DOE Symposium on Improved Oil Recovery. 2004. SPE-89343-MS. https://doi.org/10.2118/89343-ms

Kwok, D. Y. & Neumann, A. W. 1999. Contact angle measurement and contact angle interpretation. *Advances in Colloid and Interface Science,* 81(3)**,** 167-249. https://doi.org/10.1016/S0001-8686(98)00087-6

Lackner, K. S. 2003. A guide to CO_2 sequestration. *Science,* 300(5626)**,** 1677-1678. https://doi.org/10.1126/science.1079033

Lackner, K. S. & Sachs, J. 2005. A robust strategy for sustainable energy. *Brookings Papers on Economic Activity,* 2005(2)**,** 215-284. https://doi.org/10.1353/eca.2006.0007

Lamy-Chappuis, B., Angus, D., Fisher, Q., Grattoni, C. & Yardley, B. W. 2014. Rapid porosity and permeability changes of calcareous sandstone due to CO_2-enriched brine injection. *Geophysical Research Letters,* 41(2)**,** 399-406. https://doi.org/10.1002/2013GL058534

Lander, L. M., Siewierski, L. M., Brittain, W. J. & Vogler, E. A. 1993. A systematic comparison of contact angle methods. *Langmuir,* 9(8)**,** 2237-2239. https://doi.org/10.1021/la00032a055

Laplace, P. S., Bowditch, N. & Bowditch, N. I. 1829. Mécanique céleste. *Mécanique céleste*.

Lashgari, H. R., Sun, A., Zhang, T., Pope, G. A. & Lake, L. W. 2019. Evaluation of carbon dioxide storage and miscible gas EOR in shale oil reservoirs. *Fuel,* 241**,** 1223-1235. https://doi.org/10.1016/j.fuel.2018.11.076

Laszlo, P. 1987. Chemical Reactions on Clays. *Science,* 235(4795)**,** 1473-1477. https://doi.org/10.1126/science.235.4795.1473

Lebedev, M., Zhang, Y., Sarmadivaleh, M., Barifcani, A., Al-Khdheeawi, E. & Iglauer, S. 2017. Carbon geosequestration in limestone: Pore-scale dissolution and geomechanical weakening. *International Journal of Greenhouse Gas Control,* 66**,** 106-119. https://doi.org/10.1016/j.ijggc.2017.09.016

Leung, D. Y. C., Caramanna, G. & Maroto-Valer, M. M. 2014. An overview of current status of carbon dioxide capture and storage technologies. *Renewable and Sustainable Energy Reviews,* 39**,** 426-443. https://doi.org/https://doi.org/10.1016/j.rser.2014.07.093

Li, Q. & Liu, G. 2016. Risk assessment of the geological storage of CO_2: A review. *In: Vishal V., Singh T. (eds) Geologic Carbon Sequestration.* pp. 249-284. Springer, Cham. https://doi.org/10.1007/978-3-319-27019-7_13

Li, X. & Elsworth, D. 2015. Geomechanics of CO_2 enhanced shale gas recovery. *Journal of Natural Gas Science and Engineering,* 26**,** 1607-1619. https://doi.org/10.1016/j.jngse.2014.08.010

Li, Z., Dong, M., Li, S. & Dai, L. 2004. Densities and solubilities for binary systems of carbon dioxide+ water and carbon dioxide+ brine at 59 C and pressures to 29 MPa. *Journal of Chemical & Engineering Data,* 49(4)**,** 1026-1031. https://doi.org/10.1021/je049945c

Liao, B., Qiu, L., Wang, D., Bao, W., Wei, Y. & Wang, Y. 2019. The behaviour of water on the surface of kaolinite with an oscillating electric field. *RSC advances,* 9(38)**,** 21793-21803. https://doi.org/10.1039/C9RA04269E

Lindsey, R. 2020. *Climate change: Atmospheric carbon dioxide* [Online]. Available: https://www.climate.gov/news-features/understanding-climate/climate-change-atmospheric-carbon-dioxide [Accessed 23 January 2021].

Lipsicas, M., Straley, C., Costanzo, P. M. & Giese, R. F. 1985. Static and dynamic structure of water in hydrated kaolinites. II. The dynamic structure. *Journal of Colloid and Interface Science,* 107(1)**,** 221-230. https://doi.org/10.1016/0021-9797(85)90165-1

Liu, R., Heinemann, N., Liu, J., Zhu, W., Wilkinson, M., Xie, Y., Wang, Z., Wen, T., Hao, F. & Haszeldine, R. S. 2019. CO_2 sequestration by mineral trapping in natural analogues in the Yinggehai Basin, South China Sea. *Marine and Petroleum Geology,* 104**,** 190-199. https://doi.org/10.1016/j.marpetgeo.2019.03.018

Liu, Y., Mutailipu, M., Jiang, L., Zhao, J., Song, Y. & Chen, L. 2015. Interfacial tension and contact angle measurements for the evaluation of CO_2-brine two-phase flow characteristics in porous media. *Environmental Progress & Sustainable Energy,* 34(6)**,** 1756-1762. https://doi.org/10.1002/ep.12160

Love, J. C., Estroff, L. A., Kriebel, J. K., Nuzzo, R. G. & Whitesides, G. M. 2005. Self-assembled monolayers of thiolates on metals as a form of nanotechnology. *Chemical Reviews,* 105(4)**,** 1103-1170. https://doi.org/10.1021/cr0300789

Luo, P., Zhong, N., Khan, I., Wang, X., Wang, H., Luo, Q. & Guo, Z. 2019. Effects of pore structure and wettability on methane adsorption capacity of mud rock: Insights from mixture of organic matter and clay minerals. *Fuel,* 251**,** 551-561. https://doi.org/10.1016/j.fuel.2019.04.072

Marmur, A. 2006. Soft contact: Measurement and interpretation of contact angles. *Soft Matter,* 2**,** 12-17. https://doi.org/10.1039/B514811C

Mastalerz, M., Gluskoter, H. & Rupp, J. 2004. Carbon dioxide and methane sorption in high volatile bituminous coals from Indiana, USA. *International Journal of Coal Geology,* 60(1)**,** 43-55. https://doi.org/10.1016/j.coal.2004.04.001

Matter, J. M., Stute, M., Snæbjörnsdottir, S. Ó., Oelkers, E. H., Gislason, S. R., Aradottir, E. S., Sigfusson, B., Gunnarsson, I., Sigurdardottir, H. & Gunnlaugsson, E. 2016. Rapid carbon mineralization for permanent disposal of anthropogenic carbon dioxide emissions. *Science,* 352(6291)**,** 1312-1314. https://doi.org/10.1126/science.aad8132

Mazzullo, S. 2004. Overview of porosity evolution in carbonate reservoirs. *Kansas Geological Society Bulletin,* 79(1-2)**,** 1-19.

Millar, A. S. & Reeve, J. 2014. (compiler) GSWA Harvey 1 well completion and preliminary interpretation report, Southen Perth Basin: Geological Survey of Western Australia, Record 2014/12, 17p.

Mills, J., Riazi, M. & Sohrabi, M.Wettability of common rock-forming minerals in a CO_2-brine system at reservoir conditions. International Symposium of the Society of Core Analysts. 2011. Society of Core Analysts Fredericton, Canada, 19-21.

Milne, A. J. B. & Amirfazli, A. 2012. The Cassie equation: How it is meant to be used. *Advances in Colloid and Interface Science,* 170(1)**,** 48-55. https://doi.org/10.1016/j.cis.2011.12.001

Mittal, K. L. 2003. *Contact Angle, Wettability and Adhesion, Volume 3,* CRC Press.

Mo, S. & Akervoll, I.Modeling long-term CO_2 storage in aquifer with a black-oil reservoir simulator. SPE/EPA/DOE Exploration and Production Environmental Conference. 2005. SPE-93951-MS. https://doi.org/10.2118/93951-ms

Mohamed, I. M., He, J. & Nasr-El-Din, H. A.Carbon Dioxide Sequestration in Sandstone Aquifers: How Does It Affect the Permeability? 2012. Orlando, Florida, USA. CMTC: *Carbon Management Technology Conference*, 20. https://doi.org/10.7122/149958-MS

Mohammed, S. & Gadikota, G. 2020. Dynamic wettability alteration of calcite, silica and illite surfaces in subsurface environments: A case study of ssphaltene self-assembly at solid interfaces. *Applied Surface Science,* 505**,** 144516. https://doi.org/10.1016/j.apsusc.2019.144516

Moore, C. H. & Wade, W. J. 2013. *Carbonate reservoirs: Porosity and diagenesis in a sequence stratigraphic framework,* Newnes.

Moore, D. M. & Reynolds, R. C. 1997. *X-Ray Diffraction and the Identification and Analysis of Clay Minerals,* New York, Oxford Univ. Press.

Morrow, N. R. 1990. Wettability and its effect on oil recovery. *Journal of Petroleum Technology,* 42(12)**,** 1476-1484. https://doi.org/10.2118/21621-PA

Mukherjee, S. 2013. *Internal Structures of Clay Minerals,* Dordrecht, Dordrecht: Springer Netherlands. https://doi.org/10.1007/978-94-007-6683-9_3

Muller, É., Thomazo, C., Stüeken, E. E., Hallmann, C., Leider, A., Chaduteau, C., Buick, R., Baton, F., Philippot, P. & Ader, M. 2018. Bias in carbon concentration and δ13C measurements of organic matter due to cleaning treatments with organic solvents. *Chemical Geology,* 493**,** 405-412. https://doi.org/10.1016/j.chemgeo.2018.06.018

Müller, E. A. & Gelb, L. D. 2003. Molecular Modeling of Fluid-Phase Equilibria Using an Isotropic Multipolar Potential. *Industrial & Engineering Chemistry Research,* 42(17)**,** 4123-4131. https://doi.org/10.1021/ie030033y

Murray, H. 1999. Applied clay mineralogy today and tomorrow. *Clay minerals,* 34(1)**,** 39-39.

Murray, H. H. 1991. Overview—clay mineral applications. *Applied Clay Science,* 5(5-6)**,** 379-395.

Mutailipu, M., Liu, Y., Jiang, L. & Zhang, Y. 2019. Measurement and estimation of CO_2–brine interfacial tension and rock wettability under CO_2 sub- and super-critical conditions. *Journal of Colloid and Interface Science,* 534**,** 605-617. https://doi.org/10.1016/j.jcis.2018.09.031

Myshakin, E. M., Saidi, W. A., Romanov, V. N., Cygan, R. T. & Jordan, K. D. 2013. Molecular dynamics simulations of carbon dioxide intercalation in hydrated Na-montmorillonite. *The Journal of Physical Chemistry C,* 117(21)**,** 11028-11039. https://doi.org/10.1021/jp312589s

Ni, X., Yang, W., Tan, B., He, J., Xu, L., Li, H. & Wu, F. 2015. Accelerated foliar litter humification in forest gaps: dual feedbacks of carbon sequestration during winter and the growing season in an alpine forest. *Geoderma,* 241**,** 136-144. https://doi.org/10.1016/j.geoderma.2014.11.018

Nielsen, L. C., Bourg, I. C. & Sposito, G. 2012. Predicting CO_2–water interfacial tension under pressure and temperature conditions of geologic CO_2 storage. *Geochimica et Cosmochimica Acta,* 81**,** 28-38. https://doi.org/https://doi.org/10.1016/j.gca.2011.12.018

Niu, B., Al-Menhali, A. & Krevor, S. 2014. A study of residual carbon dioxide trapping in sandstone. *Energy Procedia,* 63**,** 5522-5529. https://doi.org/10.1016/j.egypro.2014.11.585

Olierook, H. K., Delle Piane, C., Timms, N. E., Esteban, L., Rezaee, R., Mory, A. J. & Hancock, L. 2014. Facies-based rock properties characterization for CO_2 sequestration: GSWA Harvey 1 well, Western Australia. *Marine and Petroleum Geology,* 50**,** 83-102. https://doi.org/10.1016/j.marpetgeo.2013.11.002

Orr, F. M. 2009. Onshore geologic storage of CO_2. *Science,* 325(5948)**,** 1656-1658. https://doi.org/10.1126/science.1175677

Osipov, V. I., Sokolov, V. a. c. N. & Eremeev, V. V. e. 2003. *Clay seals of oil and gas deposits*, CRC Press.

Pacala, S. & Socolow, R. 2004. Stabilization wedges: Solving the climate problem for the next 50 years with current technologies. *Science,* 305(5686)**,** 968-972. https://doi.org/10.1126/science.1100103

Pan, B., Gong, C., Wang, X., Li, Y. & Iglauer, S. 2020a. The interfacial properties of clay-coated quartz at reservoir conditions. *Fuel,* 262**,** 116461. https://doi.org/10.1016/j.fuel.2019.116461

Pan, B., Jones, F., Huang, Z., Yang, Y., Li, Y., Hejazi, S. H. & Iglauer, S. 2019a. Methane (CH_4) wettability of clay-coated quartz at reservoir conditions. *Energy & Fuels,* 33(2)**,** 788-795. https://doi.org/10.1021/acs.energyfuels.8b03536

Pan, B., Li, Y. J., Xie, L. J., Wang, X. P., He, Q. K., Li, Y. C., Hejazi, S. H. & Iglauer, S. 2019b. Role of fluid density on quartz wettability. *Journal of Petroleum Science and Engineering,* 172**,** 511-516. https://doi.org/10.1016/j.petrol.2018.09.088

Pan, B., Yajun, L., Wang, H., Jones, F. & Iglauer, S. 2018. CO_2 and CH_4 wettabilities of organic-rich shale. *Energy & Fuels,* 32(2)**,** 1914-1922. https://doi.org/10.1021/acs.energyfuels.7b01147

Pan, B., Yin, X. & Iglauer, S. 2020b. A review on clay wettability: From experimental investigations to molecular dynamics simulations. *Advances in Colloid and Interface Science,* 285**,** 102266. https://doi.org/10.1016/j.cis.2020.102266

Parker, J. C., Lenhard, R. J. & Kuppusamy, T. 1987. A parametric model for constitutive properties governing multiphase flow in porous media. *Water Resources Research,* 23(4)**,** 618-624. https://doi.org/10.1029/WR023i004p00618

Parks, G. A. 1967. Aqueous surface chemistry of oxides and complex oxide minerals: Isoelectric point and zero point of charge. *In: Stumm W. (Eds) Equilibrium Concepts in Natural Water System.* Vol. 67, pp. 121-160. Washington, DC: ACS Publications. https://doi.org/10.1021/ba-1967-0067.ch006

Pearce, J. K., Kirste, D. M., Dawson, G. K. W., Farquhar, S. M., Biddle, D., Golding, S. D. & Rudolph, V. 2015. SO_2 impurity impacts on experimental and simulated CO_2–water–reservoir rock reactions at carbon storage conditions. *Chemical Geology,* 399**,** 65-86. https://doi.org/10.1016/j.chemgeo.2014.10.028

Pentland, C. H., El-Maghraby, R., Georgiadis, A., Iglauer, S. & Blunt, M. J. 2011a. Immiscible Displacements and Capillary Trapping in CO_2 Storage. *Energy Procedia,* 4**,** 4969-4976. https://doi.org/10.1016/j.egypro.2011.02.467

Pentland, C. H., El-Maghraby, R., Iglauer, S. & Blunt, M. J. 2011b. Measurements of the capillary trapping of super-critical carbon dioxide in Berea sandstone. *Geophysical Research Letters,* 38(6). https://doi.org/10.1029/2011GL046683

Perera, M. S. A., Ranjith, P. G., Choi, S. K., Bouazza, A., Kodikara, J. & Airey, D. 2011. A review of coal properties pertinent to carbon dioxide sequestration in coal seams: with special reference to Victorian brown coals. *Environmental Earth Sciences,* 64(1)**,** 223-235. https://doi.org/10.1007/s12665-010-0841-7

Pevzner, R., Lumley, D., Urosevic, M., Gurevich, B., Bona, A., Alajmi, M., Shragge, J., Pervukhina, M., Mueller, T. & Shulakova, V. 2013. Advanced geophysical data analysis at Harvey-1: Storage site characterization and stability assessment. *ANLEC R&D project number 7-1111,* 198.

Qi, R., LaForce, T. C. & Blunt, M. J. 2009. Design of carbon dioxide storage in aquifers. *International Journal of Greenhouse Gas Control,* 3(2)**,** 195-205. https://doi.org/10.1016/j.ijggc.2008.08.004

Rackley, S. A. 2017. *Carbon Capture and Storage,* Oxford, United States, Elsevier Science & Technology.

Rahman, T., Lebedev, M., Barifcani, A. & Iglauer, S. 2016. Residual trapping of supercritical CO_2 in oil-wet sandstone. *Journal of Colloid and Interface Science,* 469**,** 63-68. https://doi.org/https://doi.org/10.1016/j.jcis.2016.02.020

Riaz, A. & Cinar, Y. 2014. Carbon dioxide sequestration in saline formations: Part I—Review of the modeling of solubility trapping. *Journal of Petroleum Science and Engineering,* 124**,** 367-380. https://doi.org/10.1016/j.petrol.2014.07.024

Riaz, A., Hesse, M., Tchelepi, H. A. & Orr, F. M. 2006. Onset of convection in a gravitationally unstable diffusive boundary layer in porous media. *Journal of Fluid Mechanics,* 548**,** 87-111. https://doi.org/10.1017/S0022112005007494

Robin, M., Rosenberg, E. & Fassi-Fihri, O. 1995. Wettability studies at the pore level: A new approach by the use of cryo-scanning electron microscopy. *SPE Formation Evaluation,* **10,** 11-19. https://doi.org/10.2118/22596-PA

Roshan, H., Al-Yaseri, A. Z., Sarmadivaleh, M. & Iglauer, S. 2016a. On wettability of shale rocks. *Journal of Colloid and Interface Science,* 475**,** 104-111. https://doi.org/10.1016/j.jcis.2016.04.041

Roshan, H., Andersen, M. S., Rutlidge, H., Marjo, C. E. & Acworth, R. I. 2016b. Investigation of the kinetics of water uptake into partially saturated shales. *Water Resources Research,* 52(4)**,** 2420-2438. https://doi.org/10.1002/2015WR017786

Ruprecht, C., Pini, R., Falta, R., Benson, S. & Murdoch, L. 2014. Hysteretic trapping and relative permeability of CO_2 in sandstone at reservoir conditions. *International Journal of Greenhouse Gas Control,* 27**,** 15-27. https://doi.org/10.1016/j.ijggc.2014.05.003

Saadatpoor, E., Bryant, S. L. & Sepehrnoori, K. 2010. New trapping mechanism in carbon sequestration. *Transport in Porous Media,* 82(1)**,** 3-17. https://doi.org/10.1007/s11242-009-9446-6

Saeedi, A., Delle Piane, C., Esteban, L. & Xie, Q. 2016a. Flood characteristic and fluid rock interactions of a supercritical CO_2, brine, rock system: South West Hub, Western Australia. *International Journal of Greenhouse Gas Control,* 54(1)**,** 309-321. https://doi.org/10.1016/j.ijggc.2016.09.017

Saeedi, A., Piane, C. D., Esteban, l., Noble, R., Gray, D., Iglauer, S., Lebedev, M. & Stalker, L. 2016b. Understanding fluid rock interactions and their impact on rock properties as a result of CO_2 injection in the SW Hub. *Final Project Report, SCRIPT Project RES-SE-DPE-AS-53419-2, Curtin University*.

Safarov, J., Millero, F., Feistel, R., Heintz, A. & Hassel, E. 2009. Thermodynamic properties of standard seawater: extensions to high temperatures and pressures. *Ocean Science,* 5(3)**,** 235-246. https://doi.org/10.5194/os-5-235-2009

Saraji, S., Goual, L., Piri, M. & Plancher, H. 2013. Wettability of supercritical carbon dioxide/water/quartz systems: Simultaneous measurement of contact angle and interfacial tension at reservoir conditions. *Langmuir,* 29(23)**,** 6856-6866. https://doi.org/10.1021/la3050863

Saraji, S., Piri, M. & Goual, L. 2014. The effects of SO_2 contamination, brine salinity, pressure, and temperature on dynamic contact angles and interfacial tension of supercritical CO_2/brine/quartz systems. *International Journal of Greenhouse Gas Control,* 28**,** 147-155. https://doi.org/10.1016/j.ijggc.2014.06.024

Sarmadivaleh, M., Al-Yaseri, A. Z. & Iglauer, S. 2015. Influence of temperature and pressure on quartz–water–CO_2 contact angle and CO_2–water interfacial

tension. *Journal of colloid and interface science,* 441**,** 59-64. https://doi.org/10.1016/j.jcis.2014.11.010

Sayegh, S., Krause, F., Girard, M. & DeBree, C. 1990. Rock/fluid interactions of carbonated brines in a sandstone reservoir: Pembina Cardium, Alberta, Canada. *SPE Formation Evaluation,* 5(04)**,** 399-405. https://doi.org/10.2118/19392-PA

Schrader, M. E. & Yariv, S. 1990. Wettability of clay minerals. *Journal of Colloid and Interface Science,* 136(1)**,** 85-94. https://doi.org/10.1016/0021-9797(90)90080-8

Schroth, B. K. & Sposito, G. 1997. Surface charge properties of kaolinite. *Clays Clay Miner.,* 45**,** 85-91. https://doi.org/10.1346/CCMN.1997.0450110

Seo, K., Kim, M. & Kim, D. H. 2015. Re-derivation of Young's equation, Wenzel equation, and Cassie-Baxter equation based on energy minimization. *In: Aliofkhazraei M. (Eds) Surface Energy.* pp. 3-22. InTechOpen. https://doi.org/10.5772/61066

Shang, J., Flury, M., Harsh, J. B. & Zollars, R. L. 2010. Contact angles of aluminosilicate clays as affected by relative humidity and exchangeable cations. *Colloids and Surfaces A: Physicochemical and Engineering Aspects,* 353(1)**,** 1-9. https://doi.org/10.1016/j.colsurfa.2009.10.013

Siddiqui, M. A. Q., Ali, S., Fei, H. & Roshan, H. 2018. Current understanding of shale wettability: A review on contact angle measurements. *Earth-Science Reviews,* 181**,** 1-11. https://doi.org/10.1016/j.earscirev.2018.04.002

Siddiqui, M. A. Q., Chen, X., Iglauer, S. & Roshan, H. 2019. A multiscale study on shale wettability: Spontaneous imbibition versus contact angle. *Water Resources Research,* 55(6)**,** 5012-5032. https://doi.org/10.1029/2019WR024893

Siemons, N. & Busch, A. 2007. Measurement and interpretation of supercritical CO_2 sorption on various coals. *International Journal of Coal Geology,* 69(4)**,** 229-242. https://doi.org/10.1016/j.coal.2006.06.004

Sigfusson, B., Gislason, S. R., Matter, J. M., Stute, M., Gunnlaugsson, E., Gunnarsson, I., Aradottir, E. S., Sigurdardottir, H., Mesfin, K. & Alfredsson, H. A. 2015. Solving the carbon-dioxide buoyancy challenge: The design and field testing of a dissolved CO_2 injection system. *International Journal of Greenhouse Gas Control,* 37**,** 213-219. https://doi.org/10.1016/j.ijggc.2015.02.022

Šolc, R., Gerzabek, M. H., Lischka, H. & Tunega, D. 2011. Wettability of kaolinite (001) surfaces — Molecular dynamic study. *Geoderma,* 169**,** 47-54. https://doi.org/https://doi.org/10.1016/j.geoderma.2011.02.004

Sposito, G., Skipper, N. T., Sutton, R., Park, S.-H., Soper, A. K. & Greathouse, J. A. 1999. Surface geochemistry of the clay minerals. *Proceeding of the National Academy of Sciences* 96(7)**,** 3358-3364. https://doi.org/10.1073/pnas.96.7.3358

Spycher, N., Pruess, K. & Ennis-King, J. 2003. CO_2-H_2O mixtures in the geological sequestration of CO_2. I. Assessment and calculation of mutual solubilities from 12 to 100 C and up to 600 bar. *Geochimica et cosmochimica acta,* 67(16)**,** 3015-3031. https://doi.org/10.1016/S0016-7037(03)00273-4

Stalker, L., Noble, R., Gray, D., Trefry, C., Varma, S., Ross, A., Sestak, S., Armand, S. & Gong, S. 2013a. Geochemical characterisation of gases, fluids and rocks in the Harvey-1 data well. *CSIRO Report Number EP135208*.

Stalker, L., Varma, S., Van Gent, D., Haworth, J. & Sharma, S. 2013b. South West Hub: a carbon capture and storage project. *Australian Journal of Earth Sciences,* 60(1)**,** 45-58. https://doi.org/10.1080/08120099.2013.756830

Strand, S., Standnes, D. C. & Austad, T. 2003. Spontaneous imbibition of aqueous surfactant solutions into neutral to oil-wet carbonate cores: Effects of brine salinity and composition. *Energy & Fuels,* 17(5)**,** 1133-1144. https://doi.org/10.1021/ef030051s

Suekane, T., Nobuso, T., Hirai, S. & Kiyota, M. 2008. Geological storage of carbon dioxide by residual gas and solubility trapping. *International Journal of Greenhouse Gas Control,* 2(1)**,** 58-64. https://doi.org/10.1016/S1750-5836(07)00096-5

Suekane, T., Zhou, N., Hosokawa, T. & Matsumoto, T. 2010. Direct observation of trapped gas bubbles by capillarity in sandy porous media. *Transport in Porous Media,* 82(1)**,** 111-122. https://doi.org/10.1007/s11242-009-9439-5

Surampalli, R. Y., Zhang, T. C., Brar, S. K., Gurjar, B. R., Kao, C.-M., Naidu, R., Ojha, C. S. P., Ramakrishnan, A., Tyagi, R. D. & Yan, S. 2014. *Carbon Capture and Storage : Physical, Chemical, and Biological Methods,* Reston, United States, American Society of Civil Engineers.

Swain, P. S. & Lipowsky, R. 1998. Contact angles on heterogeneous surfaces: A new look at Cassie's and Wenzel's laws. *Langmuir,* 14(23)**,** 6772-6780. https://doi.org/10.1021/la980602k

Tadmor, R. 2004. Line energy and the relation between advancing, receding, and young contact angles. *Langmuir*, 20(18)**,** 7659-7664. https://doi.org/10.1021/la049410h

Thomas, D. C. & Benson, S. M. 2005. *Carbon dioxide capture for storage in deep geologic formations-Results from the CO_2 capture project: Vol 1-Capture and separation of carbon dioxide from combustion sources*, Elsevier.

Thomazo, C., Ader, M., Farquhar, J. & Philippot, P. 2009. Methanotrophs regulated atmospheric sulfur isotope anomalies during the Mesoarchean (Tumbiana Formation, Western Australia). *Earth and Planetary Science Letters*, 279(1)**,** 65-75. https://doi.org/10.1016/j.epsl.2008.12.036

Tian, S., Erastova, V., Lu, S., Greenwell, H. C., Underwood, T. R., Xue, H., Zeng, F., Chen, G., Wu, C. & Zhao, R. 2018. Understanding model crude oil component interactions on kaolinite silicate and aluminol surfaces: Toward improved understanding of shale oil recovery. *Energy & Fuels*, 32(2)**,** 1155-1165. https://doi.org/10.1021/acs.energyfuels.7b02763

Tonnet, N., Broseta, D. & Mouronval, G.Evaluation of the petrophysical properties of a carbonate-rich caprock for CO_2 geological storage purposes. SPE EUROPEC/EAGE Annual Conference and Exhibition. 2010. SPE-131525-MS. https://doi.org/10.2118/131525-ms

Treiber, L. E. & Owens, W. W. 1972. A laboratory evaluation of the wettability of fifty oil-producing reservoirs. *Society of Petroleum Engineers Journal*, 12(06)**,** 531-540. https://doi.org/10.2118/3526-pa

Tudek, J., Crandall, D., Fuchs, S., Werth, C. J., Valocchi, A. J., Chen, Y. & Goodman, A. 2017. In situ contact angle measurements of liquid CO_2, brine, and Mount Simon sandstone core using micro X-ray CT imaging, sessile drop, and Lattice Boltzmann modeling. *Journal of Petroleum Science and Engineering*, 155**,** 3-10. https://doi.org/10.1016/j.petrol.2017.01.047

Uddin, F. 2008. Clays, nanoclays, and montmorillonite minerals. *Metallurgical and Materials Transactions A*, 39(12)**,** 2804-2814. https://doi.org/10.1007/s11661-008-9603-5

Umar, B. A., Gholami, R., Raza, A., Downey, W. S., Sarmadivaleh, M., Shah, A. A. & Nayak, P. 2019. A study on the surface wettability of clastic rocks with potential application for CO_2 storage sites. *Natural Resources Research***,** 1-11. https://doi.org/10.1007/s11053-019-09553-x

Underschultz, J. & Strand, J. 2016. Capillary seal capacity of faults under hydrodynamic conditions. *Geofluids,* 16(3)**,** 464-475. https://doi.org/10.1111/gfl.12166

Underwood, T., Erastova, V., Cubillas, P. & Greenwell, H. C. 2015. Molecular dynamic simulations of montmorillonite–organic interactions under varying salinity: An insight into enhanced oil recovery. *The Journal of Physical Chemistry C,* 119(13)**,** 7282-7294. https://doi.org/10.1021/acs.jpcc.5b00555

Vassoyevich, N., Burlin, Y. K., Konyukhov, A. & Karnyushina, Y. Y. 1976. The role of clays in oil formation. *International Geology Review,* 18(2)**,** 125-136. https://doi.org/10.1080/00206817609471181

Vishal, V. & Singh, T. 2016. *Geologic carbon sequestration*, Springer. https://doi.org/10.1007/978-3-319-27019-7

Wan, J., Kim, Y. & Tokunaga, T. K. 2014. Contact angle measurement ambiguity in supercritical CO_2–water–mineral systems: Mica as an example. *International Journal of Greenhouse Gas Control,* 31**,** 128-137. https://doi.org/10.1016/j.ijggc.2014.09.029

Wang, L., Wang, C., Yu, Y., Huang, X., Long, Z., Hou, Y. & Cui, D. 2012a. Recovery of fluorine from bastnasite as synthetic cryolite by-product. *Journal of Hazardous Materials,* 209–210**,** 77-83. https://doi.org/10.1016/j.jhazmat.2011.12.069

Wang, S., Edwards, I. M. & Clarens, A. F. 2012b. Wettability phenomena at the CO_2–brine–mineral interface: Implications for geologic carbon sequestration. *Environmental Science & Technology,* 47(1)**,** 234-241. https://doi.org/10.1021/es301297z

Wang, S., Tao, Z., Persily, S. M. & Clarens, A. F. 2013. CO_2 adhesion on hydrated mineral surfaces. *Environmental Science & Technology,* 47(20)**,** 11858-11865. https://doi.org/10.1021/es402199e

Weaver, C. E. 1989. *Clays, Muds, and Shales,* Amsterdam, Elsevier.

Wenzel, R. N. 1936. Resistance of solid surfaces to wetting by water. *Industrial and Engineering Chemistry,* 28(8)**,** 988-994. https://doi.org/10.1021/ie50320a024

White, C. M., Smith, D. H., Jones, K. L., Goodman, A. L., Jikich, S. A., LaCount, R. B., DuBose, S. B., Ozdemir, E., Morsi, B. I. & Schroeder, K. T. 2005. Sequestration of carbon dioxide in coal with enhanced coalbed methane

recovery: A review. *Energy & Fuels,* 19(3)**,** 659-724. https://doi.org/10.1021/ef040047w

Wiegand, G. & Franck, E. U. 1994. Interfacial tension between water and non-polar fluids up to 473 K and 2800 bar. *Berichte der Bunsengesellschaft für physikalische Chemie,* 98(6)**,** 809-817. https://doi.org/10.1002/bbpc.19940980608

Wiese, B., Nimtz, M., Klatt, M. & Kühn, M. 2010. Sensitivities of injection rates for single well CO_2 injection into saline aquifers. *Geochemistry,* 70**,** 165-172. https://doi.org/10.1016/j.chemer.2010.05.009

Wollenweber, J., Alles, S., Busch, A., Krooss, B. M., Stanjek, H. & Littke, R. 2010. Experimental investigation of the CO_2 sealing efficiency of caprocks. *International Journal of Greenhouse Gas Control,* 4(2)**,** 231-241. https://doi.org/10.1016/j.ijggc.2010.01.003

Worden, R. H. & Smith, L. K. 2004. Geological sequestration of CO_2 in the subsurface: lessons from CO2 injection enhanced oil recovery projects in oilfields. *Geological Society, London, Special Publications,* 233**,** 211-224. https://doi.org/10.1144/GSL.SP.2004.233.01.14

Wright, I. P., Yates, P., Hutchison, R. & Pillinger, C. 1997. The content and stable isotopic composition of carbon in individual micrometeorites from Greenland and Antarctica. *Meteoritics & Planetary Science,* 32(1)**,** 79-89. https://doi.org/10.1111/j.1945-5100.1997.tb01243.x

Xi, K., Cao, Y., Liu, K., Jahren, J., Zhu, R., Yuan, G. & Hellevang, H. 2019. Authigenic minerals related to wettability and their impacts on oil accumulation in tight sandstone reservoirs: An example from the lower Cretaceous Quantou formation in the southern Songliao Basin, China. *Journal of Asian Earth Sciences,* 178**,** 173-192. https://doi.org/10.1016/j.jseaes.2018.04.025

Xu, T., Apps, J. A. & Pruess, K. 2001. Analysis of mineral trapping for CO_2 disposal in deep aquifers. *Lawrence Berkeley National Laboratory, University of California, Berkeley, CA.*

Xu, T., Apps, J. A. & Pruess, K. 2003. Reactive geochemical transport simulation to study mineral trapping for CO_2 disposal in deep arenaceous formations. *Journal of Geophysical Research: Solid Earth,* 108(B2). https://doi.org/10.1029/2002JB001979

Yan, W., Zhao, G.-Y., Chen, G.-J. & Guo, T.-M. 2001. Interfacial tension of (methane + nitrogen) + water and (carbon dioxide + nitrogen) + water systems. *Journal of Chemical & Engineering Data,* 46(6)**,** 1544-1548. https://doi.org/10.1021/je0101505

Yang, C., He, F. & Hao, P. 2010. The apparent contact angle of water droplet on the micro-structured hydrophobic surface. *Science China Chemistry,* 53(4)**,** 912-916. https://doi.org/10.1007/s11426-010-0115-y

Yang, D., Gu, Y. & Tontiwachwuthikul, P. 2008. Wettability determination of the crude oil−reservoir brine−reservoir rock system with dissolution of CO_2 at high pressures and elevated temperatures. *Energy & Fuels,* 22(4)**,** 2362-2371. https://doi.org/10.1021/ef800012w

Yassin, M. R., Begum, M. & Dehghanpour, H. 2017. Organic shale wettability and its relationship to other petrophysical properties: A Duvernay case study. *International Journal of Coal Geology,* 169**,** 74-91. https://doi.org/10.1016/j.coal.2016.11.015

Yi, H., Jia, F., Zhao, Y., Wang, W., Song, S., Li, H. & Liu, C. 2018. Surface wettability of montmorillonite (0 0 1) surface as affected by surface charge and exchangeable cations: A molecular dynamic study. *Applied Surface Science,* 459**,** 148-154. https://doi.org/10.1016/j.apsusc.2018.07.216

Yin, X., Gupta, V., Du, H., Wang, X. & Miller, J. D. 2012. Surface charge and wetting characteristics of layered silicate minerals. *Advances in Colloid and Interface Science,* 179-182**,** 43-50. https://doi.org/10.1016/j.cis.2012.06.004

Yin, X. & Miller, J. D. 2012. Wettability of kaolinite basal planes based on surface force measurements using atomic force microscopy. *Mining, Metallurgy & Exploration,* 29(1)**,** 13-19. https://doi.org/10.1007/BF03402328

Young, T. 1805. III. An essay on the cohesion of fluids. *Philosophical Transactions of the Royal Society of London,* 95**,** 65-87. https://doi.org/doi:10.1098/rstl.1805.0005

Yu, H., Zhang, Y., Ma, Y., Lebedev, M., Ahmed, S., Li, X., Verrall, M., Squelch, A. & Iglauer, S. 2019. CO_2 saturated brine injection into unconsolidated sandstone: implications for carbon geo-sequestration. *Journal of Geophysical Research: Solid Earth,* 124. https://doi.org/10.1029/2018JB017100

Yu, K. M. K., Curcic, I., Gabriel, J. & Tsang, S. C. E. 2008. Recent Advances in CO_2 Capture and Utilization. *ChemSusChem,* 1(11)**,** 893-899. https://doi.org/10.1002/cssc.200800169

Yu, M., Liu, L., Yang, S., Yu, Z., Li, S., Yang, Y. & Shi, X. 2016. Experimental identification of CO_2–oil–brine–rock interactions: Implications for CO_2 sequestration after termination of a CO_2-EOR project. *Applied Geochemistry,* 75**,** 137-151. https://doi.org/10.1016/j.apgeochem.2016.10.018

Yuan, Y. & Lee, T. R. 2013. Contact angle and wetting properties. *In: Bracco G., Holst B. (Eds) Surface Science Techniques. Springer Series in Surface Sciences.* Vol. 51, pp. 3-34. Springer. https://doi.org/10.1007/978-3-642-34243-1_1

Zhang, D. & Song, J. 2014. Mechanisms for geological carbon sequestration. *Procedia IUTAM,* 10**,** 319-327. https://doi.org/10.1016/j.piutam.2014.01.027

Zhang, L., Lu, X., Liu, X., Yang, K. & Zhou, H. 2016a. Surface Wettability of Basal Surfaces of Clay Minerals: Insights from Molecular Dynamics Simulation. *Energy and Fuels,* 30(1)**,** 149-160. https://doi.org/10.1021/acs.energyfuels.5b02142

Zhang, L., Lu, X., Liu, X., Yang, K. & Zhou, H. 2016b. Surface wettability of basal surfaces of clay minerals: Insights from molecular dynamics simulation. *Energy & Fuels,* 30(1)**,** 149-160. https://doi.org/10.1021/acs.energyfuels.5b02142

Zhang, X., Yi, H., Bai, H., Zhao, Y., Min, F. & Song, S. 2017. Correlation of montmorillonite exfoliation with interlayer cations in the preparation of two-dimensional nanosheets. *RSC Advances,* 7(66)**,** 41471-41478. https://doi.org/10.1039/c7ra07816a

Zhao, X., Blunt, M. J. & Yao, J. 2010. Pore-scale modeling: Effects of wettability on waterflood oil recovery. *Journal of Petroleum Science and Engineering,* 71(3)**,** 169-178. https://doi.org/10.1016/j.petrol.2010.01.011

Zheng, Y. & Zaoui, A. 2017. Wetting and nanodroplet contact angle of the clay 2:1 surface: The case of Na-montmorillonite (001). *Applied Surface Science,* 396**,** 717-722. https://doi.org/10.1016/j.apsusc.2016.11.015